KTH Engineering Sciences

Doctoral Thesis

Dark Matter Phenomenology in Astrophysical Systems

Stefan Clementz

Particle and Astroparticle Physics, Department of Physics,
School of Engineering Sciences
KTH Royal Institute of Technology, SE-106 91 Stockholm, Sweden

Stockholm, Sweden 2019

Typeset in LaTeX

Akademisk avhandling för avläggande av teknologie doktorsexamen (TeknD) inom ämnesområdet fysik.

Scientific thesis for the degree of Doctor of Philosophy (PhD) in the subject area of Physics.

ISBN 978-91-7873-242-5

TRITA-SCI-FOU 2019:35

Printed in Sweden by Universitetsservice US AB

Abstract

There is now a great deal of evidence in support of the existence of a large amount of unseen gravitational mass, commonly called dark matter, from observations in astrophysical systems of sizes ranging from that of dwarf galaxies to the scale of the entire Universe. One of the most promising explanations for this unseen mass is that it consists of a species of unobserved elementary particles. An expected feature of particle dark matter is that it should form halos in the early Universe that cannot collapse due to its weak interactions with itself and baryonic matter. It is within these halos that galaxies, including the Milky Way, which is the galaxy that we inhabit, are thought to be born.

Different methods to detect dark matter that originates from the galactic halo have been devised and these generally fall into the categories of direct and indirect detection. On Earth, direct detection experiments are employed to detect the recoiling atoms that are generated through the occasional scattering between halo dark matter particles with the detector material. The indirect search for dark matter is conducted by attempting to detect the standard model particles that may be produced as dark matter annihilates or decays and by looking for the effects that dark matter may have on astrophysical bodies. The aim of this thesis is to study the effects that dark matter may have in different astrophysical systems and how its properties can be determined should an effect that is due to dark matter be detected.

The Sun currently experiences the solar composition problem, which is a mismatch between simulated and observed helioseismological properties of the Sun. A large abundance of dark matter introduces a new heat transfer mechanism that has been shown to offer a viable solution. This problem is discussed here in a particular model of dark matter where the dark matter halo is made up of equal numbers of particles and antiparticles. It is shown that dark matter arising from the thermal freeze-out mechanism might alleviate the problem, whereas only asymmetric dark matter models have previously been considered.

If a dark matter signal is seen in a direct detection experiment, the determination of the dark matter properties will be plagued by numerous uncertainties related to the halo. It has been shown that many of these uncertainties can be eliminated by comparing signals in different direct detection experiments in what is called "halo-independent" methods. These methods can also be used to predict the neutrino signal from dark matter annihilating in the Sun, further constraining DM properties, if a direct detection experiment detects a signal. This framework is here generalized to inelastic dark matter and the information concerning dark matter properties in a direct detection signal is discussed.

When the Sun captures dark matter, thermalization is a process where dark matter particles lose their remaining kinetic energy after being captured and sink into the solar core. Evaporation due to collisions with high-energy solar atoms is also possible. For inelastic dark matter, it is expected that the thermalization process stops prematurely, which will have an effect on the expected neutrino signal

from its annihilation. Moreover, evaporation may also be significant due transitions from the heavier to the lighter state. Here, the thermalization problem is discussed, and results from numerical simulations are presented that show the extent to which inelastic dark matter thermalizes and if evaporation has to be taken into account.

A number of issues have been observed in dark matter halos at smaller scales when compared to results from large simulations. Dark matter that interacts strongly with itself has been proposed as a solution. There are a number of problems associated with these models that are excluded by other means. A particular model of inelastic dark matter interacting via a light mediator is analyzed here and shown to possible alleviate at least some of the problems associated with models of this kind.

key words: dark matter, self-interactions, solar capture, helioseismology, inelastic dark matter, direct detection, indirect detection, thermalization.

Sammanfattning

Det finns nu många olika bevis som stödjer existensen av en stor mängd osynlig gravitationell massa, ofta kallad mörk materia, från observationer av astrofysikaliska system i storleksordningar från dvärggalaxer till hela Universum. En av de mest lovande förklaringarna till denna osedda massa är att den består av ännu ej observerade elementarpartiklar. En förväntad effekt av mörk materia bestående av partiklar är att den skapar halos i tidiga universum som inte kollapsar på grund av dess svaga växelverkan med sig själv och baryonisk materia. Det är inuti dessa halos som galaxer, inklusive Vintergatan som är den galax vi bor i, är tänkta att skapas.

Metoder för att detektera mörk materia som kommer från den galaktiska halon har formulerats och faller generellt under två kategorier. På jorden ämnar man att i direkt-detektionsexperiment observera den rekyl som uppstår hos atomer när mörk materia från halon kolliderar med dessa inuti experimentets detektorvolym. Indirekta sökningar sker genom att man försöker detektera partiklar i standardmodellen som skapas när mörk materia annihilerar eller sönderfaller eller att man letar efter de effekter som mörk materia kan ha i olika astrofysikaliska kroppar. Syftet med denna avhandling är att studera de effekter som mörk materia kan ha i olika astrofysikaliska system och hur dess egenskaper kan bestämmas om en effekt skapad av mörk materia detekteras.

Solen upplever för närvarande ett sammansättningssproblem som uppstått på grund av att simuleringar och observerade helioseismologiska egenskaper är inkompatibla. En stor mängd mörk materia introducerar en ny mekanism för att transportera värme som har visats kunna erbjuda en möjlig lösning. Detta problem diskuteras här med en modell av mörk materia där mörk materia består av samma antal partiklar och antipartiklar. Det visas att mörk materia som uppstår via termisk utfrysning kan förmildra problemet när det tidigare trots vara möjligt endast för asymmetrisk mörk materia modeller.

Om mörk materia observeras i ett direkt-detektionsexperiment så kommer de parametrar man bestämmer att bero på stora osäkerheter relaterade till halon. Det har visats att många av dessa osäkerheter kan elimineras genom att jämföra signaler i olika direkt detektionsexperiment i vad som kallas halo-oberoende metoder. Dessa metoder kan också användas för att förutsäga den neutrinosignal som ges upphov till från mörk materia annihilation i solen vilket kan användas för att vidare begränsa mörk materias egenskaper om en signal uppmäts i ett direkt detektionsexperiment. Detta ramverk vidareutvecklas här till att inkludera inelastisk mörk materia tillsammans med en diskussion kring den information om mörk materia som finns i signalen.

När solen fångar in mörk materia så måste termaliseringprocessen ske i vilken mörk materia efter infångning tappar sin kvarvarande kinetiska energi och sjunker in i solens kärna. Avdunstning på grund av kollisioner med högenergetiska solpartiklar kan också ske. För inelastisk mörk materia är det väntat att termaliseringsprocessen avslutas i förtid vilket har effekter på den neutrinosignal som väntas

av dess annihilation. Avdunstning kan också påverkas avsevärt vid spridning från det tyngre till det lättare tillståndet. Här diskuteras termaliseringsprocessen och resultat från numeriska simuleringar presenteras som visar till vilken grad mörk materia termaliserar och om avdunstning måste tas hänsyn till.

Ett antal problem har stötts på i mörk materia halos på mindre skalor som när dessa jämförs med resultatet från stora simuleringar. Mörk materia som växelverkar starkt med sig själv har föreslagits som lösning. Det finns dock ett antal problem associerade med dessa modeller som utesluter dessa av andra anledning. En modell för intelastisk mörk materia som växelverkar via en lätt kraftbärare analyseras här och visas möjligen lindra några av de problem som associeras med denna typ av modell.

key words: mörk materia, självväxelverkan, solinfångning, helioseismologi, inelastisk mörk materia, direkt detektion, indirekt detektion, termalisering.

Preface

This thesis is the result of my research at the Department of Theoretical Physics (now Department of Physics) from December 2014 to May 2019. The first part of the thesis presents the observational evidence for dark matter. It discusses the problems of the standard model and the motivated dark matter particles that can appear in its solutions. It describes how dark matter interactions are modelled and the treatment of non-relativistic scattering, which is highly relevant for solutions to the small scale structure problems. The early Universe, how dark matter halos form and what properties they have is also covered. Finally, means of searching for dark matter is presented. The second part contains the four papers that my research has resulted in.

List of papers

The scientific papers included in this thesis are:

1. Paper [1] (I)
   M. Blennow and *S. Clementz*
   Asymmetric capture of Dirac dark matter by the Sun
   JCAP **1508**, 036 (2015)
   arXiv:1504.05813

2. Paper [2] (II)
   M. Blennow, *S. Clementz* and J. Herrero-Garcia
   Pinning down inelastic dark matter in the Sun and in direct detection
   JCAP **1604**, 004 (2016)
   arXiv:1512.03317

3. Paper [3] (III)
   M. Blennow, *S. Clementz* and J. Herrero-Garcia
   Self-interacting inelastic dark matter: A viable solution to the small scale structure problems
   JCAP **1703**, 048 (2016)
   arXiv:1612.06681

4. Paper [4] (IV)
   M. Blennow, *S. Clementz* and J. Herrero-Garcia
   The distribution of inelastic dark matter in the Sun
   Eur. Phys. J. C78 (2018) 386
   arXiv:1802.06880

The thesis author's contribution to the papers

I participated in the scientific work as well as in the writing of all papers included in this thesis. I am also the corresponding author for all four papers.

1. I performed all numerical computations, constructed all figures except fig. 1 and wrote large parts of the paper.

2. I performed all numerical computations, constructed all figures and wrote large parts of the paper.

3. I developed the mathematical tools to find a stable numerical solution to calculate the scattering cross sections, performed all numerical computations except those of sec. 2.1, constructed all figures except fig. 1 and wrote large parts of the paper.

4. I developed many of the mathematical tools to perform the analysis, wrote all code, performed all simulations, produced all figures, and wrote large parts of the paper.

Acknowledgements

First and foremost, I want to thank my supervisor Dr. Mattias Blennow for a great number of things, not least for taking me on as a PhD student. I am very happy to have been encouraged to seek my own research interests, to have been given the opportunity to read most of his book before it was published, and for the collaboration that led to the papers of part II of the thesis. I have greatly enjoyed all the teaching where we have both been involved, I have learnt a lot! I would also like to thank Prof. Tommy Ohlsson who has been my co-supervisor and the Göran Gustafsson stiftelse for providing the financial means that allowed me to pursue a PhD in the first place.

There have been a number of people with whom I have shared office that I am glad to have been working next to. Of course, this goes for all past and present group members that I would like to thank especially for the journal clubs where many interesting discussions have taken place. I am also glad to have been placed in the office of the theoretical physics corridor where everyone has contributed to provide a great atmosphere.

I want to thank all the students who have attended my classes. I have enjoyed the teaching, probably more than I should have, and I am very glad to know that my efforts have been appreciated by some.

Finally, I want to thank my family for everything that they have ever done for me.

Contents

To my family

Part I

Introduction and background material

Chapter 1

Introduction

One of the most pressing issues of cosmology and particle physics today is the existence of dark matter (DM). In 1933, Fritz Zwicky made observations of the Coma cluster and found that the large velocity dispersion of individual galaxies required the presence of a significant amount of invisible matter in order to generate gravitational forces that were strong enough to keep the cluster together [5]. He called the invisible matter "dunkle materie" and thus coined the term DM. However, it took several decades for the scientific community to take his observations into account as being seriously problematic, when DM was observed in other types of astrophysical systems with newly developed observational techniques. There is now a wealth of data in support of the existence of DM [6].

In order to understand current efforts to explain DM, it is necessary to look at the current framework that describes the fundamental behaviour of Nature. The efforts to understand Nature at its fundamental level has culminated in two extremely successful, yet incompatible, theories. On one hand, quantum field theory (QFT) describes interactions between particles at the smallest scales imaginable and has led to the standard model of particle physics (SM). On the other hand, the theory of general relativity (GR) appears to accurately describe gravitational interactions between objects at the largest of scales.

The SM describes many phenomena to an extreme accuracy while suffering from a number of theoretical and phenomenological shortcomings. The most striking phenomenological problem is the observation of neutrino oscillations [7], which require neutrinos to have masses whereas the SM postulates them to be massless. Among many problems on the theoretical side, the strong CP problem states that the strong force should be CP violating with a strength parametrized by a number that would naturally be expected to be of the order 1, but is constrained to be less than a billionth of this value [8]. Since this parameter is free to take on whatever value Nature assigns it, the strong CP problem is not technically a problem of inconsistency, but rather a problem of naturalness.

Unlike the SM, GR appears to accommodate all observations made of gravitational interactions, including weak gravitational effects, such as the geodetic and frame-dragging effects as measured by gravity probe B [9], and strong gravitational effects, such as gravitational lensing [10], the shape of gravitational waves created by both colliding black holes [11] and neutron stars [12], and finally by direct observation of the accretion disk around a black hole [13]

Given the success of GR and the shortcomings of the SM, it is not difficult to motivate extensions of the SM that contain additional particles that successfully explain DM while simultaneously solving problems of the SM. It is thus not at all surprising that a lot of effort in explaining DM has been based around postulating new particles and the development of a number of experiments that can be used to test the most well-motivated scenarios.

This thesis deals with observational aspects of particle DM. Two ways of searching for particle DM is through direct detection (DD) and indirect detection (ID). The idea with DD is to search for the collisions that may occur between DM particles and atoms inside the experiment while ID is based around searching for the annihilation or decay products of DM particles, for example in the galactic center or inside the Sun. Theories of strongly self-interacting DM that are proposed to solve problems in small scale structure problems will also be discussed.

1.1 Outline

This thesis is organized as follows: In chapter 2, the observational evidence for the existence of DM is presented. Chapter 3 contains a short description the SM, its problems and solutions that motivate the existence of DM particles. There is also an in-depth discussion regarding DM interactions with SM particles and itself, and a simple inelastic DM model is presented. Chapter 4 discusses the thermodynamics of the early Universe, leading to the Boltzmann equations that govern the abundance of DM. Chapter 5 contains a summary of what is known about dark matter halos, such as its phase-space distribution. It also discusses the small scale structure problems and their possible solutions. In chapter 6, DD is reviewed with a discussion of how to generalize the framework to inelastic DM. Halo-independent methods is also discussed. Chapter 7 briefly reviews indirect detection in general before turning to an overview of the effects of DM in the Sun with a self-contained discussion of solar capture. Thermalization of inelastic DM is also covered. Chapter 8 concludes part I of the thesis and briefly introduces the four papers and their scientific contexts.

Chapter 2

Observational evidence for dark matter

The evidence in support for the existence of DM has been accumulated over a long time in a great number of observations [6, 14, 15]. A historical account of how DM emerged as one of the biggest mysteries of nature is nicely described in Ref. [6]. As will be described here, the evidence for DM comes from four different kinds of observations; galaxy clusters, galactic rotation curves, gravitational lensing, and the cosmic microwave background, and its history spans almost a century.

2.1 The existence of galaxy clusters

The first evidence for DM came from the observations of the Coma cluster performed by Fritz Zwicky in 1933 [5]. What he realized was that the velocity dispersion of galaxies in the cluster was much greater than the gravitational force of the luminous matter would allow. The estimate Zwicky performed is simple and relies on the virial theorem, which states that the time averaged total kinetic energy of a system of particles interacting via a potential $V(r) = r^n$ and the time averaged total potential energy are related by

$$\langle T \rangle = \frac{n}{2} \langle V \rangle \,. \tag{2.1}$$

Dealing with a gravitational potential dictates that $n = -1$. The average kinetic energy per object in the system can be approximated by $T \sim M\overline{v^2}/2$ where $\overline{v^2}$ is the averaged squared velocity of the objects and M is the mass of the object in question. The potential energy is approximately given by $V \sim -GM_{\rm tot}M/R$ where $M_{\rm tot}$ is the total mass of the cluster and R is a radius that is representative for the

distance between two galaxies within the cluster. Summing over all galaxies within the cluster and plugging into the virial theorem yields

$$M_{\rm tot}\overline{v^2} = \frac{GM_{\rm tot}^2}{R}\,. \tag{2.2}$$

Zwicky was able to estimate these parameters from his observations and found that the mass of the Coma cluster had to be several hundred times larger than the mass of all luminous matter in it. In fact, these large velocities implied that the galaxies of the Coma cluster should not even be gravitationally bound in the first place, but that the lifetime of the Coma cluster should be much shorter than the age of the Universe. It would thus be remarkable that it existed in the first place. The same observation was performed of the Virgo cluster a few years later and showed a similar mass discrepancy [16]. Unfortunately, the results were widely regarded as due to erroneous measurements and that these systems were not understood well enough to draw the attention of the scientific community.

2.2 Flat rotation curves

Thirty years after Zwicky's discovery, radio telescopes had been developed and were used to accurately measure the rotation curves of galaxies. To estimate the mass of a galaxy using rotation curves, it can be assumed that the visible mass of galaxies is mainly concentrated to the core with a smaller density of stars in the outer regions. This implies that the enclosed mass of a sphere at radii beyond the core should be relatively constant. The rotational velocity in the less dense outer regions of galaxies is then approximately given by the expression

$$v(r) \sim \sqrt{GM(r)/r}\,, \tag{2.3}$$

where G is the gravitational constant and $M(r)$ is the mass enclosed inside a sphere of radius r. If $M(r)$ is constant, this tells us that the velocity of stars should decrease as $r^{-1/2}$ in the regions where r is so large that most of the galaxy's mass is contained within. In order for rotation curves to be flat, the mass in the outer regions must grow approximately linearly, i.e.,

$$M(r) \approx M_0 r\,. \tag{2.4}$$

In 1970, two famous studies were published that were important in this context. Firstly, it was argued in the appendix of Ref. [17] that if the observations were correct, at least half of the mass in the NGC 300 and M33 galaxies is in the form of invisible matter. Secondly, the rotation curve of the Andromeda galaxy was measured and presented in Ref. [18]. It clearly shows a flat rotation curve, albeit without mention of its implication for the mass distribution within the galaxy. In the next few years, a number of studies appeared that confirmed the observations of flat rotation curves, ending with two publications stating that the mass of galaxies had thus far been seriously underestimated [19, 20].

2.3 Gravitational lensing

Gravitational lensing is the name of a phenomenon where a light ray that travels past a very massive body gets deflected. In fact, and somewhat counter-intuitively, even Newtonian mechanics predict the phenomenon even though gravity acts on massive objects and photons are massless. General relativity explains the effect as light travelling in straight lines in a curved spacetime and the effects predicted from general relativity are stronger than those of Newtonian mechanics. Depending on the gravitating body and the source of the light ray, strong, weak, and microlensing can take place.

The strong gravitational lensing effects can be very dramatic and occur for example when light is bent around very compact objects [21]. In this case, one can see several images of the same object at different sides around the gravitating body. One can also see significant distortions of the source or even so-called Einstein rings where the lensed object is located behind the lens and is distorted into an entire ring around it.

The effects of weak lensing are much more subtle, but can be used to determine the mass distribution of large objects such as galaxy clusters [22, 23]. Behind such a structure, there will be a very large number of galaxies. As the light from these galaxies pass through the lens, the images of them that can be seen will be slightly distorted and magnified. Individually, nothing can be said about the matter distribution in the lens from the single lensed galaxy as it is almost impossible to say exactly at which angle it is viewed at and at what distance it is observed. However, the statistical properties of the distribution of galaxies is known and if a large number of galaxies are lensed, their collective lensing will average out the noise from each individual galaxy, leaving behind the lensing effect.

Currently, a very strong piece of evidence for DM comes from a weak lensing analysis. The galaxy cluster 1E0657-558, more famously known as the "Bullet Cluster", is a system consisting of two galaxy clusters that have undergone collision. Out of the total mass of an average galaxy cluster, about one percent will be in the form of galaxies while about $5 - 15$ percent will be in the form of interstellar gas [24–26]. In the case of the Bullet Cluster, the interstellar hydrogen slowed down due to the friction created in collisions while the collisionless galaxies did not experience any slowing effects. Therefore, the expectation is that the overall mass peak would coincide with the interstellar gas of the clusters . This was found not to be the case but instead the mass peaks overlapped nicely with each set of galaxies from the original clusters [27]. This observation would have been impossible to explain without the existence of a very large fraction of unseen mass that appears to be collisionless.

Gravitational microlensing is similar to the strong lensing case although the effect is much weaker [28, 29]. When a massive object passes in front of a star, the light is bent around it. This leads to a focusing effect such that the star appears brighter.

An early hypothesis to explain the mass discrepancies as indicated by the flatness and galaxy cluster problems was that there existed a large population of MAssive Compact Halo Objects, or MACHOs. The MACHO population was postulated to consist of, for example, brown dwarfs, old white dwarves and neutron stars that had cooled to the point of undetectability, and stellar mass black holes. It was shown in the EROS-2 survey, which was a gravitational microlensing survey, that a population of MACHOs is not sufficient to explain the missing mass of the Milky Way [30]. This was done by monitoring some 33 million stars to look for the enhanced brightness that occur when a MACHO passes in front of them. The results of the survey was that MACHOs in the mass range $0.6 \cdot 10^{-7} M_\odot < M < 15 M_\odot$ were ruled out as the source for the total DM density. This was later confirmed in a larger mass range by another microlensing survey [31]. Gravitational microlensing has therefore helped build a case for most of the DM being non-baryonic.

2.4 Cosmic microwave background

Possibly the best evidence for non-baryonic DM comes from observations of the cosmic microwave background (CMB). When the Universe began, it was much more cramped than it is today. At the earliest times, the temperature of the plasma was so large that particles existed in chemical and thermal equilibrium. As the Universe expanded, the wavelengths of photons would decrease, and thus so would their energies. At some time, the average photon energy became so small that protons could bind electrons without photons having enough energy to scatter against the resulting hydrogen and break the bond. When this occurred, the Universe became electrically neutral and photons began to free stream. These photons can be detected in any direction of the sky and they form the CMB.

Two cosmological models were primarily discussed before the CMB was measured. The first was the Big Bang hypothesis, in which the Universe was born from a hot primordial plasma, and the second was that of an eternal static universe. Einstein himself was a proponent of the static universe theory and even introduced the cosmological constant to explain why the Universe would be static [32]. The static eternal universe does not make any prediction of a CMB while it is required in the Big Bang hypothesis as a remnant of an early hot period. Its existence was predicted and its temperature estimated to be roughly 5 K today in a discussion regarding the production of heavier elements during this time [33]. The detection of the CMB tipped the scale heavily in favour of the Big Bang theory.

The CMB has been measured very accurately by a number of experiments such as the space based observatories COBE [34], WMAP [35], and Planck [36]. Just as expected, it follows a near perfect black body profile and its temperature has been measured to roughly 2.726 K.

Another prediction is that the CMB temperature should fluctuate at the level of a few tens of μK [37], which is precisely what was observed by Planck etc. These fluctuations have turned out to be critical to our cosmological model as their

precise measurement in combination with the Big Bang hypothesis allows for the determination of the energy content of the Universe. The observation of these fluctuations was probably the most important result of the COBE experiment [38] and strongly motivated the launches of WMAP and Planck to measure the CMB to an extreme accuracy.

The CMB is often analyzed by performing a spherical harmonic expansion of the temperature fluctuations, which are then characterized by a number C_l. The coefficients of the harmonics associated with smaller l correspond to very large scale features of the CMB while larger values of l correspond to features at small scales. These corresponding scales are distinctly different in regards to which type of physics drive their temperature fluctuations.

The large scale features are due to overall denser or sparser abundances of matter. When photons are released in the pit of a gravitational well, they will redshift and thus have less energy when detected. Photons released in underdense regions will appear hotter than average as they suffer less from the redshift. Therefore, regions of higher temperature in the CMB correspond to regions with lower density than the regions that appear colder.

The small scale fluctuations are driven by baryon acoustic oscillations, which are due to interactions between the charged baryons. Before the CMB was released, regions with deeper gravitational pits would attract more mass. Since the baryons interacted, pressure would build up inside gravitational wells as matter collapsed into them. The pressure would eventually be large enough for the baryons to begin expanding outwards. Once pressure was relieved, baryons could begin flowing back into the pit. The cycle could occur once or several times before freezing out as the overall temperature fell, which induces observable fluctuations in the CMB.

A very important consequence of the arguments above is that DM cannot be baryonic and had to be cold (non-relativistic) at the time of recombination. Baryonic DM would suffer from pressure, which would prevent it from forming gravitational wells. If it was relativistic, it could not collapse into gravitationally bound objects in the first place.

The CMB also presents to us an excellent tool to determine cosmological parameters such as the density of baryons and dark matter in particular DM models. Currently, the prevailing cosmological model is called ΛCDM and it will be discussed in Chapter 4. Within this framework, one can predict the anisotropies of the CMB from the input of a number of parameters. By comparing simulations to the measurements of the CMB, one can determine which set of parameters fits the data best. This was most recently done with the Planck telescope data, which informs us that only about 5 % of the energy in the Universe is due to baryons while 25 % is made up of DM, the rest being in the form of dark energy [36].

Chapter 3

Particle dark matter

From the discussion of the observational evidence for DM in Chapter 2, it is clear that all evidence is gravitational in nature, which does not necessarily imply that DM is a particle. To find motivations for particle DM, one does not need to look further than the flaws of the SM. As will be discussed here, there are several reasons as to why the SM is not the final theory of particle physics. Various ideas to solve these problems introduce particles that may well fulfil the requirements necessary of a particle to make up the missing mass. Having established that it is not unlikely that DM is particulate in nature, it is interesting to look at a few plausible ways of generating interactions between DM and SM particles that allow for its detection. Next, a particular model of DM that three of the papers of this thesis are based around, called inelastic dark matter, is presented. Depending on the context, it is convenient to use either quantum mechanics or QFT to calculate precisely with what strength interactions take place. Thus, the quantum mechanical framework of partial waves is described, which can be used to calculate scattering cross sections in the presence of strong potentials that deform wavefunctions to the point where the Born approximation is no longer applicable. The chapter ends with a discussion on the differential cross section that is widely used in direct detection experiments.

3.1 The standard model of particle physics

The SM provides a complete model of all the known particles that we consider elementary. Yet, it suffers from numerous shortcomings that motivate extensions that introduce particles in the theory that may be DM candidates. Particle DM can not only solve the problem of the missing mass in the Universe, but its existence may also be dictated by remedies to flaws in our description of the elementary particle physics as well.

The SM is a QFT in which the gauge group composition is $SU(3)\times SU(2)\times U(1)$. The $SU(2) \times U(1)$ combination is often referred to as the electroweak interaction

and represents a unification of the electromagnetic interaction with the seemingly unrelated phenomenon of nucleon decay, and was first speculated upon at a time when the Higgs mechanism was still unknown [39]. Shortly thereafter, the Higgs mechanism was first described [40–42], which was used to formulate the electroweak theory as it stands today [43, 44]. The $U(1)$ is the hypercharge group under which all fermions and the Higgs doublet H are charged. The left-handed fermion doublets, Q^i and L^i, and the Higgs doublet, which are arranged according to

$$Q^i = \begin{pmatrix} u_L^i \\ d_L^i \end{pmatrix}, \qquad L^i = \begin{pmatrix} \nu_L^i \\ e_L^i \end{pmatrix}, \qquad H = \frac{1}{\sqrt{2}} \begin{pmatrix} \phi^1 + i\phi^2 \\ \phi^3 + i\phi^4 \end{pmatrix}, \tag{3.1}$$

where i refers to the family (of which there are three), and the subscript L refers to the chirality, are $SU(2)$ doublets. Due to the Higgs mechanism, the $SU(2) \times U(1)$ gauge group is spontaneously broken into the $U(1)$ of quantum electrondynamics, which yields a massless photon and three very massive gauge bosons. Finally, each individual quark field is in the fundamental representation of the $SU(3)$ group, which introduces the concept of colour in the theory of quantum chromodynamics (QCD). The idea of this part of the SM began to take shape after an ever increasing number of particles were detected in bubble chamber experiments, which was explained by introducing the quarks that formed various combinations of bound states that were observed [45, 46].

A peculiar feature of QCD is that its coupling constant depends strongly on the energy scale at which the interaction is taking place. In the infrared regime, QCD is extremely strong, which forces quarks to form bound states that are singlets under $SU(3)$. These combinations include mesons consisting of $q\bar{q}$ and hadrons consisting of qqq or $\bar{q}\bar{q}\bar{q}$, where q denotes a quark and $\bar{q}$ an antiquark. There is no reason as to why larger systems such as $qq\bar{q}\bar{q}$ should not appear in Nature, but it is not until recently that evidence for such systems have appeared at accelerators, see e.g., Refs [47, 48]. On the other hand, QCD possesses asymptotic freedom [49, 50], which implies that perturbation theory can be used to calculate cross sections with quarks at high enough energy scales.

The full spectrum of particles in the SM was not known at the time when the electroweak and QCD theories were developed, which is interesting as the Higgs boson is the most recent elementary particle to be observed [51, 52], roughly 50 years after its prediction. The fermion sector of the SM consists of the three lepton families

$$\begin{pmatrix} \nu_e \\ e \end{pmatrix}, \quad \begin{pmatrix} \nu_\mu \\ \mu \end{pmatrix}, \quad \begin{pmatrix} \nu_\tau \\ \tau \end{pmatrix}, \tag{3.2}$$

and the three quark families

$$\begin{pmatrix} u \\ b \end{pmatrix}, \quad \begin{pmatrix} c \\ s \end{pmatrix}, \quad \begin{pmatrix} t \\ b \end{pmatrix}. \tag{3.3}$$

The particles in each family, going from the left, are heavier than those of the previous one, apart from the neutrinos, which are all massless in the SM by design

as there are no right-chiral neutrinos. In the vector boson sector, there are 8 massless gauge bosons called gluons in the QCD sector, four gauge bosons in the electroweak sector, which upon symmetry breaking become the photon, the Z^0, and the $W^{\pm}$. Finally, the only scalar in the theory is the Higgs boson.

3.1.1 Standard model problems and motivated dark matter candidates

Neutrino oscillations

As mentioned above, the SM neutrinos are massless. However, Neutrinos undergo neutrino oscillations [7], a process in which a neutrino that is created in the flavour eigenstate ν_α can be detected as a different flavour eigenstate ν_β. The explanation for this phenomena is that the flavour eigenstates are linear combinations of mass eigenstates whose phases evolve differently during propagation. That is, neutrinos must be massive for oscillations to occur, which is in direct conflict with the SM. This phenomenon has been observed in a multitude of experiments [53, 54] and so it appears that the neutrinos are massive.

At first glance, it might be tempting to consider the neutrinos as the DM since they interact only via the weak gauge bosons, implying weak interactions. However, the results published by the Planck experiment places a bound on the sum of neutrino masses at $\sum_\nu m_\nu < 0.23$ eV [36]. Therefore, neutrinos would be relativistic in the early Universe at the time when structure formation was taking place, but for this to occur, a non-relativistic DM species is required. It can thus be concluded that the neutrinos do not make up the bulk of DM although they do make up a fraction of it. The problem of neutrino oscillations can be avoided by adding right-handed neutrinos to the theory, which allows for the generation of neutrino masses via the Higgs mechanism. Furthermore, the right-handed neutrino is a singlet under the SM gauge groups and would therefore interact very weakly with the SM particles and is therefore to be considered a DM candidate [55].

Supersymmetry

Supersymmetry (SUSY) models are probably the most well-known and studied extensions of the SM. In SUSY models, each field in the SM is complemented by a SUSY field that differs by a half unit of spin [56].

One of the big problems of the SM that SUSY was shown to alleviate is the hierarchy problem. In principle, there is no reason for the Higgs boson to have a mass at the electroweak scale [56]. This stems from the fact that if there is new physics at some scale that is coupled to the Higgs, loop corrections to the Higgs mass should drive it up to this scale. As new physics is expected at the Planck scale, where gravitational effects become important, the Higgs should gain contributions that places its mass at the Planck scale. Therefore, a very precise cancellation must take place for no apparent reason. In SUSY theories, it just so happens that the

leading contribution to the Higgs mass from any particle at this scale is to a very good degree cancelled by the contribution from the SUSY partner.

Naively invoking SUSY, one should expect interactions to take place through which baryon and lepton numbers are not conserved. Since such effects have never been observed, a quantity called R-parity is introduced to prohibit interactions of this kind. Another consequence of R-parity being conserved is that the lightest SUSY particle is automatically stable and would thus constitute a DM candidate provided that it is electrically neutral. The SUSY framework contains several DM candidates, such as the neutralino [57] and the gravitino [58].

Strong CP problem

The full SM Lagrangian contains the term

$$\mathcal{L}_{\text{SM}} \supset \bar{\theta}\frac{\alpha_s}{8\pi}G^a_{\mu\nu}\tilde{G}^{a,\mu\nu}. \tag{3.4}$$

This is problematic due to the fact that it implies that QCD is strongly CP violating unless $\bar{\theta}$ is very small, for which there is no apparent reason [8]. A non-zero value for this parameter would induce a large electric dipole moment of the neutron, which is constrained to $\lesssim 10^{-26}\, e$ cm [59, 60], which translates into $\bar{\theta} \lesssim 10^{-10}$ [61].

The strong CP problem was shown to be solved if $\bar{\theta}$ is a dynamical field and the SM is invariant under a $U(1)_{PQ}$ symmetry [62]. When this new symmetry is broken, $\bar{\theta}$ can be reduced to an extremely small number. The cost of this procedure is the introduction of a new particle called the axion [63, 64]. The interactions of the axion are expected to be very weak and it has been shown that axions can be produced efficiently in the early Universe making it a possible DM candidate [65].

Baryon-antibaryon asymmetry

The SM offers no way to account for the baryon to antibaryon asymmetry. The famous Sakharov conditions [66] state that three conditions have to be fulfilled in order for a baryon asymmetry to develop from a state where there is matter and antimatter in equal abundances. These are, in order:

- Baryon number violating processes must take place.
- There must be C and CP violating processes.
- The processes that violate baryon number must take place outside of thermal equilibrium.

The SM has baryon number violating processes called sphalerons [67], the weak interaction is C and CP violating, and out of thermal equilibrium interactions take place during, for example, the electroweak phase transition, although it seems that these effects are not strong enough to produce the observed asymmetry of the Universe [68]. In asymmetric DM models, the baryon asymmetry can be explained by

having an asymmetry that develops due to interactions connecting the SM sector to the dark sector or that one sector develops an asymmetry that is then transferred to the other [69]. It is plausible that if such an asymmetry develops, the two sectors would have very similar number densities. Bearing in mind that the mass density of DM in the Universe is about 5 times that of the baryons [36], equal number densities leads immediately to the prediction that the DM mass satisfies $m_{\mathrm{DM}} \sim 5m_p$. Leptogenesis is an alternative scenario where the original asymmetry is generated in the lepton sector rather in the baryon sector [70].

3.2 Dark matter interactions

Any detection method for particle dark matter relies on its interactions with the SM particles and the detectability of a given model will therefore rely on the relevant interactions that appear in the Lagrangian. As DM that was produced in the early Universe must be non-relativistic today, the energy scale of these interactions is generally in the case of annihilating DM at, or in the case of DM scattering possibly well below, the DM mass. On the other hand, accelerators are also used in the search for DM, where energies can be much larger than the DM mass. Depending on the scenario, one can use more or less simple models to calculate cross sections.

3.2.1 Effective operators and simplified models

When studying DM in an astrophysical context, effective operators are very commonly considered. An effective operator arises when a heavy degree of freedom, living at the energy scale Λ, is integrated out. These types of models are generally non-renormalizable and cannot be included in a complete theory where renormalizability is a requirement. Depending on the the type of DM, such an effective operator could have the form

$$\mathcal{L}_{\mathrm{scalar,int}} = \frac{c}{\Lambda}\phi\phi\bar{\psi}\psi\,, \tag{3.5}$$

where ϕ is a scalar DM particle and ψ is a SM fermion. Similarily, a vector DM particle X^μ could interact through an effective operator of the type

$$\mathcal{L}_{\mathrm{vector,int}} = \frac{c}{\Lambda}X_\mu X^\mu\bar{\psi}\psi\,. \tag{3.6}$$

The energy scale Λ can be associated with the mass of whatever heavy degree of freedom appears in the full theory and propagates in the tree level diagram for the process. Therefore, the approximation would break down when the momentum transfer becomes of the same order of magnitude as Λ. The constant c is a numerical factor that includes the coupling constants in the Lagrangian terms that define the interaction between the DM and SM fermions with the propagating heavy particle.

The same type of operators can be written down for a fermionic DM species χ,

$$\mathcal{L}_{\text{fermion,int}} = \frac{c}{\Lambda^2}(\bar{\chi}\,\Gamma\,\chi)(\bar{f}\,\Gamma' f), \tag{3.7}$$

where $\Gamma, \Gamma' \in \{1, \gamma^5, \gamma^\mu, \gamma^\mu\gamma^5, \Sigma^{\mu\nu}\}$ in such a way that the full term is Lorentz-invariant.

Effective operators are generally suppressed by $\Lambda^{-(D-4)}$, where D denotes the dimensionality of the operator, so that the the first two examples which are inversely proportional to Λ are referred to as dimension five operators and the operator in Eq. (3.7) is a dimension six operator. A large number of various effective operators depending on the nature of the DM particle can be found in references such as Refs. [71, 72].

The main motivation for discussing effective operators is that they are simple to use when placing general bounds on scattering cross sections without the need to specify the full theory. Having a particular model at hand, one may also immediately write down cross sections in the low energy limit and compare with the results from effective operator studies.

However, the story at colliders is not as simple as there is a large amount of energy available in the scattering process. As a significant amount of energy is involved in these collisions, the effective theory may break down. This was studied in, e.g., Refs. [73, 74]. To avoid the problem of effective theories breaking down, simplified models have been proposed as an alternative [75]. Generally, these are models where DM interacts with the SM through defined mediators. Their use is mainly in the fact that observable channels in larger models can be compared to the simplified models, which may help when assessing the validity of the extended model.

3.2.2 Portals

A very simple way of modelling DM interactions and to explain why they are so weak is to assume that DM hides in a different sector and interacts with the SM only through portals that connects the dark and the SM sector.

The Higgs portal is one option that introduces very weak couplings between a DM species and the SM [76]. The full Lagrangian of a very simple theory involving a complex scalar φ, which is a singlet under the SM, can be written down as [77]

$$\mathcal{L} = \partial_\mu\varphi^\dagger\partial^\mu\varphi - m^2\varphi^\dagger\varphi + \epsilon|H|^2\varphi^\dagger\varphi\,. \tag{3.8}$$

The field φ will now interact with the SM fermions via the Higgs field H and it will be stable since the model has a global $U(1)$ symmetry. Given an appropriate mass range and value of the parameter ϵ, which sets the interaction strength, it can even be a DM candidate. The dark sector may also contain other DM candidates that would interact with the SM via the φ, and subsequently via the Higgs.

Two different approaches, in which the introduction of a vector boson is made, are those of kinetic mixing [78–80] and mass-mixing [81]. In the kinetic mixing

scenario, one introduces a new vector boson, such that before electroweak symmetry breaking, the relevant part of the Lagrangian under consideration is

$$\mathcal{L} = -\frac{1}{4}B_{\mu\nu}B^{\mu\nu} - \frac{1}{4}F'_{\mu\nu}F'^{\mu\nu} - \frac{\epsilon}{2}B_{\mu\nu}F'^{\,\mu\nu} + \frac{1}{2}m^2_{A'}A'_\mu A'^\mu \,. \tag{3.9}$$

In the above, $B^{\mu\nu}$ is the field strength tensor of the hypercharge field, while A'^μ is the dark photon field and $F'^{\mu\nu}$ is its field strength tensor. By making the shift $B_\mu \to B_\mu - \epsilon A'_\mu$, the Lagrangian reads

$$\mathcal{L} = -\frac{1}{4}B_{\mu\nu}B^{\mu\nu} - \frac{1+\epsilon^2}{4}F'_{\mu\nu}F'^{\mu\nu} + \frac{1}{2}m^2_{A'}A'_\mu A'^\mu \,. \tag{3.10}$$

At this point, the A' must be rescaled such that its field strength tensor is normalized at the cost of slightly changing its mass [82–84]. The interesting point to make here is that, due to the shift in the B_μ field, any SM particle that couples to hypercharge now also couples to the dark photon, albeit with a coupling that is suppressed by ϵ. In the limit where $m_{A'}$ is much smaller than the Z mass m_Z, the mixing of the dark photon with the Z behaves as $(m_{A'}/m_Z)^2$, which implies that the dark photon mixes predominately with the photon in this limit.

In the case of mass mixing, it is not the field strength tensor that mixes but rather the fields themselves, i.e.,

$$\mathcal{L} = -\frac{1}{4}Z_{\mu\nu}Z^{\mu\nu} - \frac{1}{4}F'_{\mu\nu}F'^{\mu\nu} - \frac{1}{2}m^2_Z Z_\mu Z^\mu - \frac{1}{2}m^2_{A'}A'_\mu A'^\mu - \delta m^2 A'_\mu Z^\mu \,. \tag{3.11}$$

A redefinition of fields is necessary to find the mass eigenstates and introduces couplings between the A' and SM fields that couple to the Z.

Finally, there is also the neutrino-portal which relies on the introduction of a right-handed neutrino that couples to the left-handed lepton doublet L and the Higgs doublet as [85]

$$\mathcal{L} = \lambda \bar{L} H N \,. \tag{3.12}$$

The DM enters the picture through a similar coupling to N. Interestingly, the introduction of the right-handed neutrino and this operator can give the left-handed neutrinos a very small mass when the Higgs takes a vacuum expectation value through what is called the seesaw mechanism [86–88].

3.3 Inelastic dark matter

Inelastic DM is a framework in which DM is modelled as at least two different states with masses m_1 and m_2 that satisfy

$$m_2 - m_1 = \delta, \qquad |\delta| \ll m_2,\, m_1. \tag{3.13}$$

That is, the heavier species is only slightly heavier than the lighter species.

There are many inelastic DM models of varying complexity [89–91], and it is instructive to cover at least a simple case of these types of models to motivate the naturalness. One of the simplest is that of a Dirac fermion whose left-handed and right-handed components somehow pick up a Majorana mass term. The Lagrangian under consideration is

$$\mathcal{L} = -\frac{1}{4}(F'_{\mu\nu})^2 - \frac{1}{2}m_{A'}A'_\mu A'^\mu + \bar{\psi}\left(i\gamma^\mu\partial_\mu - M\right)\psi - g\bar{\psi}\gamma^\mu\psi A'_\mu\,, \tag{3.14}$$

where ψ is the Dirac fermion, A' is a massive dark photon, M is the Dirac mass, and the last term is the interaction term between the DM and the dark photon. If one now adds a Majorana mass term to the Lagrangian, which for simplicity set to be identical for the left- and right-handed fields, and is required to satisfy $\delta \ll M$, the mass part of the Lagrangian is given by

$$\mathcal{L}_{\text{mass}} = -M\overline{\psi}\psi - \frac{\delta}{4}\left(\overline{\psi^c}\,\psi + \overline{\psi}\,\psi^c\right)\,. \tag{3.15}$$

At this point, it is convenient to define the two left-handed spinors η and ξ and write $\psi^T = (\eta^T \;\; i\xi^\dagger\sigma^2)$. This breaks the original kinetic term in the Lagrangian into

$$\mathcal{L}_{\text{kinetic}} = \bar{\psi}i\gamma^\mu\partial_\mu\psi = i\eta^\dagger\bar{\sigma}^\mu\partial_\mu\eta + i\xi^\dagger\bar{\sigma}^\mu\partial_\mu\xi\,, \tag{3.16}$$

where $\bar{\sigma} = (1, \boldsymbol{\sigma})$ and $\boldsymbol{\sigma}$ are the Pauli spin matrices. In matrix form, the mass term can be written as

$$\mathcal{L}_{\text{mass}} = -\frac{i}{2}\begin{pmatrix}\eta^T\sigma^2 & \xi^T\sigma^2\end{pmatrix}\begin{pmatrix}\frac{\delta}{2} & M\\ M & \frac{\delta}{2}\end{pmatrix}\begin{pmatrix}\eta\\ \xi\end{pmatrix} + \text{h.c.}\,, \tag{3.17}$$

where h.c. denotes the hermitian conjugate. In order to isolate the two Majorana fermions, the fields η and ξ can be redefined according to

$$\begin{pmatrix}\eta\\ \xi\end{pmatrix} = U\begin{pmatrix}\varphi_1\\ \varphi_2\end{pmatrix}\,, \qquad U = \frac{1}{\sqrt{2}}\begin{pmatrix}i & 1\\ -i & 1\end{pmatrix}\,. \tag{3.18}$$

The Lagrangian in terms of the new fields φ_1 and φ_2 reads

$$\mathcal{L}_{\text{kinetic}} + \mathcal{L}_{\text{mass}} = \sum_{i=1,2}\left[i\varphi_i^\dagger\bar{\sigma}^\mu\partial_\mu\varphi_i - \frac{i}{2}m_i(\varphi_i^T\sigma^2\varphi_i - \varphi_i^\dagger\sigma^2\varphi_i^*)\right]\,. \tag{3.19}$$

This is precisely the Lagrangian of two Majorana fields where $m_1 = M - \delta/2$ and $m_2 = M + \delta/2$. In four-component spinor notation, one can define $\chi_i^T = (\varphi_i^T \;\; i\varphi_i^\dagger\sigma^2)$ in which case the full Lagrangian is

$$\mathcal{L} = -\frac{1}{4}(F'_{\mu\nu})^2 - \frac{1}{2}m_{A'}A'_\mu A'^\mu + \sum_{i=1,2}\frac{1}{2}\overline{\chi}_i(i\gamma^\mu\partial_\mu - m_i)\chi_i + \mathcal{L}_{\text{int}} \tag{3.20}$$

with

$$\mathcal{L}_{\text{int}} = ig\overline{\chi}_2\gamma^\mu\chi_1 A'_\mu\,. \tag{3.21}$$

It is now clear why this model is called inelastic. The tree level and first order loop diagrams for a scattering process between an incoming χ_1 and a quark are shown in

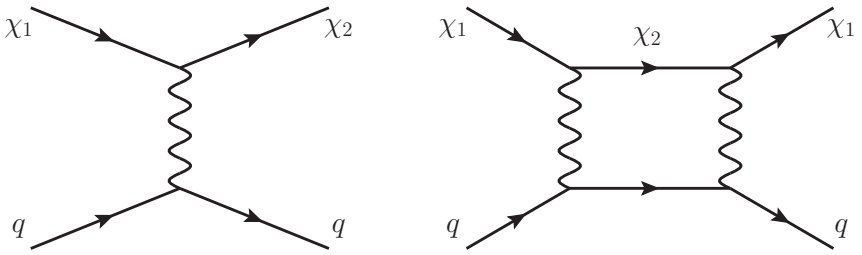

Figure 3.1. Lowest order Feynman diagrams for a simple inelastic DM model which scatters inelastically (left diagram) and elastically (right diagram) with a quark.

Fig. 3.1. The outgoing particle in the tree-level process is a χ_2. Thus, some of the kinetic energy in the center of momentum frame went into creating the additional mass of the χ_2 and so the total kinetic energy is not conserved. In this case, elastic scattering enters as a loop-level process that is significantly suppressed relative to the inelastic process. Now, this is a direct consequence of the assumption that the Majorana mass terms of the left- and right-handed components of the initial Dirac fermion were the same. Had they been different, one finds a term in the Lagrangian that gives elastic tree-level processes [90]. These are however suppressed by m_-/M where m_- is the difference between the left- and right-handed Majorana masses. Thus, inelastic scattering will be dominant also in this case.

It is also possible to design effective models of inelastic DM [92]. It is enough to start with the operator

$$L_{\text{int}} = \frac{c}{\Lambda^2} \left(\bar{\psi}\Gamma_{\text{DM}}\psi\right)\left(\bar{q}\Gamma_{\text{vis}}q\right) , \tag{3.22}$$

where ψ is the fermion field and Λ is some higher energy scale where heavy degrees of freedom were integrated out. One can then apply exactly the same procedure as above to split ψ into two Majorana fields.

3.4 Cross sections

3.4.1 Non-relativistic scattering theory

Non-relativistic scattering is important for dark matter in an astrophysical setting. It may here be more convenient to describe the scattering process in quantum mechanics using a classical potential rather than through the exchange of mediator particles in QFT. In this case, the wave function under consideration must satisfy the Schrödinger equation, which in the case of two scattering particles, one located at position $\boldsymbol{x}_1$ and the other at position $\boldsymbol{x}_2$, is given by

$$\left[-\frac{\nabla_1^2}{2m_1} - \frac{\nabla_2^2}{2m_2} + V(\boldsymbol{x}_1 - \boldsymbol{x}_2)\right]\Psi(\boldsymbol{x}_1, \boldsymbol{x}_2) = E\Psi(\boldsymbol{x}_1, \boldsymbol{x}_2). \tag{3.23}$$

In this expression, m_1 and m_2 are the particle masses, $V(\boldsymbol{x}_1 - \boldsymbol{x}_2)$ is the interaction potential between the two particles, and $E = (m_1 v_1^2 + m_2 v_2^2)/2$ is the total kinetic energy. Since only the relative motion of the particles matter, not the movement of the system as a whole, it is appropriate to change frames to the center of momentum frame by making the variable substitutions

$$\boldsymbol{x} = \boldsymbol{x}_1 - \boldsymbol{x}_2, \qquad \boldsymbol{y} = \frac{\mu}{m_2}\boldsymbol{x}_1 + \frac{\mu}{m_1}\boldsymbol{x}_2 \,. \tag{3.24}$$

In this set of coordinates,

$$E = \frac{1}{2}(m_1 + m_2)\dot{\boldsymbol{y}}^2 + \frac{1}{2}\mu\dot{\boldsymbol{x}}^2 = \frac{1}{2M}\boldsymbol{P}^2 + \frac{1}{2\mu}\boldsymbol{p}^2 \,. \tag{3.25}$$

Here, $\boldsymbol{P}$ is the momentum of the system as a whole, while $\boldsymbol{p}$ is the momentum of a particle in the center of momentum system. Since the translation of the system is trivial, it can be factored out with the substitution $\Psi(\boldsymbol{x}, \boldsymbol{y}) = \psi(\boldsymbol{x}) e^{-i\boldsymbol{P}\cdot\boldsymbol{y}}$, which leads to the differential equation

$$\left[-\frac{\nabla_x^2}{2\mu} + V(\boldsymbol{x})\right]\psi(\boldsymbol{x}) = \frac{p^2}{2\mu}\psi(\boldsymbol{x}) \,. \tag{3.26}$$

This is the fundamental equation that governs the scattering of two particles in quantum mechanics. The two-body scattering problem in quantum mechanics is equivalent to solving the single particle scattering against a fixed potential with a mass equal to the reduced mass of the two particles in the two-body scattering problem.

Discussing now the one-particle scattering process, the solution to the Schrödinger equation at large distances from the center of the potential is [93]

$$\psi(r \to \infty) = e^{i\boldsymbol{p}\cdot\boldsymbol{x}} + \frac{e^{ipr}}{r} f(\theta) \,. \tag{3.27}$$

The first term on the right-hand side is nothing but a propagating plane wave representing the incoming particle. The second term represents an outgoing particle wave travelling in a radial direction at an angle θ relative to $\boldsymbol{p}$. This term can thus be identified as the scattered particle and $f(\theta)$ is called the scattering amplitude, which relates to the differential cross section as

$$\frac{d\sigma}{d\Omega} = |f(\theta)|^2 \,. \tag{3.28}$$

It is easy to modify the scattering formalism to include the case where inelastic scattering between different states can occur, an example being atomic scattering where the atom enters an excited state in the scattering event at the cost of some initial kinetic energy, in which case the momentum of the outgoing wave function is different from that of the incoming particle. In the two state case, which is of

interest in the inelastic DM scenario, take an incoming particle of the lighter state to have momentum $\boldsymbol{p}$ and the ground state energy level of the system to $E = p^2/2\mu$. Infinitely far from the potential, the outgoing exited state particle will have the energy

$$\frac{p_{\chi^*}^2}{2\mu^2} = \frac{p^2}{2\mu} - 2\delta\,, \tag{3.29}$$

where terms suppressed by powers of δ/m_χ have been neglected. The factor 2 in front of the mass splitting is due to the outgoing state consisting of two particles of the excited kind. The scattering system is given by the two coupled equations

$$-\frac{\nabla^2}{2\mu}\psi_1(\boldsymbol{x}) + V_{1j}(\boldsymbol{x})\psi_j(\boldsymbol{x}) = \frac{p^2}{2\mu}\psi_1(\boldsymbol{x})\,, \tag{3.30}$$

$$-\frac{\nabla^2}{2\mu}\psi_2(\boldsymbol{x}) + V_{2j}(\boldsymbol{x})\psi_j(\boldsymbol{x}) = \left(\frac{p^2}{2\mu} - 2\delta\right)\psi_2(\boldsymbol{x})\,. \tag{3.31}$$

The Schrödinger equation for this coupled system can then be written

$$\left[-\frac{\nabla^2}{2\mu} + V(\boldsymbol{x})\right]\boldsymbol{\psi}(\boldsymbol{x}) = E\boldsymbol{\psi}(\boldsymbol{x})\,, \tag{3.32}$$

where $\boldsymbol{\psi}(\boldsymbol{x}) = (\psi_1(\boldsymbol{x})\ \psi_2(\boldsymbol{x}))^T$ has been promoted to a two component vector, $V(\boldsymbol{x})$ is a 2 by 2 matrix, and $E = p^2/2\mu$ is the energy. The mass splitting has been absorbed into the potential, which takes the form

$$V(\boldsymbol{x}) = \begin{pmatrix} V_{11}(\boldsymbol{x}) & V_{12}(\boldsymbol{x}) \\ V_{21}(\boldsymbol{x}) & V_{22}(\boldsymbol{x}) + 2\delta \end{pmatrix}. \tag{3.33}$$

The asymptotic form of the wave function for channel i, where $V(\boldsymbol{x})$ is negligible and j is the incoming state, looks similar to the single particle case,

$$\psi_i(r \to \infty) = \delta_{ij}e^{i\boldsymbol{p}_j\cdot\boldsymbol{x}} + \frac{1}{r}e^{ip_i r}f_i(\theta)\,. \tag{3.34}$$

The cross section is found by requiring that the flux that enters the scattering region through the area $d\sigma$ is equal to the particle flux that leaves the region through the area $r^2 d\Omega$.

$$|j_{\text{in}}|d\sigma = |j_{\text{out}}|r^2 d\Omega\,. \tag{3.35}$$

From the form of the wave function at large radii r, the relations

$$|j_{\text{in}}| = \frac{p_j}{m}\,, \qquad |j_{\text{out}}| = \frac{|f_i(\theta)|^2}{r^2}p_i \tag{3.36}$$

can be found. The form of the differential cross section becomes

$$\frac{d\sigma}{d\Omega} = \frac{p_i}{p_j}|f_i(\theta)|^2\,. \tag{3.37}$$

This expression verifies Eq. (3.28) in the case of elastic scattering where $p_i = p_j$.

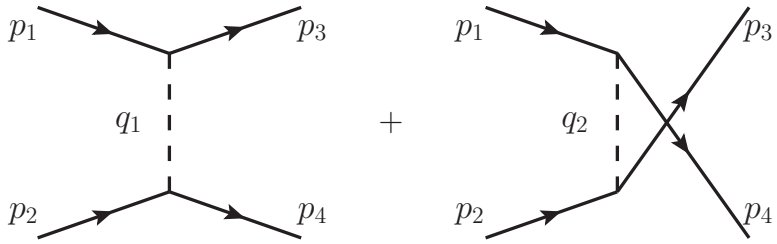

Figure 3.2. Tree level diagrams for scattering of two fermions via a scalar boson in the Yukawa theory. The left process indicates t-channel scattering while the right depicts u-channel scattering.

There is a caveat in the case where the scattering is taking place between two indistinguishable particles [93–96]. For example, if the two scattering particles are fermionic, the spatial wave function is required to be symmetric or anti-symmetric depending on whether the incoming particles form a singlet (symmetric) or a triplet (anti-symmetric) state. In this case, the amplitude is calculated according to

$$f_{\text{tot}}(\theta) = f(\theta) \pm f(\pi - \theta) \tag{3.38}$$

where + holds for the singlet and − holds for the triplet state. The cross section will then be found by taking the spin-average of the possible spin configurations.

3.4.2 The Born approximation

The Born approximation is valid in the case where the interaction potential is weak and that the scattering wave function deviates only very slightly from a plane wave inside the potential. This is the same assumption that goes into calculating matrix elements in perturbative QFT. Given that the same assumption is made in the two cases, it is interesting to compare quantum mechanical scattering to non-relativistic scattering taking place in QFT, as it gives an interesting connection between the potential in quantum mechanics and the Lagrangian density in QFT. The idea can be illustrated by considering scattering between two fermions ψ, as shown in the Feynman diagrams in Fig. 3.2.

The T-matrix element for scattering in quantum mechanics is defined as [93]

$$T_{\text{QM}} = -2\pi i \delta(E_f - E_i) T_{fi} \,. \tag{3.39}$$

In the Born approximation, the number T_{fi} is calculated as

$$T_{fi} = \langle \boldsymbol{k}_f | \, V \, | \boldsymbol{k}_i \rangle = \int d^3\boldsymbol{x} V(\boldsymbol{x}) e^{-i(\boldsymbol{k_i} - \boldsymbol{k_f})} = \tilde{V}(\boldsymbol{q}) \tag{3.40}$$

where $\boldsymbol{k}_i$ and $\boldsymbol{k}_f$ denote the momenta of incoming the incoming and outgoing particle respectively. The last identity defines the Fourier transform of the potential

in terms of the momentum transfer $\boldsymbol{q} = \boldsymbol{k}_f - \boldsymbol{k}_i$. The amplitude is then defined as

$$f(\theta) = -\frac{\mu}{2\pi} T_{fi} \,. \tag{3.41}$$

In QFT, the T-matrix element for scattering is defined as [97]

$$T_{\mathrm{QFT}} = (2\pi)^4 \delta^4(p_1 + p_2 - p_3 - p_4) i\mathcal{M}(p_1, p_2 \to p_3, p_4) \,, \tag{3.42}$$

where p_1, p_2, p_3, and p_4 are the four-momenta of incoming ($i = 1, 2$) and outgoing ($i = 3, 4$) particles. The last part, $\mathcal{M}$, is usually just called the matrix element. A couple of statements need to be made in order to relate $\mathcal{M}$ to the non-relativistic theory. Firstly, momentum conservation in the cross section is enforced by the integral of a δ function, which comes with a factor of $(2\pi)^{-3}$. Secondly, one-particle states in QFT are normalized as

$$|\boldsymbol{p}, s\rangle = \sqrt{2E_{\boldsymbol{p}}} a_{\boldsymbol{p}}^{s\,\dagger} |0\rangle \,. \tag{3.43}$$

The matrix element in the non-relativistic limit will therefore contain a factor $4m_1m_2$ relative to the QM system. By making the rearrangement

$$T_{\mathrm{QFT}} = (2\pi)^3 \delta^3(\boldsymbol{p}_1 + \boldsymbol{p}_2 - \boldsymbol{p}_3 - \boldsymbol{p}_4)(2\pi)\delta(E_f - E_i) i\mathcal{M}(p_1, p_2 \to p_3, p_4) \,, \tag{3.44}$$

and taking the considerations above into account, one can identify

$$\tilde{V}(\boldsymbol{q}) = -\mathcal{M}/4m_i m_j \,. \tag{3.45}$$

A careful derivation of this result can be found in Ref. [98].

As an example, in Yukawa theory, the Lagrangian contains the interaction term

$$\mathcal{L}_{\mathrm{int}} = -g\bar{\psi}\psi\phi \,. \tag{3.46}$$

where ψ is an interacting fermion and ϕ is a scalar mediator particle. The full matrix element for the scattering process $\psi\psi \to \psi\psi$ as shown in Fig. 3.2 is given by

$$i\mathcal{M} = \bar{u}^{k'}(p_3) u^k(p_1) \frac{i(-ig)^2}{q_1^2 - m_\phi^2} \bar{u}^{s'}(p_4) u^s(p_2) - \bar{u}^{s'}(p_4) u^k(p_1) \frac{i(-ig)^2}{q_2^2 - m_\phi^2} \bar{u}_4^{k'} u_2^s \,, \tag{3.47}$$

where m_ϕ is the mass of the scalar boson, k and s are the spins of incoming particles, and k' and s' are the spins of the outgoing particles. In the non-relativistic limit, the spinor products reduce to

$$\bar{u}^{k'}(p) u^k(p') = 2m\delta^{kk'} \,, \tag{3.48}$$

where $\delta^{kk'}$ is the Kronecker δ. The momentum transfers, evaluated in the center of momentum frame, become

$$q_1^2 = (p_1 - p_3)^2 \quad \longrightarrow \quad \boldsymbol{q}_1^2 = 2\boldsymbol{p}^2(1 - \cos(\theta)) \,, \tag{3.49}$$

$$q_2^2 = (p_1 - p_4)^2 \quad \longrightarrow \quad \boldsymbol{q}_2^2 = 2\boldsymbol{p}^2(1 - \cos(\pi - \theta)) \,. \tag{3.50}$$

The matrix element in the non-relativistic limit becomes

$$i\mathcal{M} = ig^2(2m)^2 \left[\frac{\delta^{ks}\delta^{k's'}}{\boldsymbol{q}_1^2 + m_\phi^2} - \frac{\delta^{ks'}\delta^{k's}}{\boldsymbol{q}_2^2 + m_\phi^2} \right] . \tag{3.51}$$

A first observation is that, if the particles are distinguishable, the u-channel diagram disappears immediately and only the first term in the above contributes to scattering. In this case, one can immediately make the identification

$$\tilde{V} = -\frac{g^2}{\boldsymbol{q}^2 + m_\phi^2} . \tag{3.52}$$

By taking the inverse of the Fourier transform one finds that the potential describing the scattering process in the quantum mechanical system is given by

$$V_{\text{yuk}} = -\frac{g^2}{4\pi r} e^{-m_\phi r} . \tag{3.53}$$

This attractive potential was introduced by Yukawa to explain the force binding protons and neutrons together in the atomic nucleus. Furthermore, since the potential cuts off at $r > 1/m_\phi$, which Yukawa knew to be of the order fm, he could estimate the mass of the exchanged particle, now known as the pion, to be roughly 200 times the electron mass [99].

Secondly, for indistinguishable particles, the momentum transfers in the t-channel and u-channel matches precisely the behaviour as required in Eq. (3.38). This is most easily observed for triplet state scattering, where all spins are aligned.

3.4.3 Partial wave decomposition

An alternative to the Born approximation when calculating $f(\theta)$ is to use partial wave decomposition. As will be discussed in Sec. 5.3.2, this method is of interest in DM models where self-interactions are strong enough for non-perturbative effects to become relevant and the Born approximation breaks down. In this case, the amplitude is calculated by making an expansion of the scattering wave function in terms of spherical harmonics [93]. By aligning the coordinate system such that $\boldsymbol{p} = p\hat{z}$, the wave function becomes

$$\psi(r, \theta) = \sum_l (2l + 1) P_l(\cos\theta) R_l(r) , \tag{3.54}$$

where $P_l(x)$ are Legendre polynomials. The scattering wave function of Eq. (3.27) is now given by

$$\psi(r, \theta) = \sum_l (2l + 1) P_l(\cos\theta) \left(\frac{e^{ikr} - (-1)^l e^{-ikr}}{2ikr} + \frac{f_l}{r} e^{ikr} \right) . \tag{3.55}$$

When substituting $\psi(r,\theta)$ into the Schrödinger equation, the linear independence of the Legendre polynomials implies that each term in the series must satisfy

$$\left[\frac{1}{r^2}\frac{\partial}{\partial r}\left(r^2\frac{\partial}{\partial r}\right) - \frac{l(l+1)}{r^2} + k^2 - 2\mu V(r)\right] R_l(r) = 0\,. \tag{3.56}$$

The partial wave amplitudes f_l can then be calculated by solving the Schrödinger equation numerically and then map the solutions for each l onto a solution of the form of Eq. (3.55). This can be done by writing down the solution as

$$\psi(r,\theta) = Ae^{ikr} + Be^{-ikr} \tag{3.57}$$

and determine the coefficients A and B. Once all partial waves have been computed up so some $l = l_{\max}$, beyond which all remaining contributions are negligible, the final solution will be given by

$$f(\theta) = \sum_{l=0}^{l_{\max}} (2l+1) P_l(\cos\theta) f_l\,. \tag{3.58}$$

From a classical standpoint, such an $l_{\max}$ is expected. For a fixed speed, the distance between particles increases as the angular momentum increases, which results in less of an impact from the potential on the wave function and hence in a smaller contribution to the scattering process. This is reflected by the $l(l+1)/r^2$ term in Eq. (3.56) outgrowing the potential at large l for all r.

Generalizing this procedure to the case with several scattering channels is straight forward. For example, the scattering wave function in channel i at large r will be given by

$$\psi_i(r,\theta) = \sum_l (2l+1) P_l(\cos\theta) \left[\delta_{ij}\frac{e^{ip_j r} - (-1)^l e^{-ip_j r}}{2ip_j r} + \frac{f_{i,l}}{r} e^{ip_i r}\right], \tag{3.59}$$

where j is the state to which the scattering particles belongs. In some cases, there are kinematically forbidden channels that are characterized by negative energies and can therefore not appear outside of the potential region. Forbidden channels are characterized by outgoing wavefunctions that decrease exponentially, since the associated wave number p_i for any such channel is complex. The problem is that, when solving the Schrödinger equation numerically, the solution contains both the exponentially increasing and decreasing solutions. When the system is mapped onto an exponential form, the exponentially increasing part must be cancelled by the appropriate choice of constants. This is problematic as the exponentially decaying solution is absolutely negligible in comparison to the exponentially increasing one, leading to a system that appears linearly dependent and making it impossible to extract a cross section. One of the main results of paper III was to circumvent this problem for the case of a two-component inelastic DM scenario by rewriting the wave function in terms of r-dependent coefficients and spherical Bessel and Hankel functions of the first kind. This leads to a reformulation of the Schrödinger equation that governs the behaviour of the coefficients, which is much more stable.

3.4.4 Dark matter-nucleus scattering

The cross section of DM scattering against nuclei will be a very important quantity later in this thesis. As the nucleus is an object composed of protons and neutrons, which are in turn composed of quarks and gluons, calculating the cross section for DM-nucleus scattering is not a simple matter. As will be seen, a DD experiment measures the number of scattering events as a function of atomic recoil energies. The differential cross section under consideration is therefore [57]

$$\frac{d\sigma}{dE_R} = \frac{m_N}{2\mu^2 v^2}\sigma_0 |F(E_R)|^2 \,, \tag{3.60}$$

where m_N is the mass of the nucleus, μ is the reduced mass of the nucleus-DM system, v is the relative velocity between the two colliding particles, and σ_0 is the zero-momentum transfer cross section. The recoil energy picked up by the nucleus is given by $E_R = q^2/2m_N$, where q is the momentum transfer. When the wavelength h/q becomes smaller than the nuclear radius, the structure of the nucleus becomes resolved. This is usually the case considered in DD experiments and so the nuclear structure is very important to understand. This information is encoded in the form factor $F(q)$ in the cross section. The overall factor is related to the fact that setting $|F(E_R)|$ to unity and integrating over all allowed recoil energies, σ_0 should be recovered, i.e.,

$$\int_0^{2\mu^2 v^2/m_N} \frac{d\sigma}{dE_R}\Big|_{E_R=0} dE_R = \sigma_0 \,. \tag{3.61}$$

By solving the non-relativistic energy and momentum conservation equations, it is found that the upper limit of the integral corresponds to $E_{\max} = 2\mu^2 v^2/m_N$, which is the largest possible recoil energy.

Scattering between a DM particle and a nucleus can be spin-dependent or spin-independent. Examples of effective operators that give rise to scattering of these two types are

$$\mathcal{L}_{SI} = \frac{c_q}{\Lambda^2}\bar{\chi}\gamma^\mu\chi\bar{q}\gamma_\mu q \quad \text{and} \quad \mathcal{L}_{SD} = \frac{d_q}{\Lambda^2}\bar{\chi}\gamma^\mu\gamma^5\chi\,\bar{q}\gamma_\mu\gamma^5 q \,, \tag{3.62}$$

where the former is an example of a spin-independent operator, while the latter is an example of a spin-dependent operator.

To understand the form factor that appears when calculating the cross section, it is instructive to calculate the matrix element, which is given by

$$\mathcal{M} \sim \langle \chi_f, N | \, \mathcal{L}_{\text{int}} \, | \chi_i, N \rangle \,. \tag{3.63}$$

where $\mathcal{L}_{\text{int}}$ is an interaction Lagrangian. The state $|N\rangle$ is a complicated multi-body object that describes the overall state of the bound protons and neutrons.

Focusing on the case where scattering is spin-independent, it is possible to write down an expression for the matrix element at zero momentum transfer as

$$i\mathcal{M}(\boldsymbol{q}=0) = 4m_N m_\chi \left[Zf_p + (A-Z)f_n\right] , \tag{3.64}$$

where Z and A are the number of protons and number of nucleons, respectively. The coupling constants to protons f_p and neutrons f_n depend on the operator. For example, the spin-independent vector mediated operator in Eq. (3.62) yields $f_p = (2c_u + c_d)/\Lambda^2$ and $f_n = (c_u + 2c_d)/\Lambda^2$ [100]. In the scalar mediator case, sea quarks and gluons have to be taken into account, resulting in very complex expressions for the proton and neutron couplings, see e.g., Ref [101].

The form factor is now most easily understood by considering the scattering process in the formalism of quantum mechanics. The nucleus consists of Z protons and $A - Z$ neutrons, which are distributed with probability densities $\rho_p(\boldsymbol{x})$ and $\rho_n(\boldsymbol{x})$. Furthermore, let the coupling constants be given by f_p and f_n, respectively. The full potential for the nucleus can then be written as

$$V(\boldsymbol{x}) = \sum_p f_p \rho_p(\boldsymbol{x}) + \sum_n f_n \rho_n(\boldsymbol{x}) . \tag{3.65}$$

According to the Born approximation in Eq. (3.40), the amplitude for a DM particle having incoming and outgoing momenta $\boldsymbol{p}_i$ and $\boldsymbol{p}_f$, respectively, to scatter against the nucleus is given by

$$f(\theta) = -\frac{\mu}{2\pi}\int d^3\boldsymbol{x} e^{-i\boldsymbol{x}\cdot\boldsymbol{q}}\, V(\boldsymbol{x}) = -\frac{\mu_{\chi N}}{2\pi}\tilde{V}(\boldsymbol{q}) . \tag{3.66}$$

One can immediately observe that, for zero-momentum transfer,

$$T_{fi}(q=0) = \int d^3\boldsymbol{x}\left(\sum_p f_p\rho_p(\boldsymbol{x}) + \sum_n f_n\rho_n(\boldsymbol{x})\right) = Zf_p + (A-Z)f_n , \tag{3.67}$$

which, given Eq. (3.45), confirms the choice of potential strengths. The last identity holds as the probability densities are normalized. The zero-momentum transfer cross section becomes

$$\sigma_0 = \frac{\mu^2}{\pi}\left[Zf_p + (A-Z)f_n\right]^2 = \sigma_{\chi p}\frac{\mu^2}{\mu_{\chi p}^2}\left[Z + (A-Z)\kappa\right]^2 . \tag{3.68}$$

The last step defines $\sigma_{\chi p}$ as the DM-proton cross section for which $\mu = \mu_{\chi p}$, $Z = 1$, and $A = 1$. The cross section is said to be isospin violating when $\kappa = f_n/f_p \neq 1$.

For non-zero momentum transfer, the matrix element becomes

$$T_{fi} = Zf_pF_p(q) + (A-Z)f_nF_n(q) , \tag{3.69}$$

where $F_p(q)$ and $F_n(q)$ are the Fourier transformed proton and neutron densities and it has been assumed that all nucleons of the same species are described by the

same probability distribution. It is very often assumed that $F_p(q) = F_n(q)$. In fact, calculating the differential cross section $d\sigma/d\Omega$ with the matrix element above and using that $\boldsymbol{q}^2 = 2\boldsymbol{p}_1^2(1-\cos(\theta))$, Eq. (3.60) can be derived explicitly.

There are a couple of form factors that are commonly used in the literature for the spin-independent part of the cross section. The simplest form factor is that of the exponential [102, 103]

$$F(E_R) = e^{-E_R/2E_0}\,, \tag{3.70}$$

where $E_0 = 3/2m_N R^2$, and R is the radius of the nucleus. This form factor is widely used when considering DM capture by the Sun. Another form factor, which is very often used in the context of setting limits on the DM cross section in DD experiments, is the Helm form factor [104–106],

$$F(q^2) = 3\,\frac{j_1(qR)}{qR}\,e^{-\frac{(qs)^2}{2}}\,, \tag{3.71}$$

This form factor arises from the density profile

$$\rho(\boldsymbol{x}) = \int \rho_0\theta(R-|\boldsymbol{x'}|)e^{-|\boldsymbol{x}-\boldsymbol{x'}|^2/2s^2}d^3\boldsymbol{x'}\,, \tag{3.72}$$

where ρ_0 is a normalization constant. It is evident from the convolution that R parametrizes the effective radius and s parametrizes the skin thickness of the nucleus. For large xenon nuclei, it is shown in Ref. [107] that the Helm form factor is a decent approximation but generally overpredicts the magnitude of the form factor at larger momentum transfers.

The case of spin-dependent scattering is significantly more complicated. This is due to the fact that all nuclei of the same type do not contribute to the total angular momentum of the nucleus in equal amounts. The cross section can be calculated to have the form [57, 105, 108]

$$\frac{d\sigma}{dE_R} = \frac{16m_N}{\pi v^2}\,\frac{J+1}{J}\left[a_p\langle S_p\rangle + a_n\langle S_n\rangle\right]^2\frac{S(q)}{S(0)}\,, \tag{3.73}$$

where J is the total nuclear angular momentum, $\langle S_p\rangle$ and $\langle S_n\rangle$ are the averages of the total spin carried by the protons and neutrons, a_p and a_n are the effective DM-proton and DM-neutron coupling constants, and $S(q)/S(0)$ is the squared magnitude of the form factor. Importantly, it can here be seen that the cross section has the same form as in the spin-independent case if σ_0 is defined as

$$\sigma_0 = \frac{32\mu^2}{\pi}\,\frac{J+1}{J}\left[a_p\langle S_p\rangle + a_n\langle S_n\rangle\right]^2\,. \tag{3.74}$$

Form factors for the spin-dependent case for some isotopes common in DD experiments can be found in Ref. [109]. As in the elastic case, it is also possible to write σ_0 in terms of the cross section on a single proton or neutron [57, 110].

It should be pointed out that there is a significant difference between spin-dependent and spin-independent scattering. In the case of spin-independent scattering when $\kappa > 0$, such as in the case of iso-spin conserving scattering, there is constructive interference between the proton and neutron contributions to the cross section, which implies that the cross section grows as A^2. For xenon, this factors increases the cross section up by several orders of magnitude. Since all nucleons do not contribute equally to the nuclear angular momentum, the spin-dependent cross section does not change much between nuclei with very different sizes but similar angular momenta. Explicit models of DM that is isospin-violating have been proposed and studied in, e.g., Ref. [111].

On a final note, a framework in which cross sections are calculated by using a non-relativistic framework has recently been proposed [112, 113]. The idea is to construct Hamiltonian operators that are invariant under Galilean transformations and use these for the calculations of cross sections. The form factors are replaced by response functions, which have been calculated for various nuclei in, e.g., Refs. [112, 114]. Any relativistic operator, such as those in Eq. (3.62), can then be mapped onto non-relativistic operators by following the results of, e.g., Ref. [115], where an analysis can be performed using the non-relativistic framework.

Chapter 4

The early Universe

The field of cosmology deals in part with studies of the observable effects that specific models of DM give rise to. Since the Universe expands, one encounters very interesting conditions looking back at the young Universe where particle physics played a very important role. In this very dense and hot period, thermodynamics can be used to describe various phenomena such as why the abundance of DM is what it is.

4.1 The expanding Universe

In the theory of general relativity, the geometry of spacetime is described in terms of the metric tensor $g_{\mu\nu}$, which satisfies a set of differential equations called the Einstein field equations [116–118],

$$R_{\mu\nu} - \frac{1}{2} R g_{\mu\nu} = 8\pi G T_{\mu\nu} \,. \tag{4.1}$$

In the above, $R_{\mu\nu}$ is the Ricci curvature tensor, $R = g_{\mu\nu} R^{\mu\nu}$ is the Ricci scalar, $T_{\mu\nu}$ is the energy-momentum tensor, and G is the gravitational constant. The cosmological constant Λ usually appear as a term $\Lambda g_{\mu\nu}$ on the left-hand side. This addition will be discussed later.

The most general metric that describes a homogeneous and isotropic universe is the Robertson-Walker (RW) metric [117, 118], defined through the relation

$$ds^2 = g_{\mu\nu} dx^\mu dx^\mu = dt^2 - a(t)^2 \left[\frac{1}{1 - kr^2} \, dr^2 + r^2 \, d\theta^2 + r^2 \sin^2\theta \, d\phi^2 \right] , \tag{4.2}$$

where k describes the curvature of space and the scale factor $a(t)$ parametrizes the expansion of the Universe. In relation to a RW metric, the concept of cosmic time and comoving coordinates can be introduced. The variables (r, θ, ϕ) in the metric above are comoving coordinates because an observer placed at rest in a

point (r_0, θ_0, ϕ_0) will remain at these coordinates for all times t. However, due to the appearance of $a(t)$ in the metric, the physical distance between this point and any other point, say $(0, 0, 0)$, will not remain the same. In fact, Eq. (4.2) states that the physical distance between two comoving observers will change proportionally to $a(t)$. The cosmic time is the time t that is measured by a comoving observer.

Now, it might not be obvious that we live in a homogeneous and isotropic Universe simply due to the fact that there is structure in it. Being on Earth is clearly different from being on the surface of the Sun or in the "vacuum" of intergalactic space. On the other hand, the isotropy of the CMB shows that the Universe was homogeneous at the redshift at which it was released. Substantial inhomogeneities in the Universe from the time of the CMB release until now would, via the integrated Sachs-Wolfe effect [119], induce inhomogeneities in the observed CMB. Observations of the matter distribution in the Universe at cosmologically recent times indicate that the Universe becomes homogeneous when scales of the order 100 Mpc or larger are considered [120, 121].

A Friedmann-Lemaître-Robertson-Walker (FLRW) metric is a metric as given by Eq. (4.2), but in which the behaviour of the scale factor $a(t)$ is governed by Eq. (4.1) under the assumption that the contents of the Universe can be described as perfect fluids. In a general frame, the energy-momentum tensor describing such a fluid is given by

$$T^{\mu\nu} = (p + \rho)U^\mu U^\nu - p g^{\mu\nu}, \tag{4.3}$$

where p is the fluid pressure and ρ is the energy density in the fluid rest frame, U^μ is the four-velocity of the fluid and the sign convention of $g^{\mu\nu}$ is the one conventionally used in particle physics, $(+\ -\ -\ -)$. The fluid is at rest in the comoving frame such that $U^0 = 1$ and $U^i = 0$ for $i = 1, 2, 3$. In this frame, the non-zero elements of the energy-momentum tensor are

$$T^{00} = \rho + p, \qquad T^{ij} = -p g^{ij}\,, \tag{4.4}$$

One can use the fact that the divergence of the energy-momentum tensor is zero to derive the very useful equation

$$\nabla_\nu T^{0\nu} = \frac{d\rho}{dt} + \frac{3\dot{a}}{a}(\rho + p) = 0\,. \tag{4.5}$$

The Friedmann equations, which govern the behaviour of $a(t)$, are then found from the Einstein field equations using the energy-momentum tensor for a perfect fluid. The two equations take the form

$$\left(\frac{\dot{a}}{a}\right)^2 = -\frac{k^2}{a^2} + \frac{8\pi G}{3}\rho = H^2\,, \tag{4.6}$$

$$\frac{\ddot{a}}{a} = -\frac{4\pi G}{3}(\rho + 3p)\,. \tag{4.7}$$

The second step in the first equation defines the hubble rate H in terms of a as well as its behaviour depending on the curvature and the energy density. The second

equation governs the acceleration of the scale factor depending on the energy density and the pressure exerted by the components of the fluid.

In order to understand how the different forms of energy that contribute to ρ in the Friedmann equations behave as the Universe expands, the kinematics of individual particles that make up each form of energy density must be understood. Any free particle, massless or not, travels along a geodesic, which is nothing but a straight line in curved spacetime. The geodesic equation dictates that the four coordinates $x^\mu(\lambda)$, where $\mu \in \{0, 1, 2, 3\}$ and λ parametrizes the curve, are solutions to the differential equations

$$\frac{d^2x^\mu}{d\lambda^2} + \Gamma^\mu_{\alpha\beta}\frac{dx^\alpha}{d\lambda}\frac{dx^\beta}{d\lambda} = 0\,, \tag{4.8}$$

where $\Gamma^\mu_{\alpha\beta}$ are Christoffel symbols. Now, as is widely known from Noether's theorem, symmetries in the action of a system imply that there exist conserved quantities in the system. In general relativity, the geodesic equation can be found from Hamilton's principle that the action

$$S = \int \sqrt{g_{\alpha\beta}\dot{x}^\alpha\dot{x}^\beta}d\sigma\,, \tag{4.9}$$

in which $\dot{x}^\alpha = dx^\alpha/d\sigma$, is stationary. Un-dotted coordinates appear only in the metric, which implies that if the metric remains unchanged by the shift in one of the variables $x^\gamma \to x^\gamma + \delta x^\gamma$, then a symmetry exist. The corresponding conserved quantity can be expressed through the relation

$$\frac{d}{d\sigma}\left(\xi_\mu\frac{dx^\mu}{d\sigma}\right) = 0\,, \tag{4.10}$$

where $\xi_\mu = \delta_{\mu\gamma}$ is a Killing field. The concept of Killing fields is straightforwardly generalized to higher order tensors. In particular, there is a Killing field associated with the FLRW metric that can be expressed as

$$K_{\mu\nu} = a(t)^2\left(-g_{\mu\nu} + U_\mu U_\nu\right)\,, \tag{4.11}$$

where $U^\delta = (1, 0, 0, 0)^\delta$ is the four-velocity of a comoving observer. By direct calculation, it can be shown that

$$\nabla_\alpha\left(K_{\mu\nu}V^\mu V^\nu\right) = 0\,, \tag{4.12}$$

which means that $K_{\mu\nu}V^\mu V^\nu$ is constant along the geodesic curve that a particle with four-momentum V^α follows. This allows for the identification of how the kinematic properties of massive and massless particles will evolve when repeatedly being measured by a comoving observer. For massless particles, it holds that $V_\mu V^\mu = 0$ and $U_\mu V^\mu = V_0$, the latter of which is the energy, or equivalently the magnitude of the physical momentum p, of the massless particle as measured by a comoving

observer. For massive particles, $V_\mu V^\mu = V_0^2 + g_{ij}V^iV^j$ and $U_\mu V^\mu = V_0$, and so the conserved quantity is proportional to $-a(t)^2 g_{ij}V^iV^j$, where a comoving observer would measure the physical squared momentum $p^2 = -g_{ij}V^iV^j$. Thus, if the momentum of a particle is measured twice, once at $t = t_0$ when $p = p_0$, and at some later time t, regardless of whether the particle is relativistic or not, what is found is

$$p = p_0 \frac{a(t_0)}{a(t)} \,. \tag{4.13}$$

The momentum will therefore decrease if the Universe is expanding, and the momentum will increase if the Universe is contracting. In a spatially flat FLRW universe, the metric is a function only of t, which means that there are Killing vectors associated with the spatial coordinates, which with Eq. (4.10) can be used to derive Eq. (4.13).

As far as we are aware, the Universe consists of three types of energy densities. The first type is non-relativistic non-interacting (in the sense that annihilation does not take place) matter, such as baryons and cold dark matter, commonly called "dust". There is radiation, which is composed of relativistic particle species such as photons, and finally there is dark energy. The equation of state for each of these types of energy densities can be parametrized as $p = w\rho$, in which case the solution to Eq. (4.5) is

$$\rho \propto a^{-3(1+w)} \,. \tag{4.14}$$

Given the discussion above, it is easy to understand the value of w for matter and radiation. For matter, the energy density in kinetic energy is negligible and mass per volume makes up the entire contribution to ρ. However, the volume within which N particles with mass m are contained increases in physical size as $a(t)^3$, implying that $\rho = mN/V \propto a^{-3}$ which yields $w = 0$. For radiation, if the mean energy of a photon is E, the energy density is E/V. Therefore, the redshift of photons along with the box size increasing as the Universe expands gives an energy density that behaves as a^{-4}, i.e., $w = 1/3$.

Dark energy is a form of energy density whose contribution to the energy density drives the scale factor to a positive acceleration. By Eq. (4.7), dark energy must have $w < -1/3$ [122]. Einstein initially formulated the Einstein field equations as in Eq. (4.1) [123]. However, motivated by constructing a static Universe, i.e., one that does not expand or contract, he introduced the cosmological constant Λ [32] by adding the quantity $\Lambda g_{\mu\nu}$ on the left-hand side of his field equations. This term can equally well be thought of as a contribution to $T_{\mu\nu}$ for which

$$p = -\rho = -\frac{\Lambda}{8\pi G} \,. \tag{4.15}$$

As $w = -1$ for this type of energy density, the cosmological constant will give a positive contribution to $\ddot{a}$ in Eq. (4.7), which counteracts the effects of the matter density filling the Universe. This along with postulating that the the Universe has

curvature such that k in Eq. (4.6) is non-zero, both $\dot{a}$ and $\ddot{a}$ can be made zero and Einstein can have his static universe.

Going back to the actual energy content of the Universe, the current Hubble rate H_0 relates to the critical density as

$$\rho_{0,\text{crit}} = \frac{3H_0^2}{8\pi G}\,, \tag{4.16}$$

It is called critical as the Friedmann equation dictates that the Universe is flat only if it holds today that $\rho = \rho_{0,\text{crit}}$. The quantities Ω_m, Ω_R and Ω_Λ are usually introduced using the relationship $\Omega_i = \rho_{0,i}/\rho_{0,\text{crit}}$. With the Hubble rate, normalized to its current value and using the Ω definitions, it is possible to recast the second equality in Eq. (4.6) on the form

$$\frac{H^2(a)}{H_0^2} = \left[\Omega_\Lambda + \Omega_m \left(\frac{a_0}{a}\right)^3 + \Omega_R \left(\frac{a_0}{a}\right)^4 + \Omega_K \left(\frac{a_0}{a}\right)^2\right]. \tag{4.17}$$

The evolution of each energy density as a function of a is explicitly incorporated and a_0 is the current scale factor (which can be chosen arbitrarily and is usually set to unity). The energy density of the Universe in the three various forms have been determined from the measurements of the CMB by the Planck satellite [36]. Accordingly, the fractional dark energy density is $\Omega_\Lambda \approx 0.69$ and the fractional matter density is $\Omega_m \approx 0.31$. The Planck data also gives the matter-radiation equality at $a_{\text{eq}} \approx 1/3372$. Setting $\rho_m(a_{\text{eq}}) = \rho_R(a_{\text{eq}})$ gives $\Omega_R \approx 9.16 \cdot 10^{-5}$. This gives rise to an interesting hierarchy in the evolution of H. Its evolution in the early Universe was dominated by the radiation energy density until a_{eq}, when its evolution became governed by the matter density. The very late history has been dominated by dark energy and, unless something unexpected happens, this will be the case for all eternity.

4.2 Thermodynamics

In understanding how the Universe evolved, one has to derive a few identities that hold for a gas in thermal equilibrium. A gas consisting of fermions or bosons will in thermal equilibrium be described by the probability distributions

$$f(\boldsymbol{p}, T, \mu) = \frac{g}{(2\pi)^3} \frac{1}{e^{(\sqrt{\boldsymbol{p}^2+m^2}-\mu)/T} \pm 1}\,, \tag{4.18}$$

where m is the particle mass and $\boldsymbol{p}$ its three-momentum, T is the temperature, μ is the chemical potential, and g is the internal number of degrees of freedom such

as spin. The positive sign in the denominator holds for bosons, which obey Bose-Einstein statistics, while the minus sign holds for fermions, which obey Fermi-Dirac statistics. The number density is by definition

$$n(T,\mu) = \frac{g}{(2\pi)^3}\int d^3\boldsymbol{p} f(\boldsymbol{p},T,\mu)\,. \tag{4.19}$$

The energy density and pressure of the particular state are given by

$$\rho(T,\mu) = \frac{g}{(2\pi)^3}\int d^3\boldsymbol{p}\sqrt{\boldsymbol{p}^2+m^2} f(\boldsymbol{p},T,\mu) \tag{4.20}$$

and

$$p(T,\mu) = \frac{g}{(2\pi)^3}\int d^3\boldsymbol{p}\frac{\boldsymbol{p}^2}{3\sqrt{\boldsymbol{p}^2+m^2}} f(\boldsymbol{p},T,\mu)\,, \tag{4.21}$$

respectively. It is possible to evaluate these for two cases of importance for the cosmological evolution of the Universe. At very high temperatures, where $T \gg m$ and $T \gg \mu$,

$$n(T) = \begin{cases} \text{Bosons}: & \frac{\zeta(3)}{\pi^2} g T^3 \\ \text{Fermions}: & \frac{3}{4}\frac{\zeta(3)}{\pi^2} g T^3 \end{cases}, \tag{4.22}$$

$$\rho(T) = \begin{cases} \text{Bosons}: & \frac{\pi^2}{30} g T^4 \\ \text{Fermions}: & \frac{7}{8}\frac{\pi^2}{30} g T^4 \end{cases}, \tag{4.23}$$

$$p(T) = \rho(T)/3\,, \tag{4.24}$$

where $\zeta(x)$ is the Riemann zeta function. For low temperatures $T \ll m$, the particles in the gas are non-relativistic and the expressions for fermions and bosons are identical and given by

$$n(T) = g\left(\frac{mT}{2\pi}\right)^{3/2} e^{-(m-\mu)/T}\,, \tag{4.25}$$

$$\rho(T) = mn(T)\,, \tag{4.26}$$

$$p(T) = Tn(T)\,. \tag{4.27}$$

Applying the second law of thermodynamics to the primordial plasma results in that the entropy density in a comoving box is constant and given by [117]

$$s = \frac{\rho + p}{T}\,. \tag{4.28}$$

The entropy density in the Universe is therefore almost completely defined in terms of the relativistic particles.

The redshift of particle momenta has interesting consequences for the evolution of a particle species in thermal equilibrium that decouples from, i.e., stops interacting with, the rest of the plasma. Suppose that this happens at a time when the

particle distribution is described by the temperature T_d and the magnitude of the scale factor is a_d. Since the momentum decreases inversely proportional to a after it decouples, a distribution of relativistic particles will behave as

$$f(\boldsymbol{p}a(t)/a_d, T_d, \mu) \propto \left[e^{(p\frac{a}{a_d}-\mu)/T_d} \pm 1\right]^{-1} = \left[e^{(p-\mu')/T} \pm 1\right]^{-1} . \tag{4.29}$$

In the last equality, a new temperature and chemical potential have been defined to absorb the scale factors. The implication is that that the shape of the distribution remains intact as the Universe expands, but that the temperature that describe it will be inversely proportional to a. The same discussion for the non-relativistic case leads to the conclusion that $T \propto a^{-2}$. Since the energy density of photons is proportional to T^4, its evolution with a falls perfectly in line with how the the energy density relates to the scale factor in the discussion around Eq. (4.14).

4.3 Dark matter abundances and Boltzmann equations

One of the main reasons behind the popularity of the weak scale DM particles is the thermal freeze-out scenario. A very important tool to be used to describe how the number density of DM evolves is the Boltzmann equation. At the fundamental level, the Boltzmann equation describes the evolution of the particle distribution in phase-space. To understand DM freeze-out, the three-momentum of the phase-space distribution can be integrated over, which allows us to write the Boltzmann equation in an expanding Universe as [117]

$$\frac{dn}{dt} + 3Hn = \frac{1}{a^3}\frac{d(a^3 n)}{dt} = \frac{g}{(2\pi)^2}\int C[f]\frac{d^3p}{E} . \tag{4.30}$$

Here, n is the number density of the species under consideration, H is the Hubble rate, and g is the number of degrees of freedom. The collision operator on the right-hand side is a complex object where $C[f]$ takes the particle physics of the process into account. That is, it gives the rate at which particles are created and the rate at which they annihilate. It is rather easy to interpret the terms on the left hand side of the Boltzmann equation. The first term is the change in particle number density per time, while the second term accounts for the dilution due to the expansion of the Universe.

A very simple case that illuminates the important points of the Boltzmann equation is a single self-annihilating DM particle ψ that, in thermal equilibrium, is described by a Boltzmann distribution. The Boltzmann equation is in this case given by [117]

$$\frac{dn_\psi}{dt} + 3Hn_\psi = -\langle\sigma v\rangle\left[n_\psi^2 - (n_\psi^{\mathrm{EQ}})^2\right] . \tag{4.31}$$

Here, n_ψ is the DM number density while n_ψ^{EQ} is the particle density at equilibrium. The quantity $\langle\sigma v\rangle$ corresponds to the thermal average over the rate for two

ψ particles to annihilate into some other particles. In this case, it is actually easy to argue for the right hand side using detailed balance. The annihilation rate in a gas of particles with number density n_ψ should behave as $\langle\sigma v\rangle n_\psi^2$, and the rate of change, i.e., the right hand side, should disappear when the species is in thermal equilibrium. In a scenario where the DM abundance is set by the freeze-out mechanism, DM is thought to interact strongly enough to be in thermal equilibrium with its surroundings in the early Universe. In the equation above, the right-hand side of the Boltzmann equation vanishes since $n_\psi = n_\psi^{\mathrm{EQ}}$ when $T \gtrsim m_\psi$. The equilibrium abundance of DM decreases exponentially according to Eq. (4.25) once the DM mass is larger than the temperature of whatever gas that it is coupled to. This exponential decrease can be understood as the efficient annihilation of DM while the low temperature of the gas that it is coupled to results in insufficient kinetic energies of gas particles to produce DM. At some point however, the expansion of the Universe outgrows the annihilation rate of DM after which the DM abundance in a comoving volume remains constant. Thermal freeze-out is successful when the number density of DM that survives this process is just right to match with observations.

Since the temperature and number densities were extremely large, it makes sense to consider species in thermal equilibrium since any deviation from equilibrium will be countered immediately due to the interaction term in the Boltzmann equation. However, at some point the annihilation rate falls below the Hubble rate;

$$H \gtrsim \langle\sigma v\rangle n_\psi \,. \tag{4.32}$$

When this occurs, the Universe expands faster than particles can find each other to annihilate. At this point, the species has fallen out of thermal equilibrium. Due to its simplicity, this condition is often considered as a guideline for when freeze-out occurs rather than actually solving the Boltzmann equation.

One of the crucial points in paper III is to explain why there are, in an inelastic DM model, no particles in the heavier state χ_2 in the DM halo. The number densities of χ_1 and χ_2 will depend on scattering processes such as $\chi_1\chi_1 \leftrightarrow \chi_2\chi_2$. Since a model with a light mediator was considered and these collisions were taking place in a non-relativistic setting, strong self-interactions were present. At some point, the production of χ_2 due to scattering of χ_1 becomes kinematically forbidden while χ_2 is free to downscatter. Thus, the abundance of χ_2 can be driven to completely negligible numbers as long as the interaction is strong enough. The cross section is very expensive to calculate numerically when many partial waves plays a part, which is the case in this kind of scenario. Therefore, the abundance of χ_2 was estimated at the value when $\langle\sigma_{\chi_2\chi_2} v\rangle n_{\chi_2}$ fell below the Hubble rate.

It is also interesting to mention that there are other variations of the genesis of DM that have been proposed, such as the freeze-in mechanism [124–126]. In this scenario, DM was never in thermal equilibrium but was generated gradually from zero abundance without annihilation taking place. This scenario is somewhat of an inverse to freeze-out. In freeze-out, a stronger coupling between DM and the

particles it interacts with results in a longer period of equilibrium and consequently a longer period of annihilation which drives the final abundance of DM down. In the freeze-in mechanism, a stronger coupling will only increase the final abundance of DM. Consequently, freeze-in generally require very small couplings while freeze-out requires large couplings.

Chapter 5

Dark matter halos

The CMB informs us that structure appears to have formed much earlier than the baryons had the possibility to clump up as the radiation pressure exerted by the CMB photons would destroy any such clumps. At early times, the growth of these overdensities can be described using linear perturbation theory [118]. Over time, the overdense regions may attract enough matter such that the expansion stops locally and gravitational collapse occurs [127, 128]. The non-linear regime, which is entered when enough matter has accumulated, becomes very difficult to describe. However, N-body simulations have become an invaluable tool to describe the process. To this day, they have reached an impressive number of particles, going into the billions [129, 130], and take into account effects such as baryonic physics and the presence of black holes. From the results of these, it is thought that the overdense regions will initially generate small dark matter halos that merge to form larger halos. Many of the smaller halos partaking in the merging process survive, resulting in a great deal of substructure. Since DM does not interact, the halos are protected against complete gravitational collapse. The baryons within them will however radiate energy in the form of photons in scattering processes, lose energy, and form small compact clouds within which stars, and eventually galaxies, are formed. The center of the larger halo can then form a large galaxy, while the smaller, still intact, subhalos may host dwarf galaxies. The Milky Way halo is thus thought to host not only the Milky Way but also the dwarf galaxies that appear gravitationally bound to it [131].

5.1 Dark matter halo profiles

As both DD and ID methods use DM from the halo as the source for DM, it is only natural that both depend crucially on the phase-space distribution of DM. The phase-space consists of the spatial distribution as well as the velocity distribution

of DM. Here is a summary of current knowledge and usual assumptions that are made regarding these properties.

5.1.1 Density profiles

The actual behaviour of the density profile depends heavily on specifics such as how the halo collapsed and if there were asymmetries in the initial distribution. There may also be non-trivial effects such as feedback from black holes and supernovae [132]. In larger halos, it is generally accepted that microscopic phenomena, such as feedback, play a smaller role on how the halo is shaped but, as will be discussed later, there are several issues in the halos of smaller galaxies that might be addressed with such effects. Regardless, there are several interesting spherically symmetric halo models that are used when describing the halos in the context of ID.

The most famous profile is the Navarro-Frenk-White profile [133], which can be parametrized as

$$\rho(r) = \frac{\rho_c}{(r/r_s)\left(1 + r/r_s\right)^2} \,. \tag{5.1}$$

In the above, ρ_c is a characteristic density and r_s is a characteristic radius. Originally, it is a fit to the density profile derived from N-body simulations and is constructed to have the specific behaviour of $\rho(r) \sim r^{-1}$ at $r < r_s$, while falling off as r^{-3} when $r > r_s$, and having a smooth transition between the two regimes.

Another notable profile is the Einasto profile [134]

$$\rho(r) = \rho_s \exp\left(-c\left[(r/r_s)^{1/\alpha} - 1\right]\right) \,, \tag{5.2}$$

where r_s is the radius in which half of the total halo mass is contained, ρ_s is the density at this radius, α is a constant that describes the logarithmic slope, $\mathrm{dln}\rho/\mathrm{dln}r \propto r^{1/\alpha}$, and c is a number to be fit.

There is also an isothermal distribution, which is more relevant phenomenologically than as an appropriate description of the distribution of DM [135],

$$\rho(r) = \frac{\rho_0}{a^2 + r^2} \,, \tag{5.3}$$

where ρ_0 and a are constants. A profile of this kind make sense considering the rotation curves of galaxies, as for $r \gtrsim a$, the enclosed mass grows proportionally to r, which yields exactly flat rotation curves.

For DD experiments, and certain ID methods, it is crucial to know what the density of DM is in the galactic neighbourhood of the Sun. The profiles listed above have been used in an attempt to determine this quantity, see e.g., Ref. [136]. A number of other studies using various methods seem to indicate that a value lies in the neighbourhood of [137–142].

$$\rho_\chi^{\mathrm{local}} = 0.3 - 0.4 \ \mathrm{GeV/cm^3} \,. \tag{5.4}$$

5.1.2 Velocity distribution

The velocity distribution of DM particles in the halo is also a very important quantity. For a spherically symmetric DM halo, there is an explicit formula called the Eddington formula, which immediately gives the velocity distribution as a function of energy [143],

$$f(\mathcal{E}) = \frac{1}{\sqrt{8}\pi^2}\left[\int_0^{\mathcal{E}} \frac{\mathrm{d}\Psi}{\sqrt{\mathcal{E}-\Psi}}\frac{\mathrm{d}^2\rho}{\mathrm{d}\Psi^2} + \frac{1}{\sqrt{\mathcal{E}}}\left(\frac{\mathrm{d}\rho}{\mathrm{d}\Psi}\right)_{\Psi=0}\right], \tag{5.5}$$

where $\mathcal{E} = \Psi(r) - E_{\mathrm{kin}}$, $\rho(r)$ is the density profile, and $\Psi(r) = -\phi(r) + \phi(\infty)$ where $\phi(r)$ is the gravitational potential energy.

The velocity distribution is very often assumed to be a Boltzmann distribution [144]

$$f(\vec{v}) = \frac{n_\chi}{(2\pi/3)^{3/2}\,\sigma^3}\exp\left(-\frac{3}{2}\frac{\vec{v}^{\,2}}{\sigma^2}\right). \tag{5.6}$$

Here, n_χ is the local number density of DM, which is given by $n_\chi = \rho_\chi/m_\chi$, and σ is the velocity dispersion. The assumption of this profile corresponds to having chosen a density profile as that given in Eq. (5.3), where $a = 0$ such that the density profile behave as r^{-2}.

Since the Sun moves around the galactic center with the velocity $\vec{v}_\odot$, the velocity distribution as seen by an experiment in the rest frame of the Sun is shifted by the amount $f_{\mathrm{Sun}}(v) = f(\vec{v} + \vec{v}_\odot)$. Integrating out the angular dependence of the distribution, the speed distribution in the solar frame is obtained as

$$f_{\mathrm{Sun}}(v) = \frac{3n_\chi v}{2\sqrt{\pi}\sigma^2}\left[\exp\left(-\frac{3}{2}\frac{(v-v_\odot)^2}{\sigma^2}\right) - \exp\left(-\frac{3}{2}\frac{(v+v_\odot)^2}{\sigma^2}\right)\right], \tag{5.7}$$

where $v_\odot \approx 220$ km/s and $\sigma = \sqrt{3/2}v_\odot$. The velocity of the Earth around the Sun, $v_e(t)$, will also contribute to the shift in the velocity distribution, which is now $f_{\mathrm{Earth}}(v) = f(\vec{v} + \vec{v}_\odot + \vec{v}_e)$. This gives rise to a periodicity in the flux of DM at Earth with implications for DD experiments [103, 145–147]. The velocity profile presented here is somewhat unphysical in the sense that a galactic halo will not contain particles with velocities that exceed the escape velocity of a galaxy. At the radius of the Sun, this velocity is roughly 550 km/s [148–150], albeit with fairly large uncertainties. This is sometimes incorporated by a hard cut-off at this velocity in the speed distribution, which naturally changes the normalization of the distribution slightly.

There are numerous studies of the velocity profile of the DM in Milky-Way-like galaxies using N-body simulations [151–155]. The results generally show that the Maxwell-Boltzmann assumption is a decent description, but that there is quite a large spread in profiles on a halo to halo basis.

5.2 Problems in small scale structures

While many of the ΛCDM predictions from DM only N-body simulations match up beautifully with observations at large scales, there is worry of how the theory holds up against observations of astrophysical objects on smaller scales [156]. There are several issues, commonly referred to as the small scale structure problems of which the three most prominent ones will now be discussed.

- The cusp-vs-core problem is the name of a mismatch related to the behaviour of the density of DM in the central regions of smaller galaxies. N-body simulations consistently predict cusps, where the behaviour of the DM density follows a power law $\rho \sim r^{-\gamma}$, where $\gamma \simeq 1 - 1.5$, see, e.g., Refs. [133, 157–163]. On the other hand, Observations of these smaller systems can be used to deduce the actual behaviour of ρ. It is found that most smaller halos have cores, where ρ seems to be constant at small radii, see, e.g., Refs. [164–178]. Although the mismatch between the cusps predicted by N-body simulations and the cores favoured by observations appear mainly in dwarf galaxy halos, there is also hints towards shallow cusps in galaxy cluster halos [179–181].

- The missing satellites problem is due to a discrepancy between the number of predicted and observed number of dward galaxies. As discussed above, when a large DM halo forms, it does so through the accumulation of many smaller halos. In N-body simulations, a large number of these smaller halos survive the gravitational tidal forces induced by the larger halos and their mutual interactions. The result is a large number of subhalos that are massive enough for efficient atomic cooling to take place such that star formation within them is expected to occur. When comparing the number of expected dwarf galaxies from N-body simulations to the actual number of dwarf galaxies of Milky Way sized halos, a large discrepancy is found [182, 183].

- The too-big-to-fail-problem builds somewhat upon a proposed solution to the missing satellites problem. The idea is that star formation is not efficient enough to illuminate the smaller halos and that only the largest subhalos should be inhabited by dwarf galaxies. However, the largest subhalos found in N-body simulations are significantly more massive than the subhalos hosting the Milky Way dwarves. Surely, if the smaller halos had no trouble forming stars, the largest subhalos should definitely host dwarf galaxies but these are nowhere to be found [184, 185]. This problem affects not only the Milky Way halo, but also the halo hosting the Andromeda galaxy and isolated halos appear to share the same defect [186, 187].

5.2.1 A baryon solution?

There are various proposals for solving the small scale structure problems. A popular explanation is that baryonic feedback effects from supernovae will induce a

time dependence in the dark matter halo. Even though DM is modelled as collisionless, a rapidly varying gravitational potential will affect the energy of the DM particles, which can evacuate portions of DM from the center of dwarf galaxy halos and induce cored profiles [188]. It has also been shown through simulations to be effective [176, 189–196]. On the other hand, this solution only works if there is enough star formation, which appears to be the case only in more massive dwarf galaxies [197], leaving the cusp-vs-core and too-big-to-fail problems unexplained in the lower mass dwarves. There are also other effects, such as tidal stripping of the dwarf halo by the larger halo, that can reduce the central density of DM and alleviate the small scale structure problems [198–202].

5.3 Self-interacting dark matter in halos

Taking the above discussion into account, it is not at all unlikely that the key to resolving the small scale structure problems lie in the modelling of baryonic effects. However, an alternative and very exciting way of solving the small scale structure problems is to invoke models of DM where self-interactions take place [203, 204].

5.3.1 Bounds on self-scattering cross sections

Before discussing how self-interacting DM can be used to explain the small scale structure problems, there are bounds from various astrophysical observations to be taken into account. The first way of placing such bounds is through the observations of colliding galaxy clusters. When galaxy clusters collide, DM particles in each of the two halos may interact, which results in several observational effects. Firstly, particles that scatter at angles transverse to the direction of the bulk of the DM halo will likely become gravitationally unbound from the two clusters as a whole, leading to evaporation of the DM halo. Thus, the survival of colliding halos indicate that self-interactions may not be too large. Even if particles are not ejected, transverse scattering events give rise to deceleration effects on the two halos. As was discussed briefly in Sec. 2.3, galaxies behave in a collisionless manner while the majority of visible mass, which is encapsulated in the free hydrogen, collides and slows down due to the friction induced by self-interactions. The observation of mass peaks in these objects that trail the galaxies rather than the bulk of the visible gas indicate that DM must not self-interact too strongly. The separation of the mass peak of the DM halo and galaxies in a colliding cluster scenario was studied numerically in Ref. [205] for two different types of self-interactions. It was found that, while the mass peaks of the DM generally overlap with the galaxies, the distribution is overall distorted in manners different from the distribution of galaxies depending on whether DM interactions are frequent or rare. The mass profiles deduced from observations of various colliding galaxy clusters such as the Bullet Cluster have been used to place bounds on the self-scattering cross section of DM [206–211]. Subsequent studies seem to call into question the method used to derive bounds on

the self-interacting cross sections from colliding clusters [212]. It was here noted that the method used to calculate the offset between different components of the Bullet cluster gives rise to bounds may be too strong, and that using techniques that are more closely related to observations are better suited for the job.

Constraints can also be placed based on the evaporation of DM halos of galaxies inside galactic cluster halos. The velocity dispersion of DM that is bound to the galaxy cluster halo exceeds the escape velocity of DM halos that host galaxies within the clusters. The likelihood that DM from the cluster halo transfers enough energy to eject DM from galaxy halos is therefore very large, which indicates that galaxy hosting halos will evaporate over time [213]. The requirement that these subhalos survive over a Hubble time leads to upper bounds on the self-interaction cross section.

A third way of constraining self-interactions is possible by analysing the shape of DM halos. Large DM self-interactions will tend to erase asymmetries in the DM halo core, leading to spherically symmetric profiles. These effects can be studied and initially placed very strong bounds on the self-scattering cross section [214]. On the other hand, the uncertainties in this type of analysis are huge and later numerical studies showed that the bounds are much weaker than initially thought [215]. Large self-interactions will also create cores in galaxy cluster halos which initially seemed too large to be consistent with observations [216], but was later shown to be overestimated as well [217].

Taking all constraints into account, self-interacting DM with cross sections of the order

$$\frac{\sigma_{\chi\chi}}{m_\chi} \gtrsim 1 \text{ cm}^2/\text{g} \tag{5.8}$$

are generally considered to be incompatible with observations.

5.3.2 Solving the small scale structure problems with self-interacting dark matter

The idea of solving the small scale structure problems are generally based on the same principles that are used to place bounds on them. The generation of cores by reducing the number of particles in the center of the subhalos of dwarf galaxies might solve not only the cusp-vs-core problem, but also the too-big-to-fail problem since this would necessarily reduce the rotational velocity of stars and thus imply that the dwarf galaxies really do inhabit the largest subhalos. Self-interacting DM is thought to solve the problem due to the evacuation of DM particles that make up the cusp by scattering against particles that gain large amounts of kinetic energy when falling into the core from the outer regions of the halo.

There have been numerous studies that incorporate various models of self-interacting DM in studies where the evolution of halos is simulated [216–228].

Overall, there seems to be support for the generation of cores in galaxy halos. Accordingly, cross sections with magnitudes around

$$\frac{\sigma_{\chi\chi}}{m_\chi} \sim 1 \text{ cm}^2/\text{g} \tag{5.9}$$

generate cores in dwarf galaxy halos that seem to agree with observations.

In order to explain the small scale structure problems with DM self-interactions while avoiding the bounds that arise at cluster halo sizes, one can invoke a velocity dependence in the cross section as proposed in Ref. [229]. It was here noted that the self-scattering induced by DM that interacts via a Yukawa potential can naturally have a velocity dependence that yields a large cross section at small velocities, while falling off rapidly with increasing velocities. This fits perfectly with the requirement that DM self-scattering cross sections are required to be large at velocities of the order $\mathcal{O}(10)$ km/s, which is the natural velocity range relevant for solving the small scale structure problems, while becoming small at velocities of the order $\mathcal{O}(1000)$ km/s, which is the natural velocity range at which bounds from DM cluster halos are derived. It has been verified in numerical simulations that the cross section generated by such interactions do indeed reproduce the desired behaviour in dwarf galaxy halos [222]. The appearance of Yukawa potentials in the non-relativistic limit is a natural feature in extensions of the SM containing light mediators, see, e.g., Refs. [230–236].

Models that contain light mediators, such as the ones listed above, are difficult to reconcile with cosmology. If one tries to explain the abundance of DM through the freeze-out mechanism, the mediators will be in thermal equilibrium in the early Universe. This requires the mediators to be unstable to prevent them from making up most of the DM mass, or even overclose the Universe [237]. If they are unstable, they should decay before Big Bang nucleosynthesis occurs as their presence would alter the primordial abundances of elements [238, 239]. If DM interacts via kinetic mixing or the Higgs portal, it is difficult to explain their short lifetimes with the very strong bounds on the mixing parameters from DD experiments [237, 240].

In paper III of this thesis, a scenario where DD experimental limits on the mixing parameter is evaded entirely in a model of inelastic DM, as discussed in Sec. 3.3, was considered. The idea was that if the mass splitting between the two states is large enough and self-interactions are strong enough, only the lower mass state will survive the early Universe. Due to the large mass splitting, it is kinematically impossible for scattering of the DM in the Milky Way halo to occur in DD experiments. Thus, issues associated with a light mediator in the early Universe are evaded while a solution to the small scale structure problems was provided. However, it was noted in Ref. [241] that the DM annihilation, which is greatly increased due to the Sommerfeld enhancement effect associated with strongly interacting light mediators, will produce a variety of observable signals such as distortions of the CMB. In light of this, the simple model considered in paper III might not be viable.

Chapter 6

Direct dark matter searches

Both DD and ID searches are based on the assumption that DM is a particle and that galaxies are surrounded by giant DM halos. The idea of DD and what kind of signal is expected in a DD experiment will be described here. DD searches will also be generalized to cover the case of inelastic DM, which touches upon why inelastic DM was proposed in the first place. It is also interesting to have a look at the information that is contained within a signal, should one be measured, and how this information can be used to compare results of different DD experiments in a halo-independent way.

6.1 Direct detection experiments

The idea of DD was invented very shortly after the realization that DM could very well be a weakly interacting particle [242]. There have been a very large number of experiments that have attempted to or are currently attempting to detect DM originating from the halo around the Milky Way. While their means of detection may differ, the underlying physics is the same in the sense that the recoiling target in the detector material can be detected as it is struck by a DM particle from the halo.

The differential rate at which collisions occur between a DM particle with mass m_χ and nucleus with mass m_A, where the recoil energy E_R is transferred, is given by [106]

$$\mathcal{R}(E_R, t) = \frac{\rho_\chi}{m_\chi m_A} \int_{|\vec{v}|>v_{\rm m}} f(\vec{v}, t) v \frac{d\sigma}{dE_R}\, d^3v\,, \tag{6.1}$$

which is measured in counts/kg/day/keV. In this formalism, the velocity distribution has been normalized to unity, which is why the local galactic DM density ρ_χ appears explicitly. If the experiment contains several different isotopes, the total differential rate will be given by the sum of the rates against all targets, weighed

by the fraction of detector mass that is made up of each isotope. The DM velocity distribution enters as $f(\vec{v}, t)$, where the time dependence is due to the Earth's motion around the Sun. The last quantity is the differential cross section, given by Eq. (3.60). The speed v_m that enters in the lower limit of the integral is the lowest speed that the incoming particle can have in order to be capable of giving the nucleus the recoil energy E_R and is given by

$$v_m = \sqrt{\frac{m_A E_R}{2\mu^2}}\,, \tag{6.2}$$

where μ is the reduced mass of the DM-nucleus system.

By plugging in Eq. (3.60) into Eq. (6.1), the differential rate can be cast on the form

$$\mathcal{R}(E_R, t) = \frac{\sigma_0 \rho_\chi}{2 m_\chi \mu^2} \left|F_A(E_R)\right|^2 \eta(v_m, t)\,. \tag{6.3}$$

The function $\eta(v_m, t)$ is defined here as

$$\eta(v_m, t) = \int_{v_m}^{\infty} v \tilde{f}(v) dv\,, \qquad v^2 \tilde{f}(v) = v^2 \int d\Omega\, f(v, \Omega)\,. \tag{6.4}$$

At this point, one can use the fact that σ_0 can be written in terms of cross sections on individual nucleons. For example, the rate due to spin-independent scattering will be given by

$$\mathcal{R}^{\rm SI}(E_R, t) = A_{\rm eff}^2 \mathcal{C} \eta(v_m, t) \left|F_A(E_R)\right|^2\,, \tag{6.5}$$

where the effective number of nucleons $A_{\rm eff}$ and the constant $\mathcal{C}$ have been defined as

$$A_{\rm eff} = Z + (A - Z)\kappa, \qquad \mathcal{C} = \frac{\sigma_{\chi p} \rho_\chi}{2 m_\chi \mu_{\chi p}^2}\,. \tag{6.6}$$

Since the function $\eta(v_m, t)$ is an integral over a positive function, it will necessarily decrease as v_m increases. According to Eq. (6.2), a smaller fraction of the particles in the DM halo contribute to larger recoils in a spectra. A similar expression to the one above holds for spin-dependent scattering where $A_{\rm eff}$ does not appear and $\mathcal{C}$ will be defined differently owing to the difference between Eq. (3.68) and Eq. (3.74).

6.1.1 Direct detection results

The DM-nucleus cross section can be constrained by DD experiments that over a period of time do not observe a number of events that are consistent with DM-nucleus scattering having that cross section. The procedure is generally straight forward. The standard halo model with $\rho_\chi = 0.3$ GeV as discussed in Sec. 5.1 is very often considered in this context. In the spin-independent case, the Helm form in Eq. (3.71) is also often used.

Recent results from DD experiments include those from large xenon-based experiments such as XENON1T, PandaX-II, and LUX [243–245]. The number of nucleons in natural xenon averages to about 130. Since bounds are generally reported

assuming equal coupling to protons and neutrons such that $\kappa = 1$, $A^2_{\text{eff}} \sim 10^4$, which gives extremely strong bounds on the DM-nucleon cross section $\sigma_{\chi p}$. Due to their energy thresholds, these experiments are sensitive to nuclear recoils that are larger than a couple of keV, which translates to sensitivity for DM masses above a few GeV. Other notable bounds come Darkside-50 with constraints down to just over one GeV [246] and from CRESST-III which constrains the spin-independent cross section for masses down to about 0.4 GeV [247].

On the spin-dependent side, bounds are placed on the DM-proton and DM-neutron cross section. Interestingly, natural xenon contains a lot of Xe^{129} and Xe^{131}, which have non-zero angular momentum. Since the unpaired nucleon is a neutron, the xenon based experiments constrain mostly the DM-neutron cross section [248, 249]. On the other hand, the strongest bounds from DD experiments on the spin-dependent DM-proton cross section comes from the PICO-60 experiment [250].

There have also been anomalies reported in some experiments. Most famously, the series of DAMA experiments have continously measured a modulation signal for well over a decade. Firstly, the DAMA/NaI measured a signal that was consistent with DM scattering. Subsequently, the DAMA/LIBRA-phase1 [251] and its upgrade DAMA/LIBRA-phase2 [252] show evidence of the same signal. The CoGeNT experiment has also seen a modulation signal that was consistent with DM scattering [253–255], but with a much lower statistical significance. In addition, this signal appeared to be difficult to explain with the standard halo model due to an abnormally large amplitude. Assuming that the DM particle in question would belong to one of the simpler models, numerous DD experiments have ruled out the DAMA signal. Most notably, the experiment run by the COSINE-100 experiment, using exactly the same detector material as DAMA (sodium and iodine) excludes a spin-independent DM particle explanation [256]. Of course, there have been a variety of DM models introduced to explain why a signal could appear in some experiments but not in others, see, e.g., Ref. [257] for a discussion.

6.2 Direct detection of inelastic dark matter

Inelastic DM, as was introduced in Sec. 3.3, was initially introduced to explain the DAMA signal as most of the preferred parameter region was ruled out by CDMS [258]. In this model, the DM halo consist of only the lower mass state χ, which upon scattering in the experiment creates the χ^* in an inelastic scattering event. If the mass splitting δ is of the same order of magnitude as the average kinetic energy of DM particles in the halo, the event rate in a DD experiment will be significantly affected, which might bring the experimental results into agreement. More recently, the case where there is a significant amount of χ^* in the halo has also been studied, which is interesting as the scattering process in this case is exothermic [259–261]. The scattering kinematics are significantly altered in both cases, which will also play a major role in how the observed energy recoil spectrum for each type of process is shaped.

For endothermic scattering to occur, the energy required to produce the heavier state must be provided as kinetic energy of the colliding particles. This requirement can be formulated as

$$v > \sqrt{\frac{2\delta}{\mu}}\,, \tag{6.7}$$

where v is the relative velocity of the colliding particles and μ is the reduced mass. For exothermic scattering, there is no such constraint.

In order for the target to pick up a recoil energy E_R in the collision, the relative velocity must exceed v_m, which is now given by [262]

$$v_m^2 = \left(\sqrt{\frac{m_A E_R}{2\mu^2}} + \frac{\delta}{\sqrt{2\mu E_R}}\right)^2 . \tag{6.8}$$

This reduces to the elastic case in Eq. (6.2) when $\delta \to 0$. In both cases, v_m will be minimal (and zero in the case of exothermic scattering) at a non-zero value of E_R. Specifically, this relation implies that the minimum of v_m, and the recoil energy that it corresponds to are given by

$$(v_m)_{\min} = \sqrt{2\delta/\mu}, \qquad (E_R)_{\min} = |\delta|\mu/m_A\,, \tag{6.9}$$

respectively. Since the rate is proportional to $\eta(v_m, t)$, the rate will be maximal close to $(E_R)_{\min}$, but shifted somewhat because of the form factor suppression.

The way that inelastic DM was introduced to reconcile the DAMA signal with the CDMS signal was due to the fact that since for a suitable set of parameters, v_m will be significantly smaller for scattering on iodine than on germanium (as was used in the CDMS experiment), which implied that particles in the halo could up-scatter against the targets in DAMA but not in CDMS.

Results from other DD experiments have been used to place bounds on various inelastic DM models [263–266] to the point where it is now difficult to reconcile the DAMA results with the other DD experiments also for inelastic DM. Bounds have also lately been extended to larger mass splittings than those that would necessarily reconcile the DAMA signal with other results [267]. Nevertheless, inelastic DM may still solve the problem if enough tuning is done to the model, see, e.g., Ref. [268].

6.3 Halo-independent methods

In the event that a differential rate is measured in a DD experiment, it is interesting to understand the type of DM that gave rise to it. It has also been shown that it is possible to use the information of one DD experiment to predict precisely the signal that should appear in other experiments [269, 270]. This can help to constrain various DM parameters.

The idea as noted in Refs. [269, 270] is that from a measured recoil spectrum $\mathcal{R}_1(E_R)$ in one experiment, Eq. (6.3) can be used to isolate

$$\mathcal{C}\eta_1(v_m) = \frac{1}{A_{\rm eff}^2|F(E_R)|^2}\mathcal{R}_1(E_R)\,, \tag{6.10}$$

where $\eta_1(v_m)$ can be considered as a function of the recoil energy via Eq. (6.2). The right-hand side contains everything related to the experiment, while the left-hand side contains everything DM related, save for v_m, which contains the target mass. The rate in one experiment where $\mathcal{R}(E_R)$ is measured in a range $[E^1_{\rm min}, E^1_{\rm max}]$ can then be used to calculate $\mathcal{C}\eta(v_m)$ in the corresponding velocity range $[v_{\rm min}, v_{\rm max}]$ assuming only the DM mass. The quantity $\mathcal{C}\eta(v_m)$ is universally the same for all experiments, but for different regions in E_R. Therefore, the range in v_m that this quantity is measured in corresponds to some other range in E_R in a second experiment, where the rate can then be predicted.

Going one step further, by taking the derivative of both sides with respect to v_m one obtains

$$\mathcal{C}v_m\tilde{f}_{\rm extr}(v_m) = -\frac{1}{A_{\rm eff}}\frac{d}{dv_m}\left(\frac{\mathcal{R}(E_R)}{|F(E_R)|^2}\right)\,, \tag{6.11}$$

where E_R is now considered a function of v_m. Therefore, one can actually probe the velocity distribution in a range of v_m that corresponds to the range in E_R that is found in the rate measured by the DD experiment. Of course, the lowest velocity v_m that can possibly be probed is set by $E_R = E_{\rm thr}$, the threshold energy of the experiment.

The analysis above can be generalized to inelastic scattering, as was done in paper II of this thesis. However, as indicated by Eq. (6.8), the relationship between v_m and E_R is no longer a monotonic function. Some range in v_m will now correspond to one range in $E_R < (E_R)_{\rm min}$ and one range in $E_R > (E_R)_{\rm min}$. If a signal is measured, one must first use techniques such as those developed in Ref. [271] to determine whether the signal is due to inelastic scattering or not. If inelastic scattering is taking place and the recoil spectrum has a distinct maximum, parts of the velocity distribution can be reconstructed from the derived spectrum on either side of $(E_R)_{\rm min}$ as described above.

Related to the discussion above, a curious observation is made in paper II. If a spectrum that is compatible with that expected from inelastic DM is measured and a distinct $(E_R)_{\rm min} = E^{\rm obs}_{\rm min}$ is seen in the spectrum, Eq. (6.9) gives a direct relation between m_χ and δ in terms of $E^{\rm obs}_{\rm min}$. If a second signal is seen in a DD experiment with a different target, both m_χ and δ can be uniquely determined. This is in contrast with the elastic case where mass determination from DD is not so straight forward [272].

Chapter 7

Indirect detection

7.1 Indirect detection methods

If DM is unstable or if it annihilates, an alternative way of searching for DM is via SM particles that are produced in their decay or annihilations. These annihilations may take place inside the halos of nearby galaxies, in the galactic center, or inside astrophysical bodies such as the Sun, where DM may accumulate in extremely large numbers over time. The general idea of indirect detection in various systems is discussed here, although the focus will lie mainly on the study of DM in the Sun.

7.2 Halo signatures

As the DM halos consist of a very large number of DM particles, decays or annihilations will occasionally take place and possibly produce SM particles. The end product of any SM particles that are produced will be a flux of stable particles such as protons, electrons, photons, and neutrinos. The searches for these SM particles is collectively called indirect detection searches [273].

It is straight forward to calculate the flux of particles coming from a particular direction in the sky, parametrized by ψ, provided that the annihilation rate is velocity independent. The energy spectrum of SM particle species N that hits a detector area dA per time is given by

$$\frac{dN}{dA\,dE\,dt} = \left[\frac{\langle\sigma v\rangle}{2(4)m_\chi^2}, \frac{\Gamma}{m_\chi}\right] \frac{dN}{dE} \int \frac{d\Omega}{4\pi} J\,. \tag{7.1}$$

The first and second term in the bracket holds for annihilation and decay, respectively, in which $\langle\sigma v\rangle$ is the annihilation rate and Γ is the decay rate. In the case of annihilation, the 2 in the denominator holds for self-annihilating DM while the 4 holds in the case of particle-antiparticle pair annihilation if the DM density is the

same for each species. The factor dN/dE is the energy spectrum of the species N that is generated by the annihilation or decay event. The J factor is an integral defined as

$$J_{\text{ann}} = \int \rho_\chi^2(\psi, l)\, dl\,, \qquad J_{\text{decay}} = \int \rho_\chi(\psi, l)\, dl\,, \tag{7.2}$$

where $\rho_\chi(\psi, l)$ is the DM density in the direction ψ at distance l, the first and the second J factor hold for annihilation and decay, respectively.

It is clear that, due to dilution of flux over distance, the most probable objects to search for signs of these particles are those that are closest to us, such as the Milky Way center and the surrounding dwarf galaxies. It is also clear that the calculation of J factors requires a very good understanding of the spatial density distribution of DM. For velocity-dependent annihilation, which can arise in models with light mediators and thus Sommerfeld enhanced cross sections, the J factor has to be modified to take into account the thermally averaged Sommerfeld enhancement factor [274], in which case the velocity distribution is also very important. At the annihilation site, the energy spectrum of the particle that is searched for is given by

$$\frac{dN}{dE} = \sum_f \frac{dN_f}{dE} \text{Br}_f\,. \tag{7.3}$$

In the above, it is assumed that DM annihilates or decays into a number of species f, which upon decaying generates the energy spectrum dN_f/dE. If N_f can decay into several species, the branching ratio Br_f for annihilation or decay into the species N must also be taken into account. These types of spectra have been calculated for a large range of DM masses and can be looked up in tables [275].

There are some very interesting channels, including annihilation specifically into $\gamma\gamma$, $Z\gamma$, and $h\gamma$. The common denominator of these channels is the appearance of at least one monochromatic photon, which would be detected as a line in the observed spectrum. Provided that the energy is large enough, there is no SM process that can generate such lines and this would therefore be a smoking gun for the indirect detection of decaying or annihilating DM. Current experiments used in the search for gamma rays due to DM annihilation or decay in various halos include Fermi-LAT [276], H.E.S.S [277, 278], and MAGIC [279, 280]. There have also been signals found in experimental data that could be interpreted as due to DM annihilation. These include an excess in the spectrum of photons in the few GeV range [281] and a line feature at 130 GeV [282]. While it is far from clear if the first signal can be explained by other effects, it is unclear if the line at 130 GeV is even real [273].

High energy neutrinos is another important indirect detection signal. Much like photons, DM may annihilate directly into neutrinos, producing a line feature, or generate a continuous spectra that could be observable in indirect detection experiments. Current experiments searching for high energy neutrinos due to DM annihilation in the Milky Way halo include the IceCube experiment [283] and ANTARES [284].

Finally, DM annihilations may generate cosmic rays that can be searched for. Several experiments have seen an anomalous number of cosmic ray positrons at higher energies [285–287]. The significance is that positrons tend to annihilate, and to explain the increase in the fraction of positrons to electrons, an unknown mechanism to inject high-energy positrons is required. Apart from DM, pulsars have also been proposed to solve the positron excess problem [273].

7.3 Effects of dark matter in the Sun

As the Sun revolves around the Milky Way, there will be a very large flux of DM particles passing through it. If DM interacts, some particles will scatter against the nuclei or electrons in the Sun and lose enough energy for its velocity to fall below the local escape velocity of the Sun, in which case it is said to have been captured. The accumulation of DM can after some time generate a very large number of captured DM particles. A large abundance of DM can have significant effects on the Sun. DM capture by stellar objects can significantly alter the transfer of heat inside them [288–291]. It turns out that DM particles with a cross section for scattering with nuclei in the ballpark of 10^{-36} cm^2 will travel about one orbit between each scattering event. When scattering occurs in the solar center, the kinetic energy of nuclei that it scatters against is much higher than in the outer regions of the Sun. Therefore, DM particles will scatter in the solar center and gain a large amount of kinetic energy, travel into the outskirts of the Sun, dump the energy by scattering against the colder targets, and fall back into the core to repeat the process. It was found that the heat transfer for this mechanism was extremely efficient relative to the conventional radiative and convective heat transfer effects in the Sun [289, 291, 292]. The idea was initially introduced to explain the solar neutrino problem, where only a third of the predicted flux of neutrinos was experimentally observed. Since the flux of neutrinos is very sensitive to the solar temperature, the slight cooling effect of DM could explain the deficit in the flux. However, it was later found that neutrino oscillations were the culprit when experiments became sensitive to neutral current processes such that muon and tau neutrinos originating from the Sun could be observed [293].

Today, there is a different solar problem that can be alleviated by the introduction of a large DM abundance. Detailed simulations of the solar atmosphere required a substantial change in the abundance of different elements in the Sun from previous values [294], which introduced a serious problem for helioseismology [295–299]. Since DM had been shown to possibly solve the solar neutrino problem, a large population of captured DM has naturally been proposed as a solution to the solar composition problem as well [300]. By the argument of altered helioseismology, the possibility of constraining DM via its effects has also been considered [301, 302].

If large amounts of DM are captured by the Sun and annihilate into SM particles, it is also possible to use the Sun as a laboratory for indirect detection of DM. Unfortunately, the only particles that is generated by such annihilation in most DM

models will be neutrinos, as other particles will immediately scatter with particles in the solar plasma and become lost. The flux of neutrinos in a detector will be given by

$$\frac{d\phi}{dE} = \frac{\Gamma_{\text{ann}}}{4\pi d^2} \sum_f \text{Br}_f \frac{dN_f}{dE} \,, \tag{7.4}$$

where Γ_{ann} is the annihilation rate, d is the distance from the Sun to the detector, and the sum yields the spectrum of neutrinos that is generated by DM annihilation channel f. The spectrum per annihilation event is possible to calculate as has been done in, e.g., Refs. [303, 304]. As the Sun is capable of capturing a very large number of DM particles over its lifetime and its distance is very close to the Earth, it is highly probable that the flux of neutrinos from annihilations in the Sun will be much greater than that generated by DM annihilations in the Milky Way and dwarf galaxy halos. Neutrinos that arise in the fusion processes in the Sun have energies below 20 MeV [305] and so a flux of neutrinos well beyond this energy range could be an indication that exotic physics such as DM annihilation is taking place. An important background for these searches is the high-energy neutrinos that are generated by high-energy cosmic rays that impact the Sun, producing a flux of high-energy neutrinos [306].

7.4 The capture process

When a DM particle is captured, kinematics dictates that it will generally have lost little energy in the initial scattering, or rather that it will be only loosely bound. The exception is if DM and its target have very similar masses such that the DM is able to transfer most of its kinetic energy. At this point, the process of thermalization takes place, in which a great number of subsequent scatters with the solar material takes place until the DM particle resides in the solar core. If the thermalization process is efficient, the greatly enhanced density of DM in the core will create a large annihilation rate.

The number of DM particles N that have been captured is governed by the differential equation

$$\dot{N} = C_\odot + (C_{\text{self cap}} - C_{\text{evap}})\, N - C_{\text{ann}} N^2 \,. \tag{7.5}$$

As is apparent, several terms go into this equation. Firstly, the capture rate of DM from the halo by solar nuclei enters as $C_\odot$. In case of self-interacting DM, already captured DM can capture incoming halo particles, which is given by $C_{\text{self cap}} N$. Since the Sun is a non-zero temperature body, solar nuclei can have very high velocities. It is thus possible that a high velocity nucleus transfers so much energy to the DM particle that its velocity becomes larger than the escape velocity, in which case it leaves the Sun. This is called evaporation, and its rate is given by $C_{\text{evap}} N$. Finally, the annihilation rate Γ_{ann} is given by $C_{\text{ann}} N^2/2$. The reason for

the absence of the factor 1/2 is that each annihilation event will destroy two DM particles.

When self-capture and evaporation is negligible, $\dot{N} = 0$ indicates that equilibrium between capture and equilibrium occurs when

$$\Gamma_{\rm ann} = \frac{1}{2} C_{\odot} \,. \tag{7.6}$$

This very important observation is crucial for indirect detection experiments. Intuitively, and as will be seen shortly, the capture rate is directly proportional to the DM-nucleus scattering cross section. Under this assumption, Eq. (7.4) indicates that the generated neutrino flux is directly proportional to the the scattering cross section. This has been used to place bounds on $\sigma_{\chi p}$ by using the non-observation of neutrinos in a number of neutrino experiments without the need for any other assumption than DM mass, scattering cross section, and the branching ratio into specific neutrino-generating channels [307–310].

The evolution formula is easily generalized to the case of multicomponent DM such as the case where the halo consist of particles χ with total number N, and anti-particles $\bar{\chi}$ with total number $\bar{N}$, as was considered in paper I. In this case, the two coupled equations are

$$\dot{N} = C_{\chi,\odot} + \left(C_{\rm self} - C^{\chi}_{\rm evap}\right) N + \bar{C}_{\rm self} \bar{N} - C_{\rm ann} N \bar{N} \,, \tag{7.7}$$

$$\dot{\bar{N}} = C_{\bar{\chi},\odot} + \left(C_{\rm self} - C^{\bar{\chi}}_{\rm evap}\right) \bar{N} + \bar{C}_{\rm self} N - C_{\rm ann} N \bar{N} \,. \tag{7.8}$$

The number evolution equation of each species contains an evaporation term and an annihilation term just as in the single component DM case and their capture rates may be different if they interact differently with the solar material. The new pieces that relate to self-interactions are $C_{\rm self}$ and $\bar{C}_{\rm self}$, which take into account the contribution from self-capture of halo particles on already captured particles, self-interactions leading to the target being ejected while the incoming particle is captured, and self-interactions leading to the ejection of the target while the incoming particle escapes. The individual contributions to these formulae will be discussed later.

The capture of DM by SM particles will in the following also be generalized to include the case where DM scatters inelastically, as this is the main theme of paper II and paper IV of this thesis. The number of publications related to solar capture and indirect detection using the Sun is far too numerous to point out here. In the inelastic DM case, which is relevant to this thesis, there have been some studies that consider the neutrino signal arising from inelastic DM capture [311–315] and it is also the model under consideration in paper II, where captures due to both endothermic and exothermic interactions was considered.

7.4.1 Solar capture, evaporation and annihilation

The capture rate of DM in the Sun by target i, being either free protons, electrons or larger atoms, is derived in Refs. [316, 317]. The starting point for the calculation

is to define the area of a sphere of radius R, where R is sufficiently large for the gravitational potential of the Sun to be negligible, through which flux of halo DM particles is given by

$$\frac{1}{4} u f(u)\, du\, d\cos^2\theta\,. \tag{7.9}$$

Here, u is the velocity and $f(u)$ is the galactic speed distribution, usually taken to be the one given in Eq. (5.7), and θ is the angle between $\vec{u}$ and the negative radial unit vector (pointing from R towards the solar center). Making the change of variables $J = ru\sin\theta$, such that $dJ^2 = R^2u^2 d\cos^2\theta$. The differential flux after integrating over the area of the sphere is given by

$$\pi \frac{f(u)}{u}\, du\, dJ^2\,. \tag{7.10}$$

When particles fall into the gravitational well, they accelerate to the velocity $w = \sqrt{u^2 + v_{\rm esc}^2(r)}$, where $v_{\rm esc}(r)$ is the local escape velocity at radius r. Considering a shell of thickness dr, the scattering probability of a single DM particle against the target i traversing the shell will be given by

$$P_{\rm scatter} = \frac{d\sigma}{dE_R} dE_R n_i(r) w\, dt\,, \tag{7.11}$$

where $d\sigma/dE_R$ is the differential cross section as defined in Eq. (3.60) and the time spent in the shell dt is given by

$$dt = 2\frac{dr}{w\sqrt{1 - \left(\frac{J}{rw}\right)^2}} \tag{7.12}$$

with a factor 2 due to twice passing the shell. This expression holds when the probability of scattering is very small in the first passing of the shell and $J < rw$ is guaranteed for any particle that can traverse the shell. The differential scattering rate is given by the differential flux multiplied by the scattering rate in a shell

$$dC_i = 2\pi n_i(r) \frac{f(u)}{u} \frac{d\sigma_i}{dE_R} \frac{1}{\sqrt{1 - \left(\frac{J}{rw}\right)^2}}\, dr\, du\, dJ^2\, dE_R\,. \tag{7.13}$$

Making contact with traditional definitions, the total capture rate per volume element is found by integration over u, E_R, and J^2 where the latter can be analytically integrated over in the range $0 < J^2 < r^2w^2$, as

$$\frac{dC_i}{dV} = \int_{u_{\rm min}}^{u_{\rm max}} dv\, \frac{f(u)}{u} w\Omega_i(r, w)\,, \tag{7.14}$$

where

$$\Omega_i(r, w) = w n_i(r) \int_{E_{\rm min}}^{E_{\rm max}} \frac{d\sigma_i}{dE_R} dE_R\,. \tag{7.15}$$

It is very common to use the form factor defined in Eq. (3.70) to analytically evaluate the integral over E_R as well. The integral limits are rather complicated

as $E_{\rm min}$ and $E_{\rm max}$ become difficult expressions in the case of inelastic DM. For example, the smallest $(-)$ and largest $(+)$ recoil energies possible in a collision with a nucleus of mass m_A are given by

$$E_R = \frac{\mu^2}{m_A} w^2 \left(1 \pm \sqrt{1 - \frac{\delta}{\mu w^2/2}}\right) - \frac{\mu}{m_A}\delta\,, \tag{7.16}$$

where δ is the mass splitting and μ is the reduced mass. Capture can only occur if the recoil energy carried by the nucleus is large enough for the incoming DM particle to become gravitationally bound,

$$E_{\rm capt} = m_\chi u^2/2 - \delta\,. \tag{7.17}$$

These expressions can then be used to figure out the range in u and E_R for which capture occurs [2]. They also hold in the case of elastic scattering by substituting $\delta \to 0$.

To prepare for later discussion, the solar capture rate in the spin-independent case can be cast on the form

$$C_{\rm Sun} = 4\pi \sum_i A_{{\rm eff},i}^2 \int_0^{R_\odot} dr\, r^2 \rho_i(r) \int_{u_{\rm min}}^{u_{\rm max}(r)} du\, u\, \mathcal{C} \tilde{f}(u) \int_{E_{\rm min}}^{E_{\rm max}} |F_i(E_R)|^2\, dE_R. \tag{7.18}$$

In reaching this expression, the velocity distribution $\tilde{f}(u)$ as defined in Eq. (6.4) has been plugged in as well as the the differential cross section in Eq. (3.60), where the form factor is realized to be a target dependent object. This gives rise to the factors $A_{{\rm eff},i}$ and $\mathcal{C}$ as defined in Eq. (6.6). As in the DD case, a similar expression holds for the spin-dependent case by removing the factor $A_{{\rm eff},i}$ and redefining $\mathcal{C}$ to account for the different definitions of σ_0 in Eq. (3.74) relative to the spin-independent case of Eq. (3.68).

Evaporation of DM will take place due to the fact that nuclei in the Sun have a temperature. When scattering takes place, there may be enough energy transferred to the DM particle for it to become gravitationally unbound. This phenomenon has been studied both numerically and analytically for scattering with nuclei in elastic [318–322] and in inelastic DM models [4], as well as for scattering against electrons [323, 324]. The general conclusion is that DM evaporation is completely irrelevant for $m_\chi \gtrsim 4$ GeV for elastic scattering against nuclei and $m_\chi \gtrsim 2$ GeV for scattering against electrons. There is of course a mild dependence on the scattering cross section, but its impact on the evaporation rate is surprisingly small compared to the change in mass, which is the crucial parameter.

Once captured, DM is usually assumed to fall into a thermal distribution instantaneously. Simple estimates show that this is the case for DM cross sections well below those that would generate DM abundances large enough for observable DM signals [312], but has also been shown numerically [325]. Leaving the discussion on

the thermalization process that drives particles into a distribution of captured DM for later, the annihilation rate is calculated as

$$\Gamma_{\rm ann} = \frac{\langle \sigma_{\rm ann} v \rangle}{2} \int f(\vec{x})^2 d^3x = \frac{1}{2} C_{\rm ann} N^2 \,, \tag{7.19}$$

where $f(\vec{x})$ is the DM density distribution at the location $\vec{x}$. The factor of $1/2$ appears in order to avoid double counting as there are, in the large N limit, only $N^2/2$ pairs of DM particles that can annihilate.

7.4.2 Self-capture and ejection

The aim of paper I was to study the abundance of DM that can arise in the case where the universal DM abundance is composed of DM and anti-DM whose capture rates are different. DM with large self-scattering cross sections, as motivated by the small scale structure problems, can become very relevant when an initial abundance has grown sufficiently large, ultimately leading to a self-capture rate that exceeds the rate of capture by solar material by orders of magnitude [326]. In principle, there is little difference between solar capture and self-capture and the capture rate is given by an expression identical to Eq. (7.14) except $\Omega(r, w)$ has to be redefined.

Considering the case where there are both particles and antiparticles in the DM halo and inside the Sun, there are a few interesting cases that can happen in a collision depending on how much kinetic energy the incoming DM particle has and how much energy it transfers to the target particle. Assuming that the scattering cross section is velocity and momentum independent, the probability of having a particular recoil E_R is uniformly distributed in the interval $E_{\rm min} < E_R < E_{\rm max}$. Therefore, the probability $\mathcal{P}_{\rm event}$ of a particular event to happen when a DM particle scatters will simply be a ratio between an energy range of recoil energies ΔE_R, divided by the full range in possible recoil energies,

$$\mathcal{P}_{\rm event} = \frac{\Delta E_R}{m_\chi w^2/2} \,. \tag{7.20}$$

The denominator is nothing but $E_{\rm max} - E_{\rm min}$, where Eq. (7.16) has been used, setting $\delta = 0$ and $\mu = m_\chi/2$. Therefore, the relevant $\Omega(r, w)$ for a specific event is given by

$$\Omega_{\rm event}(r, w) = \sigma f_\chi(r) \frac{\Delta E_R}{m_\chi w/2} \,, \tag{7.21}$$

where σ is the scattering cross section.

For self-capture, the largest allowed amount of energy to transfer is $m_\chi v_{\rm esc}(r)^2/2$, or the target is ejected, while the smallest amount of energy required to trap the incoming particle is $m_\chi u^2/2$. Thus, ΔE_R is the difference of the two and so

$$\Omega_{\rm sc}(r, w) = \sigma f_T(r) \frac{v_{\rm esc}(r)^2 - u^2}{w} \Theta(v_{\rm esc}(r) - u) \,, \tag{7.22}$$

where σ is the scattering cross section, f_T is the radial distribution of the target, and $\Theta(x)$ is the Heaviside function, which must here be put in by hand as an

incoming particle with $u > v_{\rm esc}$ must eject the target in order to become captured. The total rate for self-capture becomes

$$C_{\rm sc} N_T = n_{\rm inc}\sigma \int_0^{R_\odot} dr\, 4\pi r^2\, f_T(r) \int_0^{v_{\rm esc}(r)} du\, \frac{f(u)}{u} \left(v_{\rm esc}^2 - u^2\right). \tag{7.23}$$

Here, $n_{\rm inc}$ is the local galactic abundance of the incoming particle, and N_T the total number of captured target particles.

If the transferred energy exceeds $m_\chi v_{\rm esc}^2/2$, the target becomes gravitationally unbound and leaves the Sun, resulting in the ejection of a previously captured particle. In this case, $\Delta E_R = m_\chi u^2/2$ and

$$\Omega_{\rm eject}(r, w) = \sigma f_T(r) \frac{u^2}{w}. \tag{7.24}$$

The ejection rate is then given by

$$C_{\rm eject} N_T = n_{\rm inc}\sigma \int_0^{R_\odot} dr\, 4\pi r^2\, f_T(r) \int_0^{\infty} du\, \frac{f(u)}{u}. \tag{7.25}$$

One may also consider the case where the incoming particle ejects a target particle without becoming captured. However, this process requires the velocity of the incoming particle to be at least twice the escape velocity in the Sun, which implies that its velocity is much greater than the galactic escape velocity. This case was considered in paper I but shown to be negligible even if such high velocity particles exist in the halo, at least using the standard halo model. One can also define the exchange rate, which is the rate at which a particle ejects a target particle and becoming trapped in the process. This process is only interesting when the incoming and target particles are different. Again, it was shown in paper I that, due to the low velocity of halo particles relative to the escape velocity, the ejection of a target will certainly lead to capture of the incoming particle, and so the exchange rate is given by

$$C_{\rm exch} N_T = C_{\rm eject} N_T. \tag{7.26}$$

If ejection without capture occurs, the exchange rate is given by the above minus the rate for ejection without capture.

The constants $C_{\rm self}$ and $\bar{C}_{\rm self}$ in Eq. (7.7) are calculated by choosing appropriate targets and cross sections in the relations above. Neglecting ejection without capture, the parameter C gets a positive contribution from $\Omega_{\rm sc}$ and a negative contribution from $C_{\rm exch}$, while $\bar{C}$ gets only a positive contribution from $C_{\rm exch}$. Scenarios beyond the model of particles and antiparticles but rather where DM is made up of two distinct particles with different masses where the two species interact strongly has also been studied [327].

7.5 Thermalization

As is apparent from the discussion regarding both the annihilation rate and self-interaction related phenomena, the spatial distribution in the Sun is important to understand. The shape of the distribution was first studied properly when attempts were made to reconcile the solar neutrino problem with increased energy transport by DM in the Sun [291, 319, 328]. In the simple elastic DM case, the radial distribution depends on whether DM is in local thermal equilibrium or not. As discussed in Ref. [291], this is (somewhat) decided by the Knudsen number, which measures the length travelled between collisions and is given by

$$K = \frac{l}{r_\chi}\,, \tag{7.27}$$

where l is the mean free path travelled and r_χ is a number representative of the size of the DM distribution. The caveat to this is that heavy DM travels much slower than the surrounding nuclei with which it collides and will therefore scatter many times more during one mean free path length. Nevertheless, it gives a good indication on whether one is working in the local thermal equilibrium or isothermal regime.

In the limit of small mean free paths, DM is in local thermal equilibrium at each radius within the solar interior. The distribution has in this case been derived to first order in a spherical harmonics expansion of the Boltzmann equation with a collision operator where DM is coupled to the surrounding nuclei (but not to itself). The distribution is in this limit given in Ref. [291] and is a quite complicated history that depends on the temperature gradient. It is also useful only for DM with cross sections greater than $\sim 10^{-36}$ cm^2 or so, depending on whether scattering is spin-independent or spin-dependent.

The usual case to consider is that of Knudsen numbers well beyond unity. The distribution then becomes isothermal and it can be calculated under the assumption of being a Boltzmann distribution as in, e.g., Ref. [318],

$$n_{\rm iso}(\vec{r}) = n_0 e^{-m_\chi \phi(\vec{r})/T_c}\,, \tag{7.28}$$

where

$$\phi(\vec{r}) = \int_0^r G\frac{M(r)}{r^2}dr' \approx \frac{2\pi G\rho_c r^2}{3}\,, \tag{7.29}$$

is the gravitational potential assuming that the density is constant and equal to that of the solar core. The constant G is the gravitational constant, while ρ_c and T_c are the solar core density and temperature respectively. The above defines the usual parametrization of the isothermal distribution as

$$n_{\rm ISO}(\vec{r}) = n_0 e^{-r^2/r_\chi^2}\,, \tag{7.30}$$

where $n_0 = \pi^{-3/2} r_\chi^{-3} N$ and $r_\chi = 3T_c/2\pi G\rho_c m_\chi$. For a DM particle with mass $m_\chi = 10$ GeV, the radial distribution extends no more than a few percent of the

solar radius from $r = 0$ and its size decreases with increasing DM mass, motivating the approximation of setting the density and temperature to be equal to the solar core values.

Given the above, thermalization in the elastic case is under control and is generally assumed, with well defined radial distributions in each case for the Knudsen number. However, this is definitely not the case for inelastic DM. In the theory of inelastic DM, the mass separation between the two states is generally considered of the order tens to hundreds of keV while the solar core temperature is roughly 1.4 keV. The fraction of the excited DM particle χ_2 to the lower state χ_1 in thermal equilibrium is exponentially suppressed by a factor $e^{-\delta/T}$, which is essentially zero for interesting values of δ. This is due to the fact that the nuclei with velocities large enough to collide against a χ_1 and produce the χ_2 live way off in the exponentially suppressed region of the Boltzmann distribution, while the χ_2 can scatter against any nucleus, Boltzmann suppressed or not. When an inelastic DM particle is captured by the Sun, it will however carry a significant amount of kinetic energy itself. As long as it still retains some of this energy, it can scatter against at least the heavier elements in the Sun until it has reached some threshold, at which point it becomes stuck in an orbit out of which it will never scatter. Taking all of this into account, it is only natural to expect that inelastic DM does not thermalize in the Sun and that its distribution is significantly diluted relative to the case of elastic DM, which has a strong impact on the annihilation rate.

Paper IV studies the thermalization process of inelastic DM using a method with a similar approach to that of Ref. [319], which was later used to study also the effective theory framework [321] and leptophilic DM models [324], all in the context of finding when evaporation depletes the captured DM abundance. When a DM particle is captured by the Sun, it will stay in an orbit characterized by a fixed energy E and angular momentum L. The fact that a DM particle with a sufficiently small scattering cross section completes many orbits between each scattering event allows one to neglect precisely where the particle entered its orbit, as the statistical time spent within a shell in the Sun is given by the fraction of the time it takes to travel through the shell and the time it takes to complete half of an orbit. The distribution can thus be defined in the phase-space defined by the variables E and L by discretization into a number of states α, labelling the discrete distribution f_α. Given a distribution in this space, the radial distribution of particles in a given orbit is found by the total number of particles multiplied by the fraction of time spent at a particular radius. The full radial distribution is then found by summing the radial distributions from each state.

The distribution for a DM species without self-interactions will evolve according to

$$\dot{f}_\alpha = C_\alpha + \sum_\beta \Sigma_{\beta\to\alpha} f_\beta - f_\alpha \sum_\beta (1 + \delta_{\alpha\beta})\Gamma_{\alpha\beta} f_\beta \,, \tag{7.31}$$

where $\dot{f}_\alpha$ is the change in the number of particles in state α. The first term on the right-hand side corresponds to capture of halo particles into the state α, the

second describes transitions between different states as DM particles scatter against solar material, and the last term describes the annihilation of particles from states α and β. The reason for a factor 2 in the case where $\beta = \alpha$ is due to the fact that two particles are annihilated in the same state. For $\beta \neq \alpha$, one particle is removed from the state α while the second particle is removed in the equation where α and β are interchanged. The annihilation term is dropped because it induces non-linear effects that makes solving the system over a solar lifetime a very computationally expensive task. There are then two ways one can go on about calculating distributions. Firstly, one can use the Green's function for the problem and write the solution in matrix form as

$$\vec{f}(t) = \int_0^t e^{\Gamma(t-t')} \vec{C}_\odot dt' \,. \tag{7.32}$$

Upon normalization, this will give the radial distribution taking into account particles that were continously added to the distribution. Secondly, it can be interesting to follow a given initial distribution, in which case C_α is dropped and the final distribution is given by

$$\vec{f}(t) = e^{\Gamma t} \vec{f}(0) \,, \tag{7.33}$$

where $f(0)$ is the initial distribution. Although this looks simple, discretizing the phase-space into N states implies that Γ is an $N \times N$ matrix, which leads to a fairly time consuming matrix exponential to calculate. For inelastic DM, this is a $2N \times 2N$ matrix since f_α willl contain N states related to χ_1 and N states related to χ_2.

In principle, the calculation of C_α can be done using Eq. (7.13). Straight forwardly performing this integral results in the loss of any information of the outgoing DM particle except for the fact that it is gravitationally bound to the Sun. The energy and angular momentum of the outgoing DM particle can however be determined entirely in terms of the parameters that are integrated over. Therefore, discretizing the integral allows for the calculation of exactly how many particles will be captured into each state, which determines C_α. This is also simplified by the fact that the kinetic energies of solar nuclei are negligible compared to that of the incoming DM particle.

When calculating the scattering from β to α, the atomic target can no longer be considered stationary and their distribution must therefore be integrated over. The assumption that a particle travels many orbits between each scattering event allows for the rate of transitions between states to be calculated by dividing the Sun into a series of concentric shells of radii r_i. The scattering rate between states is then the product of the total scattering rate inside each shell $\mathcal{R}(r_i)$, the fraction of the time spent in each shell $\mathcal{T}(r_i)$, and the probability that the particle enters into the given α-state $\mathcal{P}_{\beta\to\alpha}(r_i)$, summed over all shells that the particle in state β traverses. Therefore, the off-diagonal elements of $\Gamma_{\beta\to\alpha}$ are given by

$$\Gamma_{\beta\to\alpha} = \sum_i \mathcal{R}(r_i)\mathcal{T}(r_i)\mathcal{P}_{\beta\to\alpha}(r_i) \,. \tag{7.34}$$

The diagonal elements of $\Gamma_{\beta\to\alpha}$ will be the negative of the sum of all off-diagonal elements in the corresponding column. This corresponds to the total rate at which particles scatter out of the state α into all other states.

An alternative way of sampling the $\Gamma_{\beta\to\alpha}$ matrix would be to randomly place particles in an orbit with a given E and L and follow its orbit over some time and take the average of final positions to sample the flow of particles. In hindsight, it would probably have been easier to randomize starting points in E and L for particles according to the fraction of particles that were captured into each state and follow the particles until they end up in a state out of which they will never scatter. This would be a much less computationally demanding way to study the thermalization process, since particles getting stuck in regions where the scattering rate exceeds the solar lifetime no longer need to be tracked, but can be distributed according to the fractional time spent at each radius as discussed above.

On a final note, the study of inelastic DM was generalized to the case where the scattering process on nuclei was governed by a light mediator and to the case where the lifetime of the χ_2 was short enough for it to not travel significantly before it decayed into a χ_1 and some light new particle that would escape the Sun [329]. The results indicated that there was a significant difference to the region in phase-space where particles were captured. However, very little difference, if any at all, was found in the final distribution of DM after the thermalization process had commenced.

7.5.1 A lower bound on the solar capture rate of dark matter

The way that the Sun captures DM depends on the galactic velocity distribution can be seen in Eq. (7.18). One may realize that the quantity $\mathcal{C}u\tilde{f}(u)$ enters both in the direct detection rate and in the solar capture rate. As was noted in Sec. 6.3, a positive signal in a DD experiment can give information on this quantity for a range of velocities corresponding to the range in recoil energies that the signal is measured in.

Armed with this knowledge, it is possible to plug the known part of the distribution function into the solar capture rate and derive the capture rate [330]

$$C_{\odot} \geq 4\pi \sum_i A_{\mathrm{eff},i}^2 \int_0^{R_\odot} dr\, r^2 \rho_i(r) \int_{u_{\mathrm{known}}} du \left(-\frac{d\tilde{\eta}(u)}{du}\right) \int_{E_{\mathrm{m}}(r,u)}^{E_{\mathrm{max}}(r,u)} |F(E_R)|^2\, dE_R. \tag{7.35}$$

Here, u_{known} is the range in velocities in which the velocity distribution is known. In the idealized case, this will be the full velocity range from $v_{\mathrm{thr}} = \sqrt{m_A E_{\mathrm{thr}}/2\mu^2}$ to infinity where according to Eq. (6.2), v_{thr} is the lowest velocity that can give rise to a detectable recoil energy, the smallest of which is set by the threshold energy $E_R = E_{\mathrm{thr}}$ in the experiment. This fact alone implies that the capture rate will be a lower bound on the capture rate as the total capture rate is found by integrating over the full velocity distribution and the part belonging to the smallest velocities

is not possible to probe in DD experiments since the recoil energies produced by these particles fall below $E_{\rm thr}$. The upper end of the integral will probably also be cut short as there are very few particles capable of producing large enough recoils to probe this region of the velocity distribution although this depends on the actual speed distribution. Assuming equilibrium between capture and annihilation, the lower bound on the capture rate is equivalent to a lower bound on the annihilation rate, which can then be used to place bounds on the annihilation cross section in a halo-independent fashion. However, it is important to point out that the underlying assumption here is that the Earth and the Sun see the same velocity distribution, which is not completely true since the earth revolves around the Sun. On the other hand, it can be argued that this should affect the velocity distributions mildly and mainly in the lowest velocity range.

The main idea of Paper II was to generalize this setting to the case of inelastic DM. This is not straight forward because of different scattering kinematics. Remembering from the discussion in Sec. 6.3 that $\eta(E_R)$ will have a maximum at some non-zero value $(E_R)_{\rm min}$, some recoil energy below $(E_R)_{\rm min}$ and some recoil energy above $(E_R)_{\rm min}$ correspond to the same value of $\eta(v_m)$. Therefore, this minimal recoil energy should be observed and the signal determined to be due to inelastic scattering. In a range in recoil energies either above or below $(E_R)_{\rm min}$, Eq. (6.8) does provide a unique relation between the recoil energy and v_m, which allows for some part of the velocity distribution to be derived using Eq. (6.11). Unfortunately, for the case where the halo consists of only χ, the velocity must generally be large, and increasing with larger δ, for scattering to possibly occur at all in a DD experiment. Thus, if δ is large enough, most of the velocity distribution is hidden and the lower bound on the capture rate is therefore small. For exothermic scattering however, which will take place if the halo contains a significant fraction of χ^*, even zero velocity DM will induce a large recoil energy in the DD experiment. In this case, it is possible (at least kinematically) to probe the entire velocity distribution, but again one should keep in mind that at least the lowest velocity region in the galactic DM velocity distribution can be significantly distorted by the Earth's orbital velocity around the Sun.

Chapter 8

Summary and conclusions

The discussion has to this point been centered around placing the papers of Part II into context. First, various sources for evidence of the existence of DM were reviewed, followed by a short discussion on standard model problems, for which possible solutions involve new particles that may play the role of DM. Then, various ways to introduce interactions between the SM and DM were discussed along with the proper treatment of a particular model of inelastic DM and a discussion regarding its peculiar scattering properties. The non-relativistic framework that is used to describe scattering processes between DM and SM particles was then introduced. The cosmological model was then presented, which ultimately leads to Boltzmann equations that describe the time evolution of number densities of DM in an expanding Universe. Next up was a discussion around the theory of DM halos and what is known about their properties as well as a presentation of the small scale structure problems and their possible solutions. Direct detection was then discussed, including the different effects of DM scattering inelastically as well as halo-independent methods. Finally, indirect detection was discussed with an extensive presentation of the current knowledge of solar capture and the observables that can be probed as DM is captured by the Sun. Each paper in Part II was also explicitly placed into context wherever the discussion was directly related.

In Paper I, the solar capture process is discussed in a scenario where the total abundance of DM in the Universe is made up in equal parts of particles and antiparticles. The goal was to see whether a large enough abundance can develop due to differences in capture rates of each species to solve the solar composition problem despite annihilation taking place. The importance of this setting is that only asymmetric DM models had previously been considered, while it was here shown that thermal relic DM can also do the job.

In paper II, the capture of inelastic DM by the Sun is considered. The goal was primarily to extend a previous study to find a lower bound on the solar capture rate, and through it a lower bound on the neutrino flux in neutrino experiments on Earth, to cover the inelastic DM scenario. The paper also discusses capture

via endothermic and exothermic reactions as well as the DM properties that can be detected by signals in multiple direct detection experiments. It is found that a direct detection signal due to exothermic DM can give information on essentially all of the weighted DM halo velocity distribution, while only the very high velocity part can be extracted for endothermic scattering, depending of course on the mass splitting δ and the actual velocity distribution. A signal in one experiment with a distinct minimum in the spectral function η as a function of E_R can relate the mass splitting to the DM mass, while signals with minima in two experiments with different targets may be used to determine both the DM mass and the mass splitting. Finally, the framework is demonstrated using the standard halo model and reasonable assumptions on the DM halo. The effects of isospin violation on the lower bound was also investigated.

In Paper III, self-interacting inelastic DM was considered in the context of solving the small scale structure problems. The set of differential equations necessary to be solved in order to calculate scattering cross sections has been found extremely numerically unstable. It is also difficult to reconcile models of this type with the number of relativistic degrees of freedom in the early Universe, and direct detection bounds. Here, a method is developed that makes the system of equations much less prone to numerical issues. The relative abundance of the heavier and lighter states are also studied. It is found that the self-scattering cross section can be large enough to solve the small scale structure problems. It is also found that it is possible to design scenarios where the abundance of the heavier state is very small, which avoids bounds from direct detection and allows the mediator to decay fast enough to not spoil Big Bang nucleosynthesis.

In Paper IV, the thermalization process of inelastic DM is studied to investigate whether the distribution of inelastic DM develops into a configuration where the annihilation rate can be assumed to be in equilibrium with the capture rate, which is a very important assumption for indirect detection experiments and to find whether evaporation due to downscattering is important to take into account. It is found that the distribution never really reaches a stationary state, but quickly reaches a state that develops very slowly. While it is not shown explicitly, it is found that in a large part of parameter space, there is good reason to believe that equilibrium between capture and annihilation has occurred in a large part of parameter space. It is also found that evaporation induced by downscattering has a very small effect on the number density evolution.

Bibliography

[1] M. Blennow and S. Clementz, *Asymmetric capture of Dirac dark matter by the Sun*, JCAP **1508**, 036 (2015), 1504.05813.

[2] M. Blennow, S. Clementz and J. Herrero-Garcia, *Pinning down inelastic dark matter in the Sun and in direct detection*, JCAP **1604**, 004 (2016), 1512.03317.

[3] M. Blennow, S. Clementz and J. Herrero-Garcia, *Self-interacting inelastic dark matter: A viable solution to the small scale structure problems*, JCAP **1703**, 048 (2017), 1612.06681.

[4] M. Blennow, S. Clementz and J. Herrero-Garcia, *The distribution of inelastic dark matter in the Sun*, Eur. Phys. J. **C78**, 386 (2018), 1802.06880.

[5] F. Zwicky, *Die Rotverschiebung von extragalaktischen Nebeln*, Helvetica Physica Acta **6**, 110 (1933).

[6] G. Bertone and D. Hooper, *History of dark matter*, Rev. Mod. Phys. **90**, 045002 (2018), 1605.04909.

[7] B. Pontecorvo, *Neutrino Experiments and the Problem of Conservation of Leptonic Charge*, Sov. Phys. JETP **26**, 984 (1968), [Zh. Eksp. Teor. Fiz.53,1717(1967)].

[8] R. D. Peccei, *The Strong CP problem and axions*, Lect. Notes Phys. **741**, 3 (2008), hep-ph/0607268.

[9] C. W. F. Everitt *et al.*, *Gravity Probe B: Final Results of a Space Experiment to Test General Relativity*, Phys. Rev. Lett. **106**, 221101 (2011), 1105.3456.

[10] M. Bartelmann, *Gravitational Lensing*, Class. Quant. Grav. **27**, 233001 (2010), 1010.3829.

[11] LIGO Scientific, Virgo, B. P. Abbott *et al.*, *Observation of Gravitational Waves from a Binary Black Hole Merger*, Phys. Rev. Lett. **116**, 061102 (2016), 1602.03837.

[12] LIGO Scientific, Virgo, B. Abbott *et al.*, *GW170817: Observation of Gravitational Waves from a Binary Neutron Star Inspiral*, Phys. Rev. Lett. **119**, 161101 (2017), 1710.05832.

[13] Event Horizon Telescope, K. Akiyama *et al.*, *First M87 Event Horizon Telescope Results. I. The Shadow of the Supermassive Black Hole*, Astrophys. J. **875**, L1 (2019).

[14] K. Freese, *Review of Observational Evidence for Dark Matter in the Universe and in upcoming searches for Dark Stars*, EAS Publ. Ser. **36**, 113 (2009), 0812.4005.

[15] L. Bergstrom, *Dark Matter Evidence, Particle Physics Candidates and Detection Methods*, Annalen Phys. **524**, 479 (2012), 1205.4882.

[16] S. Sinclaire, *The mass of the virgo cluster*, Astrophys. J. **83**, 23 (1936).

[17] K. C. Freeman, *On the disks of spiral and SO Galaxies*, Astrophys. J. **160**, 811 (1970).

[18] V. C. Rubin and W. K. Ford, Jr., *Rotation of the Andromeda Nebula from a Spectroscopic Survey of Emission Regions*, Astrophys. J. **159**, 379 (1970).

[19] J. Einasto, A. Kaasik and E. Saar, *Dynamic evidence on massive coronas of galaxies*, Nature **250** (1974).

[20] J. P. Ostriker, P. J. E. Peebles and A. Yahil, *The size and mass of galaxies, and the mass of the universe*, Astrophys. J. **193**, L1 (1974).

[21] P. V. P. Cunha and C. A. R. Herdeiro, *Shadows and strong gravitational lensing: a brief review*, Gen. Rel. Grav. **50**, 42 (2018), 1801.00860.

[22] M. Bartelmann and P. Schneider, *Weak gravitational lensing*, Phys. Rept. **340**, 291 (2001), astro-ph/9912508.

[23] H. Hoekstra and B. Jain, *Weak Gravitational Lensing and its Cosmological Applications*, Ann. Rev. Nucl. Part. Sci. **58**, 99 (2008), 0805.0139.

[24] Y. T. Lin *et al.*, *Baryon Content of Massive Galaxy Clusters at z=0-0.6*, Astrophys. J. **745**, L3 (2012), 1112.1705.

[25] SPT, I. Chiu *et al.*, *Baryon content of massive galaxy clusters at $0.57 < z < 1.33$*, Mon. Not. Roy. Astron. Soc. **455**, 258 (2016), 1412.7823.

[26] D. Eckert *et al.*, *The XXL Survey. XIII. Baryon content of the bright cluster sample*, Astron. Astrophys. **592**, A12 (2016), 1512.03814.

[27] D. Clowe *et al.*, *A direct empirical proof of the existence of dark matter*, Astrophys. J. **648**, L109 (2006), astro-ph/0608407.

[28] S. Mao, *Astrophysical Applications of Gravitational Microlensing*, Res. Astron. Astrophys. **12**, 947 (2012), 1207.3720.

[29] S. Rahvar, *Gravitational microlensing I: A unique astrophysical tool*, Int. J. Mod. Phys. **D24**, 1530020 (2015), 1503.04271.

[30] EROS-2, P. Tisserand *et al.*, *Limits on the Macho Content of the Galactic Halo from the EROS-2 Survey of the Magellanic Clouds*, Astron. Astrophys. **469**, 387 (2007), astro-ph/0607207.

[31] L. Wyrzykowski *et al.*, *The OGLE View of Microlensing towards the Magellanic Clouds. IV. OGLE-III SMC Data and Final Conclusions on MACHOs*, Mon. Not. Roy. Astron. Soc. **416**, 2949 (2011), 1106.2925.

[32] A. Einstein, *Cosmological Considerations in the General Theory of Relativity*, Sitzungsber. Preuss. Akad. Wiss. Berlin (Math. Phys.) **1917**, 142 (1917).

[33] R. A. Alpher and R. Herman, *Evolution of the Universe*, Nature **162**, 774 EP (1948).

[34] D. J. Fixsen *et al.*, *Cosmic microwave background dipole spectrum measured by the COBE FIRAS*, Astrophys. J. **420**, 445 (1994).

[35] WMAP, C. L. Bennett *et al.*, *Nine-Year Wilkinson Microwave Anisotropy Probe (WMAP) Observations: Final Maps and Results*, Astrophys. J. Suppl. **208**, 20 (2013), 1212.5225.

[36] Planck, P. A. R. Ade *et al.*, *Planck 2015 results. XIII. Cosmological parameters*, Astron. Astrophys. **594**, A13 (2016), 1502.01589.

[37] P. J. E. Peebles and J. T. Yu, *Primeval adiabatic perturbation in an expanding universe*, Astrophys. J. **162**, 815 (1970).

[38] COBE, G. F. Smoot *et al.*, *Structure in the COBE differential microwave radiometer first year maps*, Astrophys. J. **396**, L1 (1992).

[39] S. L. Glashow, *Partial Symmetries of Weak Interactions*, Nucl. Phys. **22**, 579 (1961).

[40] P. W. Higgs, *Broken Symmetries and the Masses of Gauge Bosons*, Phys. Rev. Lett. **13**, 508 (1964).

[41] F. Englert and R. Brout, *Broken Symmetry and the Mass of Gauge Vector Mesons*, Phys. Rev. Lett. **13**, 321 (1964), [,157(1964)].

[42] G. S. Guralnik, C. R. Hagen and T. W. B. Kibble, *Global Conservation Laws and Massless Particles*, Phys. Rev. Lett. **13**, 585 (1964).

[43] S. Weinberg, *A Model of Leptons*, Phys. Rev. Lett. **19**, 1264 (1967).

[44] A. Salam, *Weak and Electromagnetic Interactions*, Conf. Proc. **C680519**, 367 (1968).

[45] M. Gell-Mann, *A Schematic Model of Baryons and Mesons*, Phys. Lett. **8**, 214 (1964).

[46] G. Zweig, An SU(3) model for strong interaction symmetry and its breaking. Version 2, Developments in the quark theory of hadrons. vol. 1. 1964 - 1978., edited by D. Lichtenberg and S. P. Rosen, pp. 22–101, 1964.

[47] Belle, S. K. Choi *et al.*, *Observation of a resonance-like structure in the pi+- psi-prime mass distribution in exclusive B —¿ K pi+- psi-prime decays*, Phys. Rev. Lett. **100**, 142001 (2008), 0708.1790.

[48] LHCb, R. Aaij *et al.*, *Observation of the resonant character of the $Z(4430)^-$ state*, Phys. Rev. Lett. **112**, 222002 (2014), 1404.1903.

[49] D. J. Gross and F. Wilczek, *Ultraviolet Behavior of Nonabelian Gauge Theories*, Phys. Rev. Lett. **30**, 1343 (1973).

[50] H. D. Politzer, *Reliable Perturbative Results for Strong Interactions?*, Phys. Rev. Lett. **30**, 1346 (1973), [,274(1973)].

[51] ATLAS, G. Aad *et al.*, *Observation of a new particle in the search for the Standard Model Higgs boson with the ATLAS detector at the LHC*, Phys. Lett. **B716**, 1 (2012), 1207.7214.

[52] CMS, S. Chatrchyan *et al.*, *Observation of a new boson at a mass of 125 GeV with the CMS experiment at the LHC*, Phys. Lett. **B716**, 30 (2012), 1207.7235.

[53] Super-Kamiokande, Y. Fukuda *et al.*, *Measurement of the flux and zenith angle distribution of upward through going muons by Super-Kamiokande*, Phys. Rev. Lett. **82**, 2644 (1999), hep-ex/9812014.

[54] SNO, Q. R. Ahmad *et al.*, *Measurement of the rate of $\nu_e + d \to p + p + e^-$ interactions produced by ^8B solar neutrinos at the Sudbury Neutrino Observatory*, Phys. Rev. Lett. **87**, 071301 (2001), nucl-ex/0106015.

[55] M. Drewes, *The Phenomenology of Right Handed Neutrinos*, Int. J. Mod. Phys. **E22**, 1330019 (2013), 1303.6912.

[56] S. P. Martin, *A Supersymmetry primer*, p. 1 (1997), hep-ph/9709356, [Adv. Ser. Direct. High Energy Phys.18,1(1998)].

[57] G. Jungman, M. Kamionkowski and K. Griest, *Supersymmetric dark matter*, Phys. Rept. **267**, 195 (1996), hep-ph/9506380.

[58] J. Ellis and K. A. Olive, *Supersymmetric Dark Matter Candidates*, p. 142 (2010), 1001.3651.

[59] J. M. Pendlebury *et al.*, *Revised experimental upper limit on the electric dipole moment of the neutron*, Phys. Rev. **D92**, 092003 (2015), 1509.04411.

[60] B. Graner *et al.*, *Reduced Limit on the Permanent Electric Dipole Moment of Hg199*, Phys. Rev. Lett. **116**, 161601 (2016), 1601.04339, [Erratum: Phys. Rev. Lett.119,no.11,119901(2017)].

[61] R. J. Crewther *et al.*, *Chiral Estimate of the Electric Dipole Moment of the Neutron in Quantum Chromodynamics*, Phys. Lett. **88B**, 123 (1979), [Erratum: Phys. Lett.91B,487(1980)].

[62] R. D. Peccei and H. R. Quinn, *CP Conservation in the Presence of Instantons*, Phys. Rev. Lett. **38**, 1440 (1977).

[63] S. Weinberg, *A New Light Boson?*, Phys. Rev. Lett. **40**, 223 (1978).

[64] F. Wilczek, *Problem of Strong P and T Invariance in the Presence of Instantons*, Phys. Rev. Lett. **40**, 279 (1978).

[65] J. E. Kim and G. Carosi, *Axions and the Strong CP Problem*, Rev. Mod. Phys. **82**, 557 (2010), 0807.3125.

[66] A. D. Sakharov, *Violation of CP Invariance, C asymmetry, and baryon asymmetry of the universe*, Pisma Zh. Eksp. Teor. Fiz. **5**, 32 (1967), [Usp. Fiz. Nauk161,no.5,61(1991)].

[67] P. B. Arnold and L. D. McLerran, *Sphalerons, Small Fluctuations and Baryon Number Violation in Electroweak Theory*, Phys. Rev. **D36**, 581 (1987).

[68] M. B. Gavela *et al.*, *Standard model CP violation and baryon asymmetry*, Mod. Phys. Lett. **A9**, 795 (1994), hep-ph/9312215.

[69] K. Petraki and R. R. Volkas, *Review of asymmetric dark matter*, Int. J. Mod. Phys. **A28**, 1330028 (2013), 1305.4939.

[70] S. Davidson, E. Nardi and Y. Nir, *Leptogenesis*, Phys. Rept. **466**, 105 (2008), 0802.2962.

[71] K. Cheung *et al.*, *Global Constraints on Effective Dark Matter Interactions: Relic Density, Direct Detection, Indirect Detection, and Collider*, JCAP **1205**, 001 (2012), 1201.3402.

[72] J. Brod *et al.*, *Effective Field Theory for Dark Matter Direct Detection up to Dimension Seven*, JHEP **10**, 065 (2018), 1710.10218.

[73] G. Busoni *et al.*, *On the Validity of the Effective Field Theory for Dark Matter Searches at the LHC*, Phys. Lett. **B728**, 412 (2014), 1307.2253.

[74] G. Busoni *et al.*, *On the Validity of the Effective Field Theory for Dark Matter Searches at the LHC, Part II: Complete Analysis for the s-channel*, JCAP **1406**, 060 (2014), 1402.1275.

[75] J. Abdallah *et al.*, *Simplified Models for Dark Matter Searches at the LHC*, Phys. Dark Univ. **9-10**, 8 (2015), 1506.03116.

[76] V. Silveira and A. Zee, *Scalar phantoms*, Phys. Lett. **161B**, 136 (1985).

[77] J. McDonald, *Gauge singlet scalars as cold dark matter*, Phys. Rev. **D50**, 3637 (1994), hep-ph/0702143.

[78] L. B. Okun, *Limits on electrodynamics: paraphotons?*, Sov. Phys. JETP **56**, 502 (1982), [Zh. Eksp. Teor. Fiz.83,892(1982)].

[79] P. Galison and A. Manohar, *Two Z's or not two Z's?*, Physics Letters B **136**, 279 (1984).

[80] B. Holdom, *Two U(1)'s and Epsilon Charge Shifts*, Phys. Lett. **166B**, 196 (1986).

[81] K. S. Babu, C. F. Kolda and J. March-Russell, *Implications of generalized Z - Z-prime mixing*, Phys. Rev. **D57**, 6788 (1998), hep-ph/9710441.

[82] D. Feldman, Z. Liu and P. Nath, *The Stueckelberg Z-prime Extension with Kinetic Mixing and Milli-Charged Dark Matter From the Hidden Sector*, Phys. Rev. **D75**, 115001 (2007), hep-ph/0702123.

[83] E. Izaguirre and I. Yavin, *New window to millicharged particles at the LHC*, Phys. Rev. **D92**, 035014 (2015), 1506.04760.

[84] J. L. Feng, J. Smolinsky and P. Tanedo, *Detecting dark matter through dark photons from the Sun: Charged particle signatures*, Phys. Rev. **D93**, 115036 (2016), 1602.01465.

[85] A. Falkowski, J. Juknevich and J. Shelton, *Dark Matter Through the Neutrino Portal*, (2009), 0908.1790.

[86] T. Yanagida, *Horizontal gauge symmetry and masses of neutrinos*, Conf. Proc. **C7902131**, 95 (1979).

[87] R. N. Mohapatra and G. Senjanovic, *Neutrino Masses and Mixings in Gauge Models with Spontaneous Parity Violation*, Phys. Rev. **D23**, 165 (1981).

[88] J. Schechter and J. W. F. Valle, *Neutrino Masses in $SU(2) \times U(1)$ Theories*, Phys. Rev. **D22**, 2227 (1980).

[89] L. J. Hall, T. Moroi and H. Murayama, *Sneutrino cold dark matter with lepton number violation*, Phys. Lett. **B424**, 305 (1998), hep-ph/9712515.

[90] Y. Cui *et al.*, *Candidates for Inelastic Dark Matter*, JHEP **05**, 076 (2009), 0901.0557.

[91] S. Patra and S. Rao, *A Simple Model for Magnetic Inelastic Dark Matter (MiDM)*, (2011), 1112.3454.

[92] J. Kopp, T. Schwetz and J. Zupan, *Global interpretation of direct Dark Matter searches after CDMS-II results*, JCAP **1002**, 014 (2010), 0912.4264.

[93] J. J. Sakurai and J. Napolitano, *Modern quantum mechanics* (Addison-Wesley, 2011).

[94] L. D. Landau and E. Lifschitz, Quantum mechanics, nonrelativistic theory. 2-nd ed, 1965.

[95] J. R. Taylor *et al.*, The quantum theory of nonrelativistic collisions, 1972.

[96] R. Shankar, *Principles of quantum mechanics* (Springer Science, Business Media, 2012).

[97] M. Peskin and D. Schroeder, *An introduction to quantum field theory*, (1995).

[98] K. Petraki, M. Postma and M. Wiechers, *Dark-matter bound states from Feynman diagrams*, JHEP **06**, 128 (2015), 1505.00109.

[99] H. Yukawa, *On the Interaction of Elementary Particles I*, Proc. Phys. Math. Soc. Jap. **17**, 48 (1935), [Prog. Theor. Phys. Suppl.1,1(1935)].

[100] P. Agrawal *et al.*, *A Classification of Dark Matter Candidates with Primarily Spin-Dependent Interactions with Matter*, (2010), 1003.1912.

[101] H. Y. Cheng and C. W. Chiang, *Revisiting Scalar and Pseudoscalar Couplings with Nucleons*, JHEP **07**, 009 (2012), 1202.1292.

[102] S. P. Ahlen *et al.*, *Limits on Cold Dark Matter Candidates from an Ultralow Background Germanium Spectrometer*, Phys. Lett. **B195**, 603 (1987).

[103] K. Freese, J. A. Frieman and A. Gould, *Signal Modulation in Cold Dark Matter Detection*, Phys. Rev. **D37**, 3388 (1988).

[104] R. H. Helm, *Inelastic and Elastic Scattering of 187-Mev Electrons from Selected Even-Even Nuclei*, Phys. Rev. **104**, 1466 (1956).

[105] J. Engel, *Nuclear form-factors for the scattering of weakly interacting massive particles*, Phys. Lett. **B264**, 114 (1991).

[106] J. D. Lewin and P. F. Smith, *Review of mathematics, numerical factors, and corrections for dark matter experiments based on elastic nuclear recoil*, Astropart. Phys. **6**, 87 (1996).

[107] L. Vietze *et al.*, *Nuclear structure aspects of spin-independent WIMP scattering off xenon*, Phys. Rev. **D91**, 043520 (2015), 1412.6091.

[108] J. Engel, S. Pittel and P. Vogel, *Nuclear physics of dark matter detection*, Int. J. Mod. Phys. **E1**, 1 (1992).

[109] P. Klos *et al.*, *Large-scale nuclear structure calculations for spin-dependent WIMP scattering with chiral effective field theory currents*, Phys. Rev. **D88**, 083516 (2013), 1304.7684, [Erratum: Phys. Rev.D89,no.2,029901(2014)].

[110] XENON, E. Aprile *et al.*, *First results on the scalar WIMP-pion coupling, using the XENON1T experiment*, Phys. Rev. Lett. **122**, 071301 (2019), 1811.12482.

[111] J. L. Feng *et al.*, *Isospin-Violating Dark Matter*, Phys. Lett. **B703**, 124 (2011), 1102.4331.

[112] A. L. Fitzpatrick *et al.*, *The Effective Field Theory of Dark Matter Direct Detection*, JCAP **1302**, 004 (2013), 1203.3542.

[113] A. L. Fitzpatrick *et al.*, *Model Independent Direct Detection Analyses*, (2012), 1211.2818.

[114] R. Catena and B. Schwabe, *Form factors for dark matter capture by the Sun in effective theories*, JCAP **1504**, 042 (2015), 1501.03729.

[115] E. Del Nobile, *Complete Lorentz-to-Galileo dictionary for direct dark matter detection*, Phys. Rev. **D98**, 123003 (2018), 1806.01291.

[116] A. Friedman, *On the Curvature of space*, Z. Phys. **10**, 377 (1922), [Gen. Rel. Grav.31,1991(1999)].

[117] E. W. Kolb and M. S. Turner, *The Early Universe*, Front. Phys. **69**, 1 (1990).

[118] S. Weinberg, *Cosmology* (, 2008).

[119] R. K. Sachs and A. M. Wolfe, *Perturbations of a cosmological model and angular variations of the microwave background*, Astrophys. J. **147**, 73 (1967), [Gen. Rel. Grav.39,1929(2007)].

[120] M. Scrimgeour *et al.*, *The WiggleZ Dark Energy Survey: the transition to large-scale cosmic homogeneity*, Mon. Not. Roy. Astron. Soc. **425**, 116 (2012), 1205.6812.

[121] P. Laurent *et al.*, *A 14 h^{-3} Gpc^3 study of cosmic homogeneity using BOSS DR12 quasar sample*, JCAP **1611**, 060 (2016), 1602.09010.

[122] P. Brax, *What makes the Universe accelerate? A review on what dark energy could be and how to test it*, Rept. Prog. Phys. **81**, 016902 (2018).

[123] A. Einstein, *The Foundation of the General Theory of Relativity*, Annalen Phys. **49**, 769 (1916), [65(1916)].

[124] J. McDonald, *Thermally generated gauge singlet scalars as selfinteracting dark matter*, Phys. Rev. Lett. **88**, 091304 (2002), hep-ph/0106249.

[125] L. J. Hall *et al.*, *Freeze-In Production of FIMP Dark Matter*, JHEP **03**, 080 (2010), 0911.1120.

[126] N. Bernal *et al.*, *The Dawn of FIMP Dark Matter: A Review of Models and Constraints*, Int. J. Mod. Phys. **A32**, 1730023 (2017), 1706.07442.

[127] H. Mo, F. Van den Bosch and S. White, *Galaxy formation and evolution* (Cambridge University Press, 2010).

[128] A. Kravtsov and S. Borgani, *Formation of Galaxy Clusters*, Ann. Rev. Astron. Astrophys. **50**, 353 (2012), 1205.5556.

[129] A. Klypin, S. Trujillo-Gomez and J. Primack, *Halos and galaxies in the standard cosmological model: results from the Bolshoi simulation*, Astrophys. J. **740**, 102 (2011), 1002.3660.

[130] M. Vogelsberger *et al.*, *Introducing the Illustris Project: Simulating the coevolution of dark and visible matter in the Universe*, Mon. Not. Roy. Astron. Soc. **444**, 1518 (2014), 1405.2921.

[131] R. S. Somerville and R. Davé, *Physical Models of Galaxy Formation in a Cosmological Framework*, Ann. Rev. Astron. Astrophys. **53**, 51 (2015), 1412.2712.

[132] J. Silk, *Feedback in Galaxy Formation*, IAU Symp. **277**, 273 (2011), 1102.0283.

[133] J. F. Navarro, C. S. Frenk and S. D. M. White, *The Structure of cold dark matter halos*, Astrophys. J. **462**, 563 (1996), astro-ph/9508025.

[134] J. Einasto, Trudy Astrofizicheskogo Instituta Alma-Ata **5**, 87 (1965).

[135] J. E. Gunn and J. R. Gott, III, *On the Infall of Matter into Clusters of Galaxies and Some Effects on Their Evolution*, Astrophys. J. **176**, 1 (1972).

[136] R. Catena and P. Ullio, *A novel determination of the local dark matter density*, JCAP **1008**, 004 (2010), 0907.0018.

[137] M. Weber and W. de Boer, *Determination of the Local Dark Matter Density in our Galaxy*, Astron. Astrophys. **509**, A25 (2010), 0910.4272.

[138] M. Pato *et al.*, *Systematic uncertainties in the determination of the local dark matter density*, Phys. Rev. **D82**, 023531 (2010), 1006.1322.

[139] J. Bovy and S. Tremaine, *On the local dark matter density*, Astrophys. J. **756**, 89 (2012), 1205.4033.

[140] S. Garbari *et al.*, *A new determination of the local dark matter density from the kinematics of K dwarfs*, Mon. Not. Roy. Astron. Soc. **425**, 1445 (2012), 1206.0015.

[141] J. I. Read, *The Local Dark Matter Density*, J. Phys. **G41**, 063101 (2014), 1404.1938.

[142] S. Sivertsson *et al.*, *The local dark matter density from SDSS-SEGUE G-dwarfs*, Mon. Not. Roy. Astron. Soc. **478**, 1677 (2018), 1708.07836.

[143] S. Tremaine and J. Binney, *Galactic Dynamics* (Princeton University Press, 1987).

[144] L. Hernquist, *N-body realizations of compound galaxies*, Astrophys. J. Suppl. **86**, 389 (1993).

[145] A. K. Drukier, K. Freese and D. N. Spergel, *Detecting Cold Dark Matter Candidates*, Phys. Rev. **D33**, 3495 (1986).

[146] D. N. Spergel, *The Motion of the Earth and the Detection of weakly interacting massive particles*, Phys. Rev. **D37**, 1353 (1988).

[147] K. Freese, M. Lisanti and C. Savage, *Colloquium: Annual modulation of dark matter*, Rev. Mod. Phys. **85**, 1561 (2013), 1209.3339.

[148] T. Piffl *et al.*, *The RAVE survey: the Galactic escape speed and the mass of the Milky Way*, Astron. Astrophys. **562**, A91 (2014), 1309.4293.

[149] P. R. Kafle *et al.*, *On the Shoulders of Giants: Properties of the Stellar Halo and the Milky Way Mass Distribution*, Astrophys. J. **794**, 59 (2014), 1408.1787.

[150] G. Monari *et al.*, *The escape speed curve of the Galaxy obtained from Gaia DR2 implies a heavy Milky Way*, Astron. Astrophys. **616**, L9 (2018), 1807.04565.

[151] M. Vogelsberger *et al.*, *Phase-space structure in the local dark matter distribution and its signature in direct detection experiments*, Mon. Not. Roy. Astron. Soc. **395**, 797 (2009), 0812.0362.

[152] M. Kuhlen *et al.*, *Dark Matter Direct Detection with Non-Maxwellian Velocity Structure*, JCAP **1002**, 030 (2010), 0912.2358.

[153] F. S. Ling *et al.*, *Dark Matter Direct Detection Signals inferred from a Cosmological N-body Simulation with Baryons*, JCAP **1002**, 012 (2010), 0909.2028.

[154] I. Butsky *et al.*, *NIHAO project II: Halo shape, phase-space density and velocity distribution of dark matter in galaxy formation simulations*, Mon. Not. Roy. Astron. Soc. **462**, 663 (2016), 1503.04814.

[155] N. Bozorgnia *et al.*, *Simulated Milky Way analogues: implications for dark matter direct searches*, JCAP **1605**, 024 (2016), 1601.04707.

[156] J. S. Bullock and M. Boylan-Kolchin, *Small-Scale Challenges to the ΛCDM Paradigm*, Ann. Rev. Astron. Astrophys. **55**, 343 (2017), 1707.04256.

[157] J. F. Navarro, C. S. Frenk and S. D. M. White, *A Universal density profile from hierarchical clustering*, Astrophys. J. **490**, 493 (1997), astro-ph/9611107.

[158] B. Moore *et al.*, *Resolving the structure of cold dark matter halos*, Astrophys. J. **499**, L5 (1998), astro-ph/9709051.

[159] A. Klypin *et al.*, *Resolving the structure of cold dark matter halos*, Astrophys. J. **554**, 903 (2001), astro-ph/0006343.

[160] J. F. Navarro *et al.*, *The Inner structure of Lambda-CDM halos 3: Universality and asymptotic slopes*, Mon. Not. Roy. Astron. Soc. **349**, 1039 (2004), astro-ph/0311231.

[161] J. Diemand *et al.*, *Cusps in cold dark matter haloes*, Mon. Not. Roy. Astron. Soc. **364**, 665 (2005), astro-ph/0504215.

[162] J. Diemand *et al.*, *Clumps and streams in the local dark matter distribution*, Nature **454**, 735 (2008), 0805.1244.

[163] V. Springel *et al.*, *The Aquarius Project: the subhalos of galactic halos*, Mon. Not. Roy. Astron. Soc. **391**, 1685 (2008), 0809.0898.

[164] R. A. Flores and J. R. Primack, *Observational and theoretical constraints on singular dark matter halos*, Astrophys. J. **427**, L1 (1994), astro-ph/9402004.

[165] B. Moore, *Evidence against dissipationless dark matter from observations of galaxy haloes*, Nature **370**, 629 (1994).

[166] W. J. G. de Blok *et al.*, *Mass density profiles of LSB galaxies*, Astrophys. J. **552**, L23 (2001), astro-ph/0103102.

[167] W. J. G. de Blok and A. Bosma, *High-resolution rotation curves of low surface brightness galaxies*, Astron. Astrophys. **385**, 816 (2002), astro-ph/0201276.

[168] R. A. Swaters *et al.*, *The Central mass distribution in dwarf and low-surface brightness galaxies*, Astrophys. J. **583**, 732 (2003), astro-ph/0210152.

[169] J. D. Simon *et al.*, *High-resolution measurements of the halos of four dark matter-dominated galaxies: Deviations from a universal density profile*, Astrophys. J. **621**, 757 (2005), astro-ph/0412035.

[170] K. Spekkens and R. Giovanelli, *The Cusp/core problem in Galactic halos: Long-slit spectra for a large dwarf galaxy sample*, Astron. J. **129**, 2119 (2005), astro-ph/0502166.

[171] M. Spano *et al.*, *GHASP: An H-alpha kinematic survey of spiral and irregular galaxies. 5. Dark matter distribution in 36 nearby spiral galaxies*, Mon. Not. Roy. Astron. Soc. **383**, 297 (2008), 0710.1345.

[172] R. Kuzio de Naray, S. S. McGaugh and W. J. G. de Blok, *Mass Models for Low Surface Brightness Galaxies with High Resolution Optical Velocity Fields*, Astrophys. J. **676**, 920 (2008), 0712.0860.

[173] W. J. G. de Blok *et al.*, *High-Resolution Rotation Curves and Galaxy Mass Models from THINGS*, Astron. J. **136**, 2648 (2008), 0810.2100.

[174] F. Donato *et al.*, *A constant dark matter halo surface density in galaxies*, Mon. Not. Roy. Astron. Soc. **397**, 1169 (2009), 0904.4054.

[175] S. H. Oh *et al.*, *Dark and luminous matter in THINGS dwarf galaxies*, Astron. J. **141**, 193 (2011), 1011.0899.

[176] S. H. Oh *et al.*, *The central slope of dark matter cores in dwarf galaxies: Simulations vs. THINGS*, Astron. J. **142**, 24 (2011), 1011.2777.

[177] M. G. Walker and J. Penarrubia, *A Method for Measuring (Slopes of) the Mass Profiles of Dwarf Spheroidal Galaxies*, Astrophys. J. **742**, 20 (2011), 1108.2404.

[178] J. J. Adams *et al.*, *Dwarf Galaxy Dark Matter Density Profiles Inferred from Stellar and Gas Kinematics*, Astrophys. J. **789**, 63 (2014), 1405.4854.

[179] A. B. Newman *et al.*, *The Distribution of Dark Matter Over 3 Decades in Radius in the Lensing Cluster Abell 611*, Astrophys. J. **706**, 1078 (2009), 0909.3527.

[180] A. B. Newman *et al.*, *The Dark Matter Distribution in Abell 383: Evidence for a Shallow Density Cusp from Improved Lensing, Stellar Kinematic and X-ray Data*, Astrophys. J. **728**, L39 (2011), 1101.3553.

[181] A. B. Newman *et al.*, *The Density Profiles of Massive, Relaxed Galaxy Clusters: II. Separating Luminous and Dark Matter in Cluster Cores*, Astrophys. J. **765**, 25 (2013), 1209.1392.

[182] A. A. Klypin *et al.*, *Where are the missing Galactic satellites?*, Astrophys. J. **522**, 82 (1999), astro-ph/9901240.

[183] B. Moore *et al.*, *Dark matter substructure within galactic halos*, Astrophys. J. **524**, L19 (1999), astro-ph/9907411.

[184] M. Boylan-Kolchin, J. S. Bullock and M. Kaplinghat, *Too big to fail? The puzzling darkness of massive Milky Way subhaloes*, Mon. Not. Roy. Astron. Soc. **415**, L40 (2011), 1103.0007.

[185] M. Boylan-Kolchin, J. S. Bullock and M. Kaplinghat, *The Milky Way's bright satellites as an apparent failure of LCDM*, Mon. Not. Roy. Astron. Soc. **422**, 1203 (2012), 1111.2048.

[186] E. J. Tollerud, M. Boylan-Kolchin and J. S. Bullock, *M31 Satellite Masses Compared to LCDM Subhaloes*, Mon. Not. Roy. Astron. Soc. **440**, 3511 (2014), 1403.6469.

[187] E. Papastergis *et al.*, *Is there a "too big to fail" problem in the field?*, Astron. Astrophys. **574**, A113 (2015), 1407.4665.

[188] J. Silk and M. J. Rees, *Quasars and galaxy formation*, Astron. Astrophys. **331**, L1 (1998), astro-ph/9801013.

[189] S. Mashchenko, J. Wadsley and H. M. P. Couchman, *Stellar Feedback in Dwarf Galaxy Formation*, Science **319**, 174 (2008), 0711.4803.

[190] A. Pontzen and F. Governato, *How supernova feedback turns dark matter cusps into cores*, Mon. Not. Roy. Astron. Soc. **421**, 3464 (2012), 1106.0499.

[191] F. Governato *et al.*, *Cuspy No More: How Outflows Affect the Central Dark Matter and Baryon Distribution in Lambda CDM Galaxies*, Mon. Not. Roy. Astron. Soc. **422**, 1231 (2012), 1202.0554.

[192] A. M. Brooks and A. Zolotov, *Why Baryons Matter: The Kinematics of Dwarf Spheroidal Satellites*, Astrophys. J. **786**, 87 (2014), 1207.2468.

[193] J. Oñorbe *et al.*, *Forged in FIRE: cusps, cores, and baryons in low-mass dwarf galaxies*, Mon. Not. Roy. Astron. Soc. **454**, 2092 (2015), 1502.02036.

[194] P. Madau, S. Shen and F. Governato, *Dark Matter Heating and Early Core Formation in Dwarf Galaxies*, Astrophys. J. **789**, L17 (2014), 1405.2577.

[195] J. I. Read, O. Agertz and M. L. M. Collins, *Dark matter cores all the way down*, Mon. Not. Roy. Astron. Soc. **459**, 2573 (2016), 1508.04143.

[196] A. R. Wetzel *et al.*, *Reconciling dwarf galaxies with ΛCDM cosmology: Simulating a realistic population of satellites around a Milky Way-mass galaxy*, Astrophys. J. **827**, L23 (2016), 1602.05957.

[197] A. Fitts *et al.*, *FIRE in the Field: Simulating the Threshold of Galaxy Formation*, Mon. Not. Roy. Astron. Soc. **471**, 3547 (2017), 1611.02281.

[198] A. Zolotov *et al.*, *Baryons Matter: Why Luminous Satellite Galaxies Have Reduced Central Masses*, Astrophys. J. **761**, 71 (2012), 1207.0007.

[199] K. S. Arraki *et al.*, *Effects of baryon removal on the structure of dwarf spheroidal galaxies*, Mon. Not. Roy. Astron. Soc. **438**, 1466 (2014), 1212.6651.

[200] T. Sawala *et al.*, *The APOSTLE simulations: solutions to the Local Group's cosmic puzzles*, Mon. Not. Roy. Astron. Soc. **457**, 1931 (2016), 1511.01098.

[201] A. A. Dutton *et al.*, *NIHAO V: too big does not fail - reconciling the conflict between ΛCDM predictions and the circular velocities of nearby field galaxies*, Mon. Not. Roy. Astron. Soc. **457**, L74 (2016), 1512.00453.

[202] M. Tomozeiu, L. Mayer and T. Quinn, *Tidal stirring of satellites with shallow density profiles prevents them from being too big to fail*, Astrophys. J. Lett. **827** (2016).

[203] D. N. Spergel and P. J. Steinhardt, *Observational evidence for selfinteracting cold dark matter*, Phys. Rev. Lett. **84**, 3760 (2000), astro-ph/9909386.

[204] C. Firmani *et al.*, *Evidence of self-interacting cold dark matter from galactic to galaxy cluster scales*, Mon. Not. Roy. Astron. Soc. **315**, L29 (2000), astro-ph/0002376.

[205] F. Kahlhoefer *et al.*, *Colliding clusters and dark matter self-interactions*, Mon. Not. Roy. Astron. Soc. **437**, 2865 (2014), 1308.3419.

[206] M. Markevitch *et al.*, *Direct constraints on the dark matter self-interaction cross-section from the merging galaxy cluster 1E0657-56*, Astrophys. J. **606**, 819 (2004), astro-ph/0309303.

[207] S. W. Randall *et al.*, *Constraints on the Self-Interaction Cross-Section of Dark Matter from Numerical Simulations of the Merging Galaxy Cluster 1E 0657-56*, Astrophys. J. **679**, 1173 (2008), 0704.0261.

[208] M. Bradac *et al.*, *Revealing the properties of dark matter in the merging cluster MACSJ0025.4-1222*, Astrophys. J. **687**, 959 (2008), 0806.2320.

[209] J. Merten *et al.*, *Creation of cosmic structure in the complex galaxy cluster merger Abell 2744*, Mon. Not. Roy. Astron. Soc. **417**, 333 (2011), 1103.2772.

[210] W. A. Dawson *et al.*, *Discovery of a Dissociative Galaxy Cluster Merger with Large Physical Separation*, Astrophys. J. **747**, L42 (2012), 1110.4391.

[211] D. Harvey *et al.*, *The non-gravitational interactions of dark matter in colliding galaxy clusters*, Science **347**, 1462 (2015), 1503.07675.

[212] A. Robertson, R. Massey and V. Eke, *What does the Bullet Cluster tell us about self-interacting dark matter?*, Mon. Not. Roy. Astron. Soc. **465**, 569 (2017), 1605.04307.

[213] O. Y. Gnedin and J. P. Ostriker, *Limits on collisional dark matter from elliptical galaxies in clusters*, Astrophys. J. **561**, 61 (2001), astro-ph/0010436.

[214] J. Miralda-Escude, *A test of the collisional dark matter hypothesis from cluster lensing*, Astrophys. J. **564**, 60 (2002), astro-ph/0002050.

[215] A. H. G. Peter *et al.*, *Cosmological Simulations with Self-Interacting Dark Matter II: Halo Shapes vs. Observations*, Mon. Not. Roy. Astron. Soc. **430**, 105 (2013), 1208.3026.

[216] N. Yoshida *et al.*, *Weakly self-interacting dark matter and the structure of dark halos*, Astrophys. J. **544**, L87 (2000), astro-ph/0006134.

[217] M. Rocha *et al.*, *Cosmological Simulations with Self-Interacting Dark Matter I: Constant Density Cores and Substructure*, Mon. Not. Roy. Astron. Soc. **430**, 81 (2013), 1208.3025.

[218] N. Yoshida *et al.*, *Collisional dark matter and the structure of dark halos*, Astrophys. J. **535**, L103 (2000), astro-ph/0002362.

[219] A. Burkert, *The Structure and evolution of weakly selfinteracting cold dark matter halos*, Astrophys. J. **534**, L143 (2000), astro-ph/0002409.

[220] R. Dave *et al.*, *Halo properties in cosmological simulations of selfinteracting cold dark matter*, Astrophys. J. **547**, 574 (2001), astro-ph/0006218.

[221] P. Colin *et al.*, *Structure and subhalo population of halos in a selfinteracting dark matter cosmology*, Astrophys. J. **581**, 777 (2002), astro-ph/0205322.

[222] M. Vogelsberger, J. Zavala and A. Loeb, *Subhaloes in Self-Interacting Galactic Dark Matter Haloes*, Mon. Not. Roy. Astron. Soc. **423**, 3740 (2012), 1201.5892.

[223] J. Zavala, M. Vogelsberger and M. G. Walker, *Constraining Self-Interacting Dark Matter with the Milky Way's dwarf spheroidals*, Monthly Notices of the Royal Astronomical Society: Letters **431**, L20 (2013), 1211.6426.

[224] M. Vogelsberger *et al.*, *Dwarf galaxies in CDM and SIDM with baryons: observational probes of the nature of dark matter*, Mon. Not. Roy. Astron. Soc. **444**, 3684 (2014), 1405.5216.

[225] M. Vogelsberger *et al.*, *ETHOS - An Effective Theory of Structure Formation: Dark matter physics as a possible explanation of the small-scale CDM problems*, Mon. Not. Roy. Astron. Soc. **460**, 1399 (2016), 1512.05349.

[226] A. B. Fry *et al.*, *All about baryons: revisiting SIDM predictions at small halo masses*, Mon. Not. Roy. Astron. Soc. **452**, 1468 (2015), 1501.00497.

[227] G. A. Dooley *et al.*, *Enhanced Tidal Stripping of Satellites in the Galactic Halo from Dark Matter Self-Interactions*, Mon. Not. Roy. Astron. Soc. **461**, 710 (2016), 1603.08919.

[228] V. H. Robles *et al.*, *SIDM on FIRE: hydrodynamical self-interacting dark matter simulations of low-mass dwarf galaxies*, Mon. Not. Roy. Astron. Soc. **472** (2017).

[229] A. Loeb and N. Weiner, *Cores in Dwarf Galaxies from Dark Matter with a Yukawa Potential*, Phys. Rev. Lett. **106**, 171302 (2011), 1011.6374.

[230] M. R. Buckley and P. J. Fox, *Dark Matter Self-Interactions and Light Force Carriers*, Phys. Rev. **D81**, 083522 (2010), 0911.3898.

[231] S. Tulin, H. B. Yu and K. M. Zurek, *Beyond Collisionless Dark Matter: Particle Physics Dynamics for Dark Matter Halo Structure*, Phys. Rev. **D87**, 115007 (2013), 1302.3898.

[232] K. Schutz and T. R. Slatyer, *Self-Scattering for Dark Matter with an Excited State*, JCAP **1501**, 021 (2015), 1409.2867.

[233] K. Kainulainen, K. Tuominen and V. Vaskonen, *Self-interacting dark matter and cosmology of a light scalar mediator*, Phys. Rev. **D93**, 015016 (2016), 1507.04931.

[234] M. Kaplinghat, S. Tulin and H. B. Yu, *Dark Matter Halos as Particle Colliders: Unified Solution to Small-Scale Structure Puzzles from Dwarfs to Clusters*, Phys. Rev. Lett. **116**, 041302 (2016), 1508.03339.

[235] K. K. Boddy *et al.*, *Hidden Sector Hydrogen as Dark Matter: Small-scale Structure Formation Predictions and the Importance of Hyperfine Interactions*, Phys. Rev. **D94**, 123017 (2016), 1609.03592.

[236] Y. Zhang, *Self-interacting Dark Matter Without Direct Detection Constraints*, Phys. Dark Univ. **15**, 82 (2017), 1611.03492.

[237] M. Kaplinghat, S. Tulin and H. B. Yu, *Direct Detection Portals for Self-interacting Dark Matter*, Phys. Rev. **D89**, 035009 (2014), 1310.7945.

[238] M. Hufnagel, K. Schmidt-Hoberg and S. Wild, *BBN constraints on MeV-scale dark sectors. Part I. Sterile decays*, JCAP **1802**, 044 (2018), 1712.03972.

[239] M. Hufnagel, K. Schmidt-Hoberg and S. Wild, *BBN constraints on MeV-scale dark sectors. Part II. Electromagnetic decays*, JCAP **1811**, 032 (2018), 1808.09324.

[240] E. Del Nobile, M. Kaplinghat and H. B. Yu, *Direct Detection Signatures of Self-Interacting Dark Matter with a Light Mediator*, JCAP **1510**, 055 (2015), 1507.04007.

[241] T. Bringmann *et al.*, *Strong constraints on self-interacting dark matter with light mediators*, Phys. Rev. Lett. **118**, 141802 (2017), 1612.00845.

[242] M. W. Goodman and E. Witten, *Detectability of Certain Dark Matter Candidates*, Phys. Rev. **D31**, 3059 (1985).

[243] XENON, E. Aprile *et al.*, *Dark Matter Search Results from a One Ton-Year Exposure of XENON1T*, Phys. Rev. Lett. **121**, 111302 (2018), 1805.12562.

[244] PandaX-II, X. Cui *et al.*, *Dark Matter Results From 54-Ton-Day Exposure of PandaX-II Experiment*, Phys. Rev. Lett. **119**, 181302 (2017), 1708.06917.

[245] LUX, D. S. Akerib *et al.*, *Results from a search for dark matter in the complete LUX exposure*, Phys. Rev. Lett. **118**, 021303 (2017), 1608.07648.

[246] DarkSide, P. Agnes *et al.*, *Low-Mass Dark Matter Search with the DarkSide-50 Experiment*, Phys. Rev. Lett. **121**, 081307 (2018), 1802.06994.

[247] CRESST, F. Petricca *et al.*, 15th International Conference on Topics in Astroparticle and Underground Physics (TAUP 2017) Sudbury, Ontario, Canada, July 24-28, 2017, 2017, 1711.07692.

[248] PandaX-II, C. Fu *et al.*, *Spin-Dependent Weakly-Interacting-Massive-ParticleNucleon Cross Section Limits from First Data of PandaX-II Experiment*, Phys. Rev. Lett. **118**, 071301 (2017), 1611.06553, [Erratum: Phys. Rev. Lett.120,no.4,049902(2018)].

[249] LUX, D. S. Akerib *et al.*, *Limits on spin-dependent WIMP-nucleon cross section obtained from the complete LUX exposure*, Phys. Rev. Lett. **118**, 251302 (2017), 1705.03380.

[250] PICO, C. Amole *et al.*, *Dark Matter Search Results from the PICO-60 C_3F_8 Bubble Chamber*, Phys. Rev. Lett. **118**, 251301 (2017), 1702.07666.

[251] R. Bernabei *et al.*, *Final model independent result of DAMA/LIBRA-phase1*, Eur. Phys. J. **C73**, 2648 (2013), 1308.5109.

[252] R. Bernabei *et al.*, *First Model Independent Results from DAMA/LIBRAPhase2*, Universe **4**, 116 (2018), 1805.10486, [At. Energ.19,307(2018)].

[253] CoGeNT, C. E. Aalseth *et al.*, *Results from a Search for Light-Mass Dark Matter with a P-type Point Contact Germanium Detector*, Phys. Rev. Lett. **106**, 131301 (2011), 1002.4703.

[254] C. E. Aalseth *et al.*, *Search for an Annual Modulation in a P-type Point Contact Germanium Dark Matter Detector*, Phys. Rev. Lett. **107**, 141301 (2011), 1106.0650.

[255] CoGeNT, C. E. Aalseth *et al.*, *Search for An Annual Modulation in Three Years of CoGeNT Dark Matter Detector Data*, (2014), 1401.3295.

[256] G. Adhikari *et al.*, *An experiment to search for dark-matter interactions using sodium iodide detectors*, Nature **564**, 83 (2018).

[257] L. Roszkowski, E. M. Sessolo and S. Trojanowski, *WIMP dark matter candidates and searches - current status and future prospects*, Rept. Prog. Phys. **81**, 066201 (2018), 1707.06277.

[258] D. Tucker-Smith and N. Weiner, *Inelastic dark matter*, Phys. Rev. **D64**, 043502 (2001), hep-ph/0101138.

[259] P. W. Graham *et al.*, *Exothermic Dark Matter*, Phys. Rev. **D82**, 063512 (2010), 1004.0937.

[260] M. T. Frandsen and I. M. Shoemaker, *Up-shot of inelastic down-scattering at CDMS-Si*, Phys. Rev. **D89**, 051701 (2014), 1401.0624.

[261] N. Chen *et al.*, *Exothermic isospin-violating dark matter after SuperCDMS and CDEX*, Phys. Lett. **B743**, 205 (2015), 1404.6043.

[262] D. Tucker-Smith and N. Weiner, *The Status of inelastic dark matter*, Phys. Rev. **D72**, 063509 (2005), hep-ph/0402065.

[263] XENON100, E. Aprile *et al.*, *Implications on Inelastic Dark Matter from 100 Live Days of XENON100 Data*, Phys. Rev. **D84**, 061101 (2011), 1104.3121.

[264] G. Barello, S. Chang and C. A. Newby, *A Model Independent Approach to Inelastic Dark Matter Scattering*, Phys. Rev. **D90**, 094027 (2014), 1409.0536.

[265] PandaX-II, X. Chen *et al.*, *Exploring the dark matter inelastic frontier with 79.6 days of PandaX-II data*, Phys. Rev. **D96**, 102007 (2017), 1708.05825.

[266] XENON, E. Aprile *et al.*, *Search for magnetic inelastic dark matter with XENON100*, JCAP **1710**, 039 (2017), 1704.05804.

[267] J. Bramante *et al.*, *Inelastic frontier: Discovering dark matter at high recoil energy*, Phys. Rev. **D94**, 115026 (2016), 1608.02662.

[268] S. Kang *et al.*, *Proton-philic spin-dependent inelastic dark matter as a viable explanation of DAMA/LIBRA-phase2*, Phys. Rev. **D99**, 023017 (2019), 1810.09674.

[269] P. J. Fox, J. Liu and N. Weiner, *Integrating Out Astrophysical Uncertainties*, Phys. Rev. **D83**, 103514 (2011), 1011.1915.

[270] P. J. Fox, G. D. Kribs and T. M. P. Tait, *Interpreting Dark Matter Direct Detection Independently of the Local Velocity and Density Distribution*, Phys. Rev. **D83**, 034007 (2011), 1011.1910.

[271] N. Bozorgnia *et al.*, *Halo-independent methods for inelastic dark matter scattering*, JCAP **1307**, 049 (2013), 1305.3575.

[272] M. Drees and C. L. Shan, *Model-Independent Determination of the WIMP Mass from Direct Dark Matter Detection Data*, JCAP **0806**, 012 (2008), 0803.4477.

[273] J. M. Gaskins, *A review of indirect searches for particle dark matter*, Contemp. Phys. **57**, 496 (2016), 1604.00014.

[274] K. K. Boddy, J. Kumar and L. E. Strigari, *Effective J -factor of the Galactic Center for velocity-dependent dark matter annihilation*, Phys. Rev. **D98**, 063012 (2018), 1805.08379.

[275] P. Ciafaloni *et al.*, *Weak Corrections are Relevant for Dark Matter Indirect Detection*, JCAP **1103**, 019 (2011), 1009.0224.

[276] Fermi-LAT, DES, A. Albert *et al.*, *Searching for Dark Matter Annihilation in Recently Discovered Milky Way Satellites with Fermi-LAT*, Astrophys. J. **834**, 110 (2017), 1611.03184.

[277] HESS, H. Abdalla *et al.*, *Searches for gamma-ray lines and 'pure WIMP' spectra from Dark Matter annihilations in dwarf galaxies with H.E.S.S*, JCAP **1811**, 037 (2018), 1810.00995.

[278] HESS, H. Abdallah *et al.*, *Search for γ-Ray Line Signals from Dark Matter Annihilations in the Inner Galactic Halo from 10 Years of Observations with H.E.S.S.*, Phys. Rev. Lett. **120**, 201101 (2018), 1805.05741.

[279] MAGIC, V. A. Acciari *et al.*, *Constraining Dark Matter lifetime with a deep gamma-ray survey of the Perseus Galaxy Cluster with MAGIC*, Phys. Dark Univ. **22**, 38 (2018), 1806.11063.

[280] MAGIC, M. L. Ahnen *et al.*, *Indirect dark matter searches in the dwarf satellite galaxy Ursa Major II with the MAGIC Telescopes*, JCAP **1803**, 009 (2018), 1712.03095.

[281] L. Goodenough and D. Hooper, *Possible Evidence For Dark Matter Annihilation In The Inner Milky Way From The Fermi Gamma Ray Space Telescope*, (2009), 0910.2998.

[282] C. Weniger, *A Tentative Gamma-Ray Line from Dark Matter Annihilation at the Fermi Large Area Telescope*, JCAP **1208**, 007 (2012), 1204.2797.

[283] IceCube, M. G. Aartsen *et al.*, *Search for Neutrinos from Dark Matter Self-Annihilations in the center of the Milky Way with 3 years of IceCube/DeepCore*, Eur. Phys. J. **C77**, 627 (2017), 1705.08103.

[284] A. Albert *et al.*, *Results from the search for dark matter in the Milky Way with 9 years of data of the ANTARES neutrino telescope*, Phys. Lett. **B769**, 249 (2017), 1612.04595.

[285] PAMELA, O. Adriani *et al.*, *An anomalous positron abundance in cosmic rays with energies 1.5-100 GeV*, Nature **458**, 607 (2009), 0810.4995.

[286] Fermi-LAT, M. Ackermann *et al.*, *Measurement of separate cosmic-ray electron and positron spectra with the Fermi Large Area Telescope*, Phys. Rev. Lett. **108**, 011103 (2012), 1109.0521.

[287] AMS, M. Aguilar *et al.*, *First Result from the Alpha Magnetic Spectrometer on the International Space Station: Precision Measurement of the Positron Fraction in Primary Cosmic Rays of 0.5-350 GeV*, Phys. Rev. Lett. **110**, 141102 (2013).

[288] G. Steigman *et al.*, *Dynamical interactions and astrophysical effects of stable heavy neutrinos*, Astron. J. **83**, 1050 (1978).

[289] D. N. Spergel and W. H. Press, *Effect of hypothetical, weakly interacting, massive particles on energy transport in the solar interior*, Astrophys. J. **294**, 663 (1985).

[290] A. Gould and G. Raffelt, *Cosmion Energy Transfer in Stars: The Knudsen Limit*, Astrophys. J. **352**, 669 (1990).

[291] A. Gould and G. Raffelt, *Thermal conduction by massive particles*, Astrophys. J. **352**, 654 (1990).

[292] L. M. Krauss *et al.*, *Cold dark matter candidates and the solar neutrino problem*, Astrophys. J. **299**, 1001 (1985).

[293] SNO, Q. R. Ahmad *et al.*, *Direct evidence for neutrino flavor transformation from neutral current interactions in the Sudbury Neutrino Observatory*, Phys. Rev. Lett. **89**, 011301 (2002), nucl-ex/0204008.

[294] M. Asplund, N. Grevesse and J. Sauval, *The Solar chemical composition*, Nucl. Phys. **A777**, 1 (2006), astro-ph/0410214, [ASP Conf. Ser.336,25(2005)].

[295] S. Basu and H. M. Antia, *Constraining solar abundances using helioseismology*, Astrophys. J. **606**, L85 (2004), astro-ph/0403485.

[296] J. N. Bahcall *et al.*, *Helioseismological implications of recent solar abundance determinations*, Astrophys. J. **618**, 1049 (2005), astro-ph/0407060.

[297] S. Basu and H. M. Antia, *Helioseismology and Solar Abundances*, Phys. Rept. **457**, 217 (2008), 0711.4590.

[298] M. Asplund *et al.*, *The chemical composition of the Sun*, Ann. Rev. Astron. Astrophys. **47**, 481 (2009), 0909.0948.

[299] A. Serenelli *et al.*, *New Solar Composition: The Problem With Solar Models Revisited*, Astrophys. J. **705**, L123 (2009), 0909.2668.

[300] M. T. Frandsen and S. Sarkar, *Asymmetric dark matter and the Sun*, Phys. Rev. Lett. **105**, 011301 (2010), 1003.4505.

[301] M. Taoso *et al.*, *Effect of low mass dark matter particles on the Sun*, Phys. Rev. **D82**, 083509 (2010), 1005.5711.

[302] D. T. Cumberbatch *et al.*, *Light WIMPs in the Sun: Constraints from Helioseismology*, Phys. Rev. **D82**, 103503 (2010), 1005.5102.

[303] M. Cirelli *et al.*, *Spectra of neutrinos from dark matter annihilations*, Nucl. Phys. **B727**, 99 (2005), hep-ph/0506298, [Erratum: Nucl. Phys.B790,338(2008)].

[304] M. Blennow, J. Edsjö and T. Ohlsson, *Neutrinos from WIMP annihilations using a full three-flavor Monte Carlo*, JCAP **0801**, 021 (2008), 0709.3898.

[305] J. N. Bahcall, *Solar neutrinos: Where we are, where are we going*, Astrophys. J. **467**, 475 (1996), hep-ph/9512285.

[306] J. Edsjo *et al.*, *Neutrinos from cosmic ray interactions in the Sun*, JCAP **1706**, 033 (2017), 1704.02892.

[307] IceCube, M. G. Aartsen *et al.*, *Search for annihilating dark matter in the Sun with 3 years of IceCube data*, Eur. Phys. J. **C77**, 146 (2017), 1612.05949.

[308] ANTARES, S. Adrian-Martinez *et al.*, *Limits on Dark Matter Annihilation in the Sun using the ANTARES Neutrino Telescope*, Phys. Lett. **B759**, 69 (2016), 1603.02228.

[309] ANTARES, S. Adrin-Martnez *et al.*, *A search for Secluded Dark Matter in the Sun with the ANTARES neutrino telescope*, JCAP **1605**, 016 (2016), 1602.07000.

[310] Baikal, A. D. Avrorin *et al.*, *Search for neutrino emission from relic dark matter in the Sun with the Baikal NT200 detector*, Astropart. Phys. **62**, 12 (2015), 1405.3551.

[311] S. Nussinov, L. T. Wang and I. Yavin, *Capture of Inelastic Dark Matter in the Sun*, JCAP **0908**, 037 (2009), 0905.1333.

[312] A. Menon *et al.*, *Capture and Indirect Detection of Inelastic Dark Matter*, Phys. Rev. **D82**, 015011 (2010), 0905.1847.

[313] J. Shu, P. f. Yin and S. h. Zhu, *Neutrino Constraints on Inelastic Dark Matter after CDMS II*, Phys. Rev. **D81**, 123519 (2010), 1001.1076.

[314] J. Smolinsky and P. Tanedo, *Dark Photons from Captured Inelastic Dark Matter Annihilation: Charged Particle Signatures*, Phys. Rev. **D95**, 075015 (2017), 1701.03168, [Erratum: Phys. Rev.D96,no.9,099902(2017)].

[315] R. Catena and F. Hellström, *New constraints on inelastic dark matter from IceCube*, JCAP **1810**, 039 (2018), 1808.08082.

[316] W. H. Press and D. N. Spergel, *Capture by the sun of a galactic population of weakly interacting massive particles*, Astrophys. J. **296**, 679 (1985), [277(1985)].

[317] A. Gould, *Resonant Enhancements in WIMP Capture by the Earth*, Astrophys. J. **321**, 571 (1987).

[318] K. Griest and D. Seckel, *Cosmic Asymmetry, Neutrinos and the Sun*, Nucl. Phys. **B283**, 681 (1987), [Erratum: Nucl. Phys.B296,1034(1988)].

[319] A. Gould, *WIMP Distribution in and Evaporation From the Sun*, Astrophys. J. **321**, 560 (1987).

[320] G. Busoni, A. De Simone and W. C. Huang, *On the Minimum Dark Matter Mass Testable by Neutrinos from the Sun*, JCAP **1307**, 010 (2013), 1305.1817.

[321] Z. L. Liang *et al.*, *On the evaporation of solar dark matter: spin-independent effective operators*, JCAP **1609**, 018 (2016), 1606.02157.

[322] G. Busoni *et al.*, *Evaporation and scattering of momentum- and velocity-dependent dark matter in the Sun*, JCAP **1710**, 037 (2017), 1703.07784.

[323] R. Garani and S. Palomares-Ruiz, *Dark matter in the Sun: scattering off electrons vs nucleons*, JCAP **1705**, 007 (2017), 1702.02768.

[324] Z. L. Liang, Y. L. Tang and Z. Q. Yang, *The leptophilic dark matter in the Sun: the minimum testable mass*, JCAP **1810**, 035 (2018), 1802.01005.

[325] A. Widmark, *Thermalization time scales for WIMP capture by the Sun in effective theories*, JCAP **1705**, 046 (2017), 1703.06878.

[326] A. R. Zentner, *High-Energy Neutrinos From Dark Matter Particle Self-Capture Within the Sun*, Phys. Rev. **D80**, 063501 (2009), 0907.3448.

[327] C. S. Chen and Y. H. Lin, *On the evolution process of two-component dark matter in the Sun*, JHEP **04**, 074 (2018), 1802.06956.

[328] M. Nauenberg, *Energy Transport and Evaporation of Weakly Interacting Particles in the Sun*, Phys. Rev. **D36**, 1080 (1987).

[329] S. Israelsson, Thermalisation of inelastic dark matter in the sun with a light mediator, Master's thesis, KTH, urn:nbn:se:kth:diva-233754, 2018.

[330] M. Blennow, J. Herrero-Garcia and T. Schwetz, *A halo-independent lower bound on the dark matter capture rate in the Sun from a direct detection signal*, JCAP **1505**, 036 (2015), 1502.03342.

Part II

Scientific papers

Paper I

M. Blennow and S. Clementz

Asymmetric capture of Dirac dark matter by the Sun

JCAP **1508**, 036 (2015)

arXiv:1504.05813

Paper II

M. Blennow, S. Clementz and J. Herrero-Garcia

Pinning down inelastic dark matter in the Sun and in direct detection

JCAP **1604**, 004 (2016)

arXiv:1512.03317

Paper III

M. Blennow, S. Clementz and J. Herrero-Garcia

Self-interacting inelastic dark matter: A viable solution to the small scale structure problems

JCAP 1703 (2017) 048

arXiv:1612.06681

Paper IV

M. Blennow, S. Clementz and J. Herrero-Garcia

The distribution of inelastic dark matter in the Sun

Eur. Phys. J. C78 (2018) 386

arXiv:1802.06880